Preprint no ...

Studies of the QED/EW corrections to $Z \to ll$ observables at the LHC

LHC EW working group

ABSTRACT

Draft as of: **March 27, 2020**.

Contents

1 Change Log

1.1 version v03, January 2020

- Updated plots/table in Appendix E and D
- Updated plots/table in Section 2.4, still old binning for Tables.
- Updated plots/table in Section 1.2, still old binning for Tables.

1.2 Version v04, February 2020

- Introduced three variants of "Effective Born", tuned to predictions from Dizet 6.45.
- New results in Appendix C about Z-boson propagator, text needs more discussion, plots/tables final.
- Updated plots/table in Section 1.2, new binning for tables.
- Updated layout of Tables in Section 2.4, updated numbers from `TauSpinner`+wt^{EW}
- Updated plots/table in Appendix E and D, results with diferent 'Born Effective" variants added.

1.3 Version v05, March 2020

- Added Appendix K with multi-MC tuned comparisons in EW G_μ scheme. Results from `Powheg_ew`, `MCSANC` and `ZGRAD2`.
- Added additional bin for comparison between fixed and runing width propagators, Appendix H.
- Added subsection in Appendix E with estimated A_4 in the experimental bins, using `TauSpinner` weights wt^{EW}, with full EW corrections and Effective Born.

2 Introduction

Content:
Short historical overview of LEP/Tevatron/early LHC.

2.1 Electroweak pseudo-observables at LEP

Authors: Fulvio, Elzbieta

The concept of electroweak pseudo-observables (EWPO) was essential in the final analysis of LEP1 data of [1]. The EWPO's at LEP were quantities like Z mass and width; the various $2 \to 2$ Z peak cross-sections, most of the $2 \to 2$ charge and spin asymmetries at the Z peak, plus the equivalent effective weak mixing angle, which is the main SM parameter under study in this article. They were derived directly from the experimental data in such a way that QED contributions and the kinematic cut-off effects were removed. The art of the Z line-shape and asymmetry analyses at LEP relied on the ability to reduce the many degrees of freedom from the experimental measurements to a sufficiently small set of intermediate variables, which could be precisely described by theory. With full one-loop accuracy in QED/EW theory (and even a bit beyond) this was prepared in the ZFITTER package [2, 3].

A theoretically sound separation of the QED/EW effects between the QED emissions and genuine virtual weak effects was essential for the phenomenology of LEP precision physics [1]. It was motivated by the structure of the amplitudes for single Z-boson production or (to a lesser degree) WW-pair production in e^+e^- collisions, as well as by the fact that QED bremsstrahlung occurs at a different energy scale than the electroweak processes. Even more importantly, with this approach, multi-loop calculations for the complete electroweak sector could be avoided. The QED terms were thus resummed in an exclusive exponentiation scheme implemented in Monte Carlo [4]. Note that these QED corrections modify the cross-section at the peak by as much as 40%. The details of this paradigm are explained for example in Ref. [5]. It was obtained as the result of a massive effort by the theory community, which will not be recalled in any detail here. From the practical phenomenology perspective, spin amplitudes are semi-factorised into a Born-like term(s) and functional factors responsible for bremsstrahlung [6].

A similar separation can also be achieved for dynamics of production process in pp collisions, which can be isolated from QED/EW corrections. It was explored recently in the case of configurations with high-p_T jets associated with the Drell-Yan production of Z [7] or W bosons [8] at the LHC. The potentially large electroweak Sudakov logarithmic corrections discussed in [9] represent yet another class of weak effects, separable from those discussed above and throughout this paper, and they are not discussed here because they are mainly relevant for dilepton masses beyond the range considered for the weak mixing angle measurement.

To assess precisely the size and impact of the so-called genuine weak corrections to the Born-like cross section for lepton pair production with a virtuality well below the threshold for WW pair production, the precision calculations and programs prepared for the LEP era: `KKMC` Monte Carlo [10] and `Dizet` electroweak (EW) library, were adapted to provide pre-tabulated EW corrections which could be used by LHC-specific programs like the `TauSpinner` package [11]. Currently, the `KKMC` Monte Carlo used is `Dizet` version `6.21` [12, 2]. Since the LEP times, the version of the `Dizet` library has been updated eg. [13, 14]. For the sake of compatibility, results from this version are shown as well, however the final numbers will be evaluated with the most recent versions of the program, the `Dizet` version `6.45` [15].

2.2 The weak mixing angle and effective weak mixing angle

There are multiple approaches and conventions used to define the effective weak mixing angle(s), as illustrated e.g. in the Particle Data Group 2018 review [16]. This naming is therefore overloaded and may lead to confusion.

The fundamental quantity is the weak mixing angle, $\sin^2\theta_W$. In the on-shell convention and $\alpha(0)$ EW scheme, as discussed in more detail in Appendix **??**, the weak mixing angle is defined uniquely through the gauge-boson masses at tree level:

$$\sin^2\theta_W = s_W^2 = 1 - \frac{m_W^2}{m_Z^2}. \tag{1}$$

and this relation holds to all orders. If m_W is a derived input parameter calculated using higher-order corrections, the corresponding $\sin^2\theta_W$ gets updated. For example, in the $\alpha(0)$ v0 scheme at EW LO, the value of $\sin^2\theta_W$ =

Table 1: The theory predictions for on-shell and effective leptonic weak angle. Number from Particle Data Group 2018 review [16].

Weak angle	Notation	Value	Parametric uncertainty
On-shell weak angle	s_W^2	0.22343	$\pm$ 0.00007
Effective weak angle	$\sin^2\theta_{eff}^{\ell}$	0.23154	$\pm$ 0.00003

0.21215 (see Table 13). With EW NLO+HO corrections applied to calculate m_W, the value of $\sin^2\theta_W = 0.22352$ (see Table 18).

In the same EW $\alpha(0)$ v0 scheme there is also a clear definition of the observable $\sin^2\theta_{eff}^f(M_Z)$, which is called the effective weak mixing angle at the Z-pole, which is related to the ratio of the effective axial and vector couplings, g_Z^f (here we use "f" for quark or lepton):

$$g_Z^f = \frac{v_Z^f}{a_Z^f} = 1 - 4|q_f|(K_Z^f s_W^2 + I_f^2), \tag{2}$$

with

$$I_f^2 = \alpha^2(s)\frac{35}{18}[1 - \frac{8}{3}Re(K_Z^f)s_W^2], \tag{3}$$

and the flavour-dependent *effective weak mixing angles* as

$$\sin^2\theta_{eff}^f = Re(\mathscr{K}_Z^f)s_W^2 + I_f^2 \tag{4}$$

While the $\sin^2\theta_W$ generic for all flavours, and energy-scale not dependent, the $\sin^2\theta_{eff}^f$ is not. It is specifficaly for a given flavour, and only at the Z-pole. In the name already is suggested as effective theory quantity, not necessarily the Standard Model gauge theory one. In Table 1 we quote the most updated numbers from Particle Data Group 2018 review [16].

Estimates for the total theoretical error from leading unknown higher order corrections on $\sin^2\theta_{eff}^{\ell}$ has been recently updated in [17]. The leading missing orders are three- and four-loop corrections, $O(\alpha^3)$, $O(\alpha\alpha_s^2)$ and $O(\alpha\alpha_s^3)$. The final estimate is $4.3\cdot 10^{-5}$, compatible with number quoted by final LEP publications [1] of $5.0\cdot 10^{-5}$. This is precision fully adequate for measurement at LHC.

While the measurement at LEP were done at different energies and then corrected with theoretical predictions to the values at Z-pole, at LHC it will be done differently. The measurements will be done in different mass and rapidity ranges, and then combined. At least it is present strategy. It is therefore of interest to extend the definition of $\sin^2\theta_{eff}^f$ outside the Z-pole region. This could be done in straightforward way

$$g_{eff}^f(s,t) = \frac{v_{eff}^f(s,t)}{a_{eff}^f(s,t)} = 1 - 4|q_f|(K^f(s,t)s_W^2 + I_f^2(s,t)) \tag{5}$$

where s,t stand for Mandelstam variables. and correspondingly

$$\sin^2\theta_{eff}^f(s,t) = Re(\mathscr{K}^f(s,t))s_W^2 + I_f^2(s,t) \tag{6}$$

The flavour dependent effective weak mixing angles, calculated using: Eq. (6), EW form-factors of `Dizet` library, and $\alpha(0)v0$ scheme, with on-shell $s_W^2 = 0.22352$ are shown on Fig. 1 as a function of the invariant mass of outgoing lepton pair and for $\cos\theta = 0.5$. In Table 2 we display value of effective weak missing angles averaged over specified mass windows.

Prepare in the $\sin^2\theta_{eff}$ *schemes, similar figure and table. Ask Fulvio et al.*

Table 2: The effective weak mixing angles $\sin^2\theta^f_{eff}$, for different mass windows and with/without box corrections. The form-factor corrections are averaged with realistic line-shape and $\cos\theta$ distribution.
Updated with `Dizet 6.45` *form-factors*

Parameter	$\sin^2\theta^{\ell}_{eff}$	$\sin^2\theta^{up-quark}_{eff}$	$\sin^2\theta^{down-quark}_{eff}$
	EW loops without box corrections		
$89 < m_{ee} < 93$ GeV	0.231485	0.231484	0.231465
$60 < m_{ee} < 81$ GeV	0.231734	0.231659	0.231552
$81 < m_{ee} < 101$ GeV	0.231488	0.231487	0.231474
$101 < m_{ee} < 150$ GeV	0.208106	0.208145	0.208210
	EW loops with box corrections		
$89 < m_{ee} < 93$ GeV	0.231480	0.231467	0.231474
$60 < m_{ee} < 81$ GeV	0.231619	0.230903	0.231441
$81 < m_{ee} < 101$ GeV	0.231484	0.231476	0.231478
$101 < m_{ee} < 150$ GeV	0.208043	0.208945	0.208146

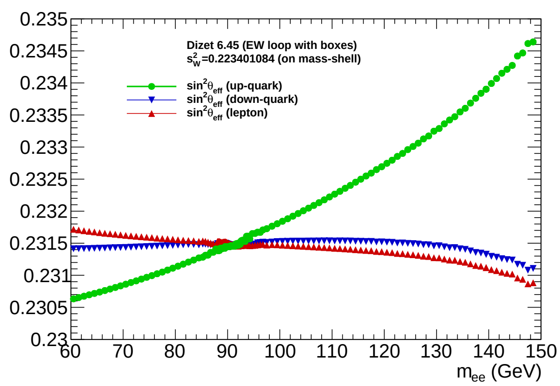

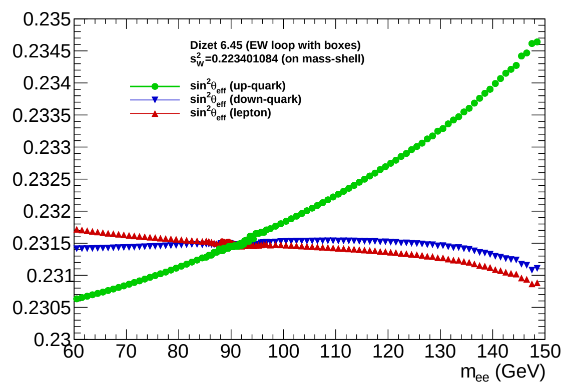

Figure 1: Effective weak mixing angles $\sin^2\theta^f_{eff}$ with EW corrections calculated using `Dizet` library form-factors and on mass-shell $s^2_W = 0.223401084$ as a function of m_{ee} and $\cos\theta = 0$, without (left) and with (right) box corrections are shown.
Updated with `Dizet 6.45` *form-factors.*

2.3 Observables sensitive to the weak mixing angle at hadron colliders

2.4 Interpretation of early hadron collider measurements in terms of the effective weak mixing angle

3 Virtual EW corrections

Authors: Elzbieta (`Dizet`), Fulvio (`Powheg_ew`), Serge/Lida (`MCSANC`), Doreen?(`ZGRAD2`)

Content:

- *Loops and box corrections with different EW schemes.*
- *Treatment of* $\alpha(M_Z)$ *with different EW schemes. Show numerical results.*
- *Treatment of* $\sin^2\theta_W$ *with different schemes. Show numerical results.*
- *Genuine EW and line-shape corrections to* $d\sigma/dm_{ll}$, A_{FB}. *Comparisons of* `Powheg_ew`, `MCSANC` *and* `PowhegZj`+wt^{EW}
- *Improved Born Approximation vs Effective Born. Comparisons from* `PowhegZj`+wt^{EW}.

3.1 Introduction

3.2 Overview of calculations/tools and input schemes

3.3 Numerical results for virtual EW corrections

3.3.1 Loops and box corrections with different EW schemes

In this Section we show comparison between `Dizet` and `MCSANC` EW libraries. For details on the calculations see respectively [12, 2] and [18, 19]. The input parameters, which could be set consistently in both programs, are collected in Table **??**.

The definition of the *effective* quark masses used in both initialisation and shown in Table **??** is such that they are some fitted values which allows to reproduce in the one-loop order the quantity of $\Delta\alpha_h^{(5)}(M_Z^2)$.

Comments:

For `Dizet 6.21` *parametrisation of* α *not updated, used the one of published version. For measurements at LEP used probably updates of [20]. The comparison between* `MCSANC` *and* `Dizet` *should be updated to* `Dizet 6.XX`

Table 3: The EW parameters at EW NLO+HO, with on-mass-shell definition (LEP convention).

Parameter	$(\alpha(0), G_\mu, M_Z)$ $\alpha(0)$ v0	$(\alpha(0), M_W, M_Z)$ $\alpha(0)$ v1	(G_μ, M_Z, M_W) G_μ	$(\alpha(0), s_W^2, M_Z)$ $\sin^2_{eff}$ v1	(G_μ, s_W^2, M_Z) sin^2_{eff} v2
M_Z (GeV)	91.1876	91.1876	91.1876	91.1876	91.1876
Γ_Z (GeV)	2.4953785				
$1/\alpha(M_Z)$	0.0077549256		0.0077546943		
$\alpha(M_Z)$	128.9503022		128.954148618738		
G_μ (GeV^{-2})	$1.1663787 \cdot 10^{-5}$		$1.1663787 \cdot 10^{-5}$		$1.1663787 \cdot 10^{-5}$
M_W (GeV)	80.358935	80.385	80.385		
s_W^2	0.223401084	0.22289722	0.22289722		
$\sin^2\theta^\ell_{eff}$	0.231499			0.231499	0.231499
$\sin^2\theta^u_{eff}$	0.231392				
$\sin^2\theta^d_{eff}$	0.231265				
$\sin^2\theta^b_{eff}$	0.232733				

3.3.2 α_{QED} with different EW schemes

3.3.3 $\sin^2\theta_W$ with different EW schemes

Table 4: The EW parameters used for: (i) the EW LO $\alpha(0)$ v0 scheme, (ii) effective Born spin amplitude around the Z-pole. The $G_\mu = 1.1663887 \cdot 10^{-5}$ GeV^{-2}, $M_Z = 91.1876$ GeV and $\mathscr{K}_f, \mathscr{K}_e, \mathscr{K}_{\ell f} = 1$.
.

EW LO $\alpha(0)$ scheme	Effective Born *v0*	Effective Born *v1*	Effective Born *v2*
$\alpha = 1/137.03599$	$\alpha = 1/128.9503022$	$\alpha = 1/128.9503022$	$\alpha = 1/128.9503022$
$s_W^2 = 0.21215$	$s_W^2 = 0.231499$	$s_W^2 = 0.231499$	${s_W^2}^{\ell} = 0.231499$ ${s_W^2}^{up} = 0.231392$ ${s_W^2}^{down} = 0.231265$
$\rho_{\ell f} = 1.0$	$\rho_{\ell f} = 1.0$	$\rho_{\ell f} = 1.005$	$\rho_{\ell up} = 1.005403$ $\rho_{\ell down} = 1.005889$

3.3.4 Improved Born Approximation and Effective Born

Comment: Content of this subsection was published in [21].

The *Improved Born Approximation* (IBA) is discussed in more details in Appendix B. In IBA, the complete $O(\alpha)$ EW corrections, supplemented by selected higher order terms, are handled with form-factor corrections, dependent on (s,t), multiplying couplings and propagators of the usual Born expressions.

At this point we would like to introduce two options for the Born spin amplitudes *parametrisation*, which we will refer to as *Effective Born*, which work as very good approximations of the EW corrections near the Z-pole. The *Effective Born* absorbs bulk of EW corrections into redefinition of few fixed parameters (couplings) instead.

- The *v0* parametrisation is using formula (26) for spin amplitude but with $\alpha(s) = \alpha(M_Z) = 1./128.9503022$, $s_W^2 = \sin^2\theta_W^{eff}(M_Z) = 0.231499$ and all form factors equal to 1.0.
- The *v1* parametrisation is using formula (26) for spin amplitude, parameters are set as for *v0* parametrisation, and all form-factors equal 1, except $\rho_{\ell f} = 1.005$.
- The *v2* parametrisation is using formula (26) for spin amplitude, parameters are set as that both s_W^2 and $\rho_{\ell f}$ are flavour dependent, and equal to predicted by `Dizet 6.45`.

Table 4 shows effective Born parametrisation for *v0, v1, v2* versions.

In the following, we will systematically compare predictions of EW corrections and those calculated with Born effective approximations. As we will see later, effective Born with *v2* works remarkably well around Z-pole both for predicting the lineshape and forward-backward asymmetry.

3.3.5 The Z-boson lineshape

In the EW LO, the Z-boson lineshape, assuming that the constraint (38) holds, depends only on two parameters (M_Z, Γ_z). The effect on the lineshape from EW loop corrections are due to corrections to the propagators: vacuum polarisation corrections (running α) and ρ form-factor, causing change in relative contributions of the Z and γ, and change of the Z-boson vector to axial coupling ratio ($\sin^2\theta_{eff}$). The above affect not only shape but also normalisation of the cross-section.

In Fig. 2 (top-left) distributions of generated and EW corrected lineshape are shown. On the logarithmic scale difference is barely visible. In the following plots of the same Figure we study it in more details. The ratios of the lineshape distributions with gradually introduced EW corrections are shown. For reference ones (denominator) the following: (i) EW LO $\alpha(0)$, (ii) effective Born *v0* and (iii) effective Born *(v2)* are used. At the Z-pole, complete EW corrections are at about 0.1% for the one with effective Born *(v2)*. It shows that using for events generation EW LO matrix element but with different parametrisations will significantly reduce the size of missing EW corrections.

Table 5: EW corrections to cross-sections in the specified mass windows. The EW weight is calculated with $\cos\theta^*$ definition for scattering angle.
Updated with Dizet 6.45 form factors and running width.

Corrections to cross-section	$89 < m_{ee} < 93$ GeV	$81 < m_{ee} < 101$ GeV
σ(EW corr. to m_W)/σ(EW LO $\alpha(0)$)	0.97145	0.97185
σ(EW corr. to $\chi(Z),\chi(\gamma)$)/σ(EW LO $\alpha(0)$)	0.98271	0.98362
σ(EW/QCD FF no boxes)/σ(EW LO $\alpha(0)$)	0.96505	0.96626
σ(EW/QCD FF with boxes)/σ(EW LO $\alpha(0)$)	0.96510	0.96631
σ(Eff. v0)/σ(EW/QCD FF with boxes)	1.01142	1.01135
σ(Eff. v1)/σ(EW/QCD FF with boxes)	1.00130	1.00132
σ(Eff. v2)/σ(EW/QCD FF with boxes)	0.99989	0.99987

Table 5 details numerical values for EW corrections to the normalisation (ratios of the cross-section), integrated in the range $81 < m_{ee} < 101$ GeV and $89 < m_{ee} < 93$ GeV. Results from calculating EW weight using $\cos\theta^*$ definition of the scattering angle are shown. Total EW correction to normalisation at EW LO G_μ is 1.010. Total EW correction to normalisation at EW LO $\alpha(0)$ is about 0.965, while total corrections to the effective Born *(v2)* is of about 1.001.

3.3.6 The A_{FB} distribution

The forward-backward asymmetry defined for pp collisions in a standard way reads

$$A_{FB} = \frac{\sigma(\cos\theta > 0) - \sigma(\cos\theta < 0)}{\sigma(\cos\theta > 0) + \sigma(\cos\theta < 0)}, \tag{7}$$

where $\cos\theta$ is taken in the *Collins-Soper* frame.

The EW corrections change overall normalisation and the shape of A_{FB}, particularly around the Z-pole. In Fig. 3 (top-left), the A_{FB} distribution as generated (EW LO) and EW corrected are shown. In the following plots of this Figure, we study it in more details. The difference $\Delta A_{FB} = A_{FB} - A_{FB}^{ref}$ with gradually introduced EW corrections are shown. For reference the following ones: (i) EW LO $\alpha(0)$, (ii) effective Born *v0* and (iii) effective Born *v2* are used.

Complete EW corrections to A_{FB} integrated around Z-pole, are about ΔA_{FB} = -0.00075 with respect to EW LO G_μ predictions and about ΔA_{FB} = -0.03534 with respect to EW LO with $\alpha(0)$ predictions. The total corrections to A_{FB} of effective Born *v2* is ΔA_{FB} = -0.00005. Using effective Born *v2* configuration reproduces EW loop corrections predictions with precision better than ΔA_{FB} = -0.0001 in the full mass range shown, but the remaining box corrections are at ΔA_{FB} = -0.002 around $m_{ee} = 150$ GeV.

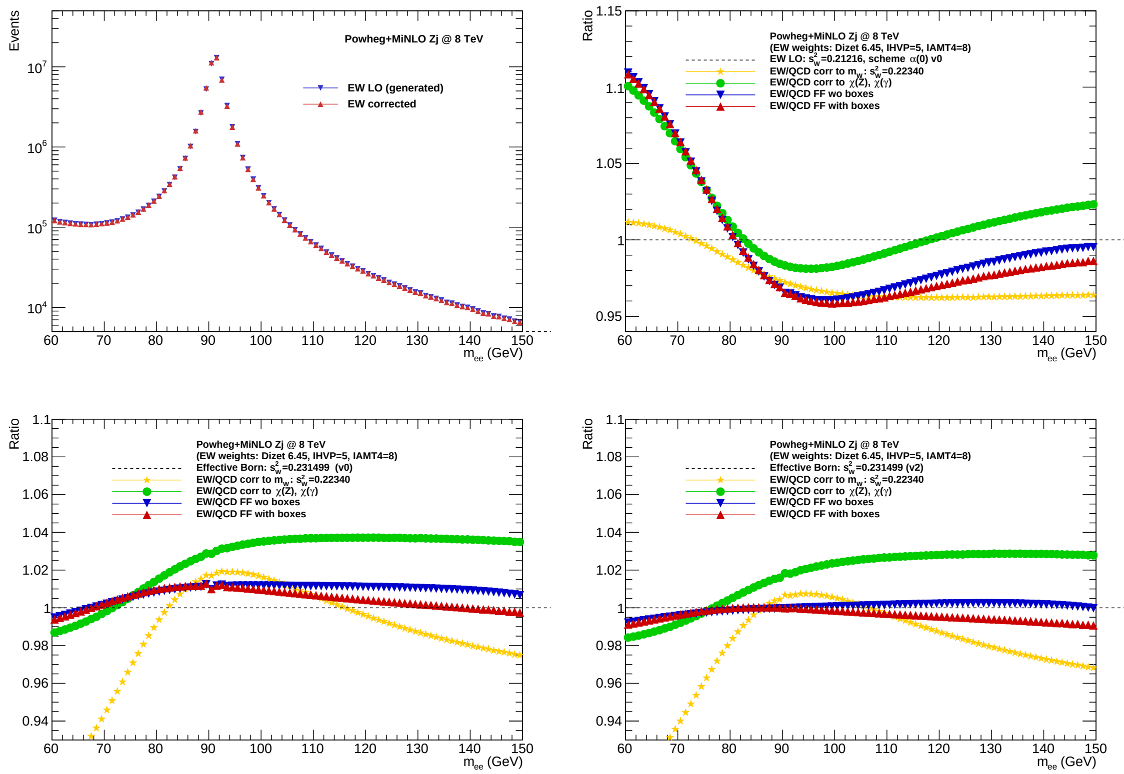

Figure 2: Top-left: lineshape distribution as generated with `Powheg+MiNLO` (blue triangles) and after reweighting introducing all EW corrections discussed (red triangles). The points are barely distinguishable. Ratios of the lineshapes with gradually introduced EW corrections. In consecutive plots as a reference (black dashed line): (i) reweighted to EW LO $\alpha(0)$ scheme (top-right), (ii) reweighted to effective Born *v0* (bottom-left) and (iii) reweighted to effective Born *v2* (bottom-right) was used.
Updated with Dizet 6.45 form factors and running width.

Table 6: The difference in forward-backward asymmetry, ΔA_{FB}, in the specified mass windows. The difference is calculated using $\cos\theta^{CS}$ to define forward and backward hemisphere. The EW weight is calculated with $\cos\theta^{*}$ definition for scattering angle.
Updated with Dizet 6.45 form factors and running width.

Corrections to A_{FB}	$89 < m_{ee} < 93$ GeV	$81 < m_{ee} < 101$ GeV
A_{FB}(EW corr. m_W) - A_{FB}(EW LO $\alpha(0)$)	-0.02076	-0.02079
A_{FB}(EW corr. prop. $\chi(Z), \chi(\gamma)$) - A_{FB}(EW LO $\alpha(0)$)	-0.02047	-0.02071
A_{FB}(EW/QCD FF no boxes) - A_{FB}(EW LO $\alpha(0)$)	-0.03491	-0.03515
A_{FB}(EW/QCD FF with boxes) - A_{FB}(EW LO $\alpha(0)$)	-0.03489	-0.03514
A_{FB}(Eff. v0) - A_{FB}(EW/QCD FF with boxes)	-0.00039	-0.00042
A_{FB}(Eff. v1) - A_{FB}(EW/QCD FF with boxes)	-0.00042	-0.00042
A_{FB}(Eff. v2) - A_{FB}(EW/QCD FF with boxes)	-0.00022	-0.00024

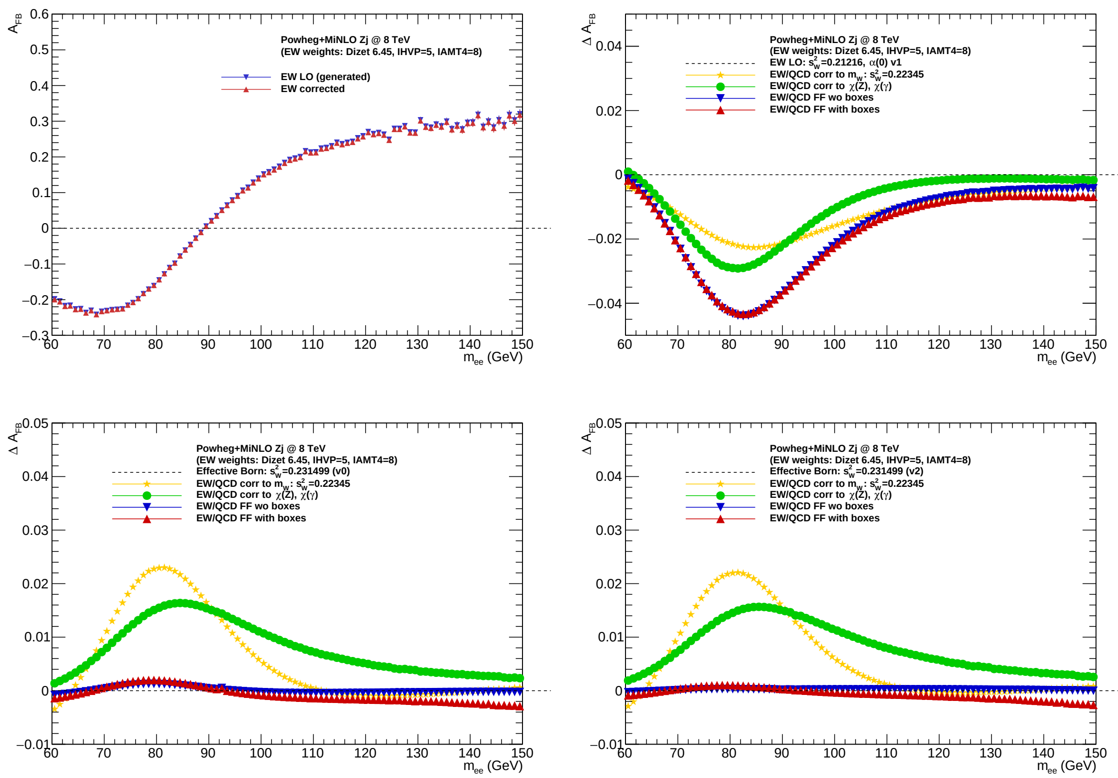

Figure 3: Top-left: the A_{FB} distribution as generated in `Powheg+MiNLO` sample (blue triangles) and after reweighting introducing all EW corrections (red triangles). The two choices are barely distinguishable.The differences $\Delta A_{FB} = A_{FB} - A_{FB}^{ref}$, due to gradually introduced EW corrections. In consecutive plots as a reference (black dashed line): (i) reweighted to EW LO $\alpha(0)$ scheme (top-right), (ii) reweighted to effective Born *v0* (bottom-left) and (iii) reweighted to effective Born *v2* (bottom-right) was used.
Updated with Dizet 6.45 form factors and runnign width.

Table 7: Shown availability for QCD corrections and EW schemes with different codes.

Program	QCD	EW	EW scheme	Comments
`Powheg_ew`	LO	LO	$\alpha(0)$ v0	pole mass, fixed Γ_Z
		LO, NLO, NLO+HO	$\alpha(0)$ v1	
		LO, NLO, NLO+HO	G_μ	
		LO, NLO, NLO+HO	$\sin^2\theta_{eff}$ v1	
		LO, NLO, NLO+HO	$\sin^2\theta_{eff}$ v2	
	NLO	NLO+HO	G_μ	
`MCSANC`	LO	LO, NLO, NLO+HO	$\alpha(0)$ v1	pole mass, fixed Γ_Z
		LO, NLO, NLO+HO	G_μ	
`Powheg Zj` +wt^{EW}	MC event	LO, NLO+HO	$\alpha(0)$ v0	on-shell mass, running Γ_Z[1]
		LO	$\alpha(0)$ v1	
		LO	G_μ	
		LO	$\sin^2\theta_{eff}$ v2	

3.4 Benchmark results from Powheg_ew, MCSANC, PowhegZj+wt^{EW}

In this section we collect results for `Powheg_ew`, `MCSANC` and `PowhegZj`+wt^{EW}, for benchmark EW schemes defined as in Table 13. Not all EW schemes where implemented in all programs. Table 7 specify the order of QCD and EW corrections which were used for the comparisons presented in this Section.

Comparisons between different programs and EW calculations are performed for the ratios of differential cross-sections and the differences of forward-backward asymmetries, between EW LO and NLO or NLO+HO predictions, always calculated with the same program. Those ratios or differences are then compared between different calculations. This approach to large extend minimises impact from not *tuned* QCD component of the predictions: structure functions, QCD scale, matrix element order, etc. Also, as pointed in Table 7, two out of three programs are using pole mass and fixed Γ_Z, while the third one is using on-shell mass and running Γ_Z.

The `PowhegZj`+wt^{EW} which is using form-factors from `Dizet` library, also provides predictions for the (NLO+HO - LO) corrections in other schemes. The wt^{EW}, as exlained in Appendix E is used to are reweighted at EW LO to different schemes. Then it is assumed that absolute predictions in different EW schemes should agree at NLO+HO, which indeed is the case for `Powheg_ew` estimates, see Tables 36 and 37. With this assumptions, the ratios NLO+HO/LO or differences NLO+HO - LO can be calculated with `PowhegZj`+wt^{EW}, using predictions of EW NLO+HO with $\alpha(0)$ v0 scheme and EW LO with either of three schemes.

Table 8: Cross-sections and cross-section ratios estimated at EW LO with `Powheg_ew` and `PowhegZj`+wt^{EW}, for three mass windows.
Results with `PowhegZj`+wt^{EW} *updated (running width,* `Dizet 6.45`*).*
TODO: update/complete `Powheg_ew` and `MCSANC` numbers.

	m_{ee} = 89 - 93 GeV	m_{ee} = 60 - 81 GeV	m_{ee} = 81 - 101 GeV	m_{ee} = 101 - 150 GeV
Cross-section [pb]				
`Powheg_ew`				
$\alpha(0)$ v0	630.848722		906.156051	
$\alpha(0)$ v1	571.411296		821.363274	
G_μ	612.514433		880.446121	
$\sin^2_{eff}$ v1				
$\sin^2_{eff}$ v2				
Cross-section ratios				
$\alpha(0)$ v1/ $\alpha(0)$ v0				
`Powheg_ew`	0.905782		0.906426	
`PowhegZj`+wt^{EW}	0.90570	0.95271	0.90637	0.90872
G_μ / $\alpha(0)$ v0				
`Powheg_ew`	0.970937		0.971627	
`PowhegZj`+wt^{EW}	0.97278	1.02320	0.97347	0.97596
G_μ / $\alpha(0)$ v1				
`Powheg_ew`	1.071933		1.071933	
`MCSANC`				
`PowhegZj`+wt^{EW}	1.07405	1.07399	1.07404	1.07400
$\alpha(0)$ v0 /$\sin^2_{eff}$ v2				
`Powheg_ew`				
`PowhegZj`+wt^{EW}	1.04798	0.95795	1.04659	1.04212
G_μ/ $\sin^2_{eff}$ v2				
`Powheg_ew`				
`PowhegZj`+wt^{EW}	1.01945	0.98018	1.01883	1.01707

3.4.1 Benchmarks at EW LO

Comparison of the cross-sections ratios for different EW schemes, predicted by `Powheg_ew` and `PowhegZj`+wt^{EW} are shown in Table 8. Similar comparison for forward-backward asymmetry is shown in Table 9. The ratio of line-shapes and difference for forward-backward asymmetry are shown in Fig. 4. comparison between `MCSANC` and `PowhegZj`+wt^{EW}. Similar agreement was obtained when comparing with `Powheg_ew`. They confirm very good tuning at EW LO and also that comparisons between programs with different implementation of QCD components can be done quite precisely, ones comparing ratios or differences of ratios. For `Powheg_ew` shown are also absolute predictions, while for `PowhegZj`+wt^{EW} are not[2]. Note for example that as at EW LO, schemes $\alpha(0)$ v1 and G_μ were tuned to share the same value of s_W^2, the difference $A_{FB}(G_\mu)$ - $A_{FB}(\alpha(0)$ v1) is equal to zero,

[2]The reason is that `PowhegZj` events were generated with somewhat arbitrary setting for QCD and EW parts (e.g. $sin^2\theta_W$=0.23113, fixed Γ_Z in the propagator, on-shell Z mass), so obtained results should not be quoted as the reference ones. They are however reweighted to EW $\alpha(0)$ v0 scheme before any benchmarks are evaluated.

Table 9: Cross-sections difference in forward and backward hemispheres and forward-backward asymmetry as estimated at EW LO with Powheg_ew and PowhegZj+wt^{EW}, for three mass windows. The pole definition is used for input parameters as in Table 14.
Results with PowhegZj+wt^{EW} updated (running width).
TODO: update/complete Powheg_ew and MCSANC numbers.

	m_{ee} = 89 - 93 GeV	m_{ee} = 60 - 81 GeV	m_{ee} = 81 - 101 GeV	m_{ee} = 101 - 150 GeV
A_{FB}				
Powheg_ew				
$\alpha(0)$ v0	0.06691361		0.06392369	
$\alpha(0)$ v1	0.04653886		0.04343789	
G_μ	0.04653886		0.04343789	
$\sin^2_{eff}$ v1				
$\sin^2_{eff}$ v2				
ΔA_{FB}				
$\alpha(0)$ v1 - $\alpha(0)$ v0				
Powheg_ew	0.020375		0.020486	
PowhegZj+wt^{EW}	- 0.01981	-0.01776	- 0.01999	-0.00650
G_μ - $\alpha(0)$ v0				
Powheg_ew	0.020375		0.020486	
PowhegZj+wt^{EW}	- 0.01983	-0.01776	- 0.020000	-0.00650
G_μ - $\alpha(0)$ v1				
Powheg_ew				
MCSANC				
PowhegZj+wt^{EW}	- 0.00002	-0.00000	- 0.00001	-0.00000
$\alpha(0)$ v0 - $\sin^2_{eff}$ v2				
Powheg_ew				
PowhegZj+wt^{EW}	0.03528	0.02995	0.03556	0.01163
$G_\mu - \sin^2_{eff}$ v2				
Powheg_ew				
PowhegZj+wt^{EW}	0.01545	0.01219	0.01557	0.00513

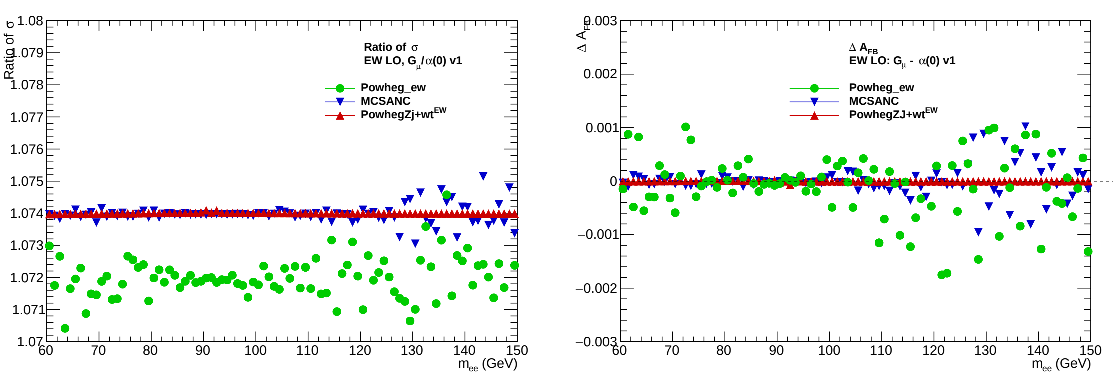

Figure 4: The EW LO predictions for radio of cross-sections and ΔA_{FB} between different EW schemes: $\alpha(0)$ v0 and G_μ. Shown results with MCSANC, Powheg_ew and PowhegZj + wt^{EW}.
Results with PowhegZj+wt^{EW} updated (running width).

3.4.2 Benchmarks at EW NLO, NLO+HO

The following tables and figures contain comparisons between ratio of cross-sections or differences of forward-backward asymmetries between different EW schemes or same EW scheme but different level of corrections.

Tables:

- Table 10: Cross-sections ratios estimated with `Powheg_ew` and `PowhegZj`+wt^{EW}, different EW schemes, comparison at EW LO and NLO+HO.
- Table 11: Forward-backward asymmetry differences as estimated by `PowhegZj`+wt^{EW} and `Powheg_ew`, different EW schemes, comparison at EW LO and NLO+HO.

Figures:

- Figure 5: The lineshape predictions with `Powheg_ew` and `MCSANC`. Comparison of ratios EW NLO/LO and NLO+HO/LO.
- Figure 6: The lineshape predictions with `Powheg_ew`, `MCSANC` and `PowhegZj`+wt^{EW}. Comparison of EW NLO+HO/LO, different EW schemes.
- Figure 7: The ΔA_{FB} predictions with `Powheg_ew` and `MCSANC`. Comparison at EW LO, NLO, NLO+HO, different EW schemes.
- Figure 8: The ΔA_{FB} predictions with `Powheg_ew` and `MCSANC` and `PowhegZj`+wt^{EW}. Comparisons of EW LO, NLO, NLO+HO, different EW schemes.

Observations:

- Tables 10 and 11 shows very good agreement between `Powheg_ew` and `PowhegZj`+wt^{EW} predictions for cross-section NLO+HO/LO and A_{FB} NLO+HO -HO corrections in $\alpha(0)$ v1 and G_μ schemes.
- Figure 5:
  Top plots: Very good agreement between `MCSANC` and `Powheg_ew` for σ_{NLO}/σ_{LO}. Both EW schemes: $\alpha(0)$ v1 and G_μ.
  Bottom plots: Apparent shift in $\sigma_{NLO+HO}/\Delta\sigma_{LO}$ for $\alpha(0)$ v1 scheme. Almost OK for G_μ scheme.
- Figure 6:
  Top plots: same observation as above about disagreement on HO corrections between `MCSANC` and `Powheg_ew` for $\alpha(0)$ v1 scheme.
  Bottom plot: `PowhegZj`+wt^{EW} and `Powheg_ew` in good agreement for NLO+HO at Z-pole, but discrepant at the level on 0.005 in relative corrections below and above Z peak.
- Figure 7:
  Top plots: Very good agreement between `MCSANC` and `Powheg_ew` for $\Delta A_{FB}(NLO-LO)$. Both EW schemes: $\alpha(0)$ v1 and G_μ.
  Bottom plots: Apparent shift in $\Delta A_{FB}(NLO+HO-LO)$ for $\alpha(0)$ v1 scheme. Almost OK for G_μ scheme.
- Figure 8:
  Top plots: same observation as above about disagreement on HO corrections between `MCSANC` and `Powheg_ew` for $\alpha(0)$ v1 scheme.
  Bottom plot: `PowhegZj`+wt^{EW} and `Powheg_ew` in good agreement for NLO+HO at Z-pole and below, but discrepant at the level up to 0.005 in absolute corrections above Z peak.

Table 10: Cross-sections ratios estimated with `MCSANC`, `Powheg_ew` and `PowhegZj`+wt^{EW} for three mass windows. (For `PowhegZj`+wt^{EW} predictions EW NLO+HO calculated with $\alpha(0)$ v0 scheme.)
Results with `PowhegZj`+wt^{EW} *updated with* `Dizet 6.45` *and running width.*
TODO: update/complete `Powheg_ew` **and** `MCSANC` **numbers.**

	EW order	m_{ee} = 89 - 93 GeV	m_{ee} = 60 - 81 GeV	m_{ee} = 81 - 101 GeV	m_{ee} = 101 - 150 GeV
`Powheg_ew`	NLO+HO/LO				
$\alpha(0)$ v1		1.06325		1.06374	
G_μ		0.99104		0.99229	
$\sin^2_{eff}$ v1					
$\sin^2_{eff}$ v2					
`MCSANC`	NLO+HO/LO				
$\alpha(0)$ v1		1.051194		1.066182	
G_μ		0.992299		0.992740	
`PowhegZj`+wt^{EW}	NLO+HO/LO				
$\alpha(0)$ v0		0.96510	1.04624	0.96631	0.96508
$\alpha(0)$ v1		1.06558	1.09892	1.06613	1.06202
G_μ		0.99211	1.02321	0.99264	0.98884
$\sin^2_{eff}$ v2		1.01141	1.00293	1.01132	1.00572

Table 11: Forward-backward asymmetry differences as estimated by `PowhegZj`+wt^{EW} and `Powheg_ew`, for three mass windows. (For `PowhegZj`+wt^{EW} predictions EW NLO+HO calculated with $\alpha(0)$ v0 scheme.)
Results with `PowhegZj`+wt^{EW} *updated with* `Dizet 6.45` *and running width. Updated results from* `Powheg_ew` *in* G_μ *scheme.*
TODO: update/complete `Powheg_ew` **and** `MCSANC` **numbers.**

ΔA_{FB}	EW order	m_{ee} = 89 - 93 GeV	m_{ee} = 60 - 81 GeV	m_{ee} = 81 - 101 GeV	m_{ee} = 101 - 150 GeV
`Powheg_ew`	NLO+HO - LO				
$\alpha(0)$ v1		-0.015706		-0.015733	
G_μ		-0.015636		-0.015660	
$\sin^2_{eff}$ v1					
$\sin^2_{eff}$ v2					
`MCSANC`	NLO+HO - LO				
$\alpha(0)$ v1		-0.001444		-0.001444	
G_μ		-0.001523		-0.001525	
`PowhegZj`+wt^{EW}	NLO+HO - LO				
$\alpha(0)$ v0		-0.03489	-0.02880	-0.03514	-0.01334
$\alpha(0)$ v1		-0.01508	-0.01104	-0.01515	-0.00684
G_μ)		-0.01507	-0.01104	-0.01514	-0.00684
$\sin^2_{eff}$ v2		0.00039	0.00115	0.00042	-0.00171

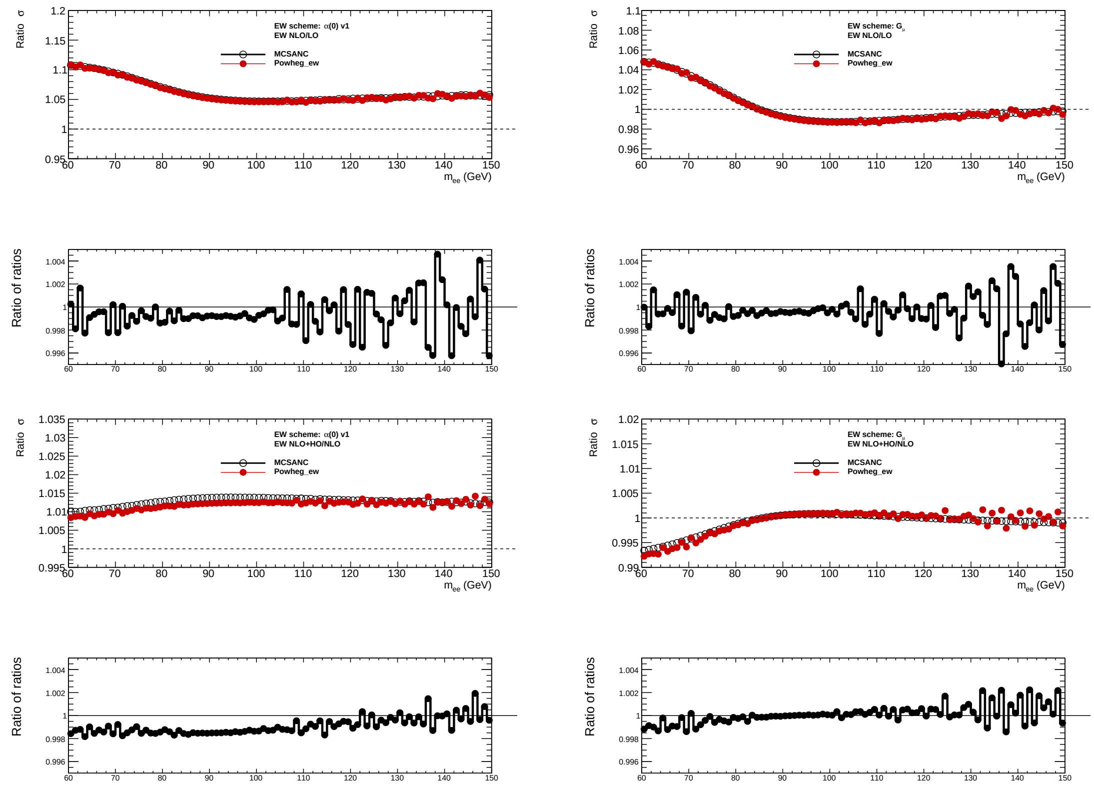

Figure 5: The lineshape predictions with `Powheg_ew` and `MCSANC`. Comparison of the EW NLO/LO and NLO+HO/NLO ratios for $\alpha(0)$ v1 and G_μ schemes.

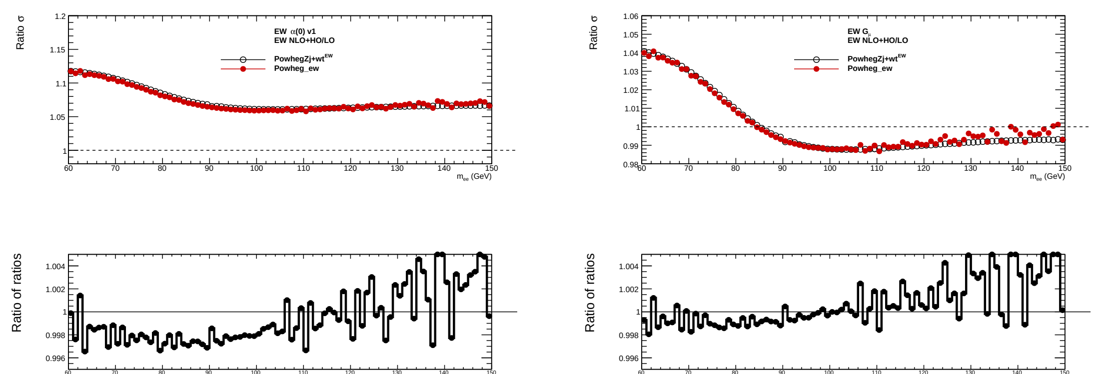

Figure 6: The lineshape predictions with `Powheg_ew` and `PowhegZj`+wt^{EW}. Comparisons of the EW NLO+HO/LO ratios for $\alpha(0)$ v1 and G_μ schemes. For `PowhegZj`+wt^{EW} EW NLO+HO predictions are calculated with $\alpha(0)$ v0 scheme.

Results with `PowhegZj`+wt^{EW} *updated with* `Dizet 6.45` *and running width.*

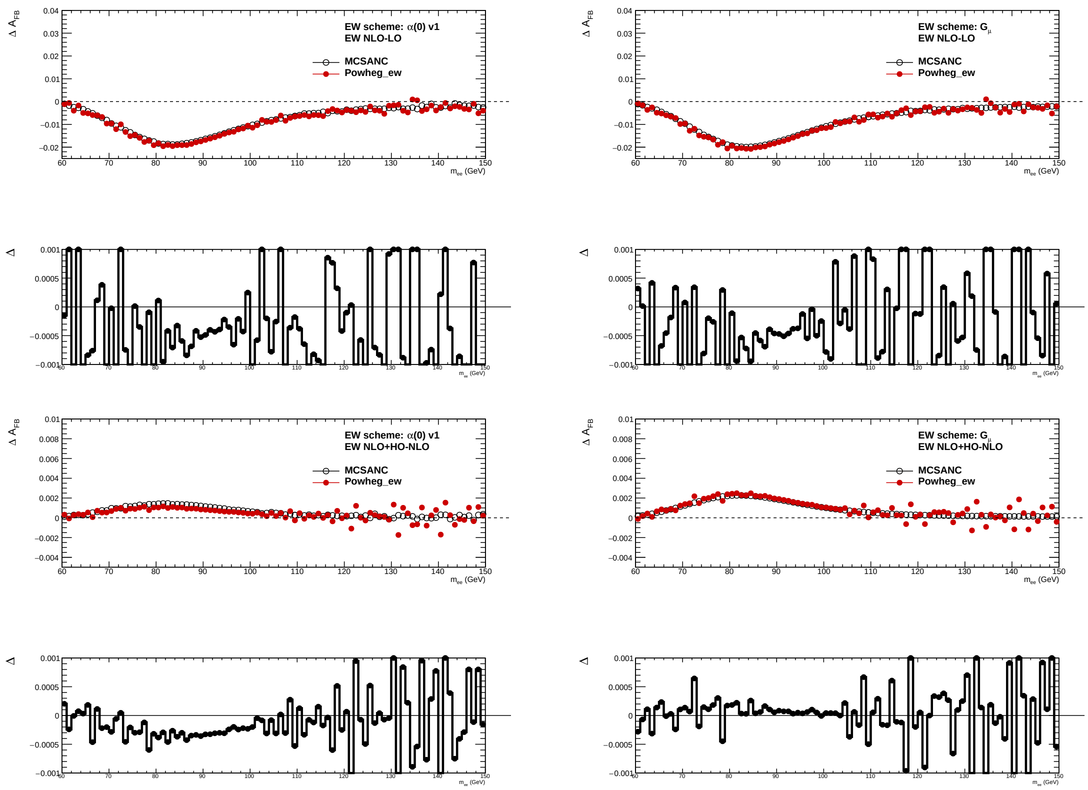

Figure 7: The ΔA_{FB} predictions with `Powheg_ew` and `MCSANC`. Comparisons of the EW LO, NLO, NLO+HO for $\alpha(0)$ v1 and G_μ schemes.
Results with `PowhegZj`+wt^{EW} *updated with* `Dizet 6.45` *and running width.*

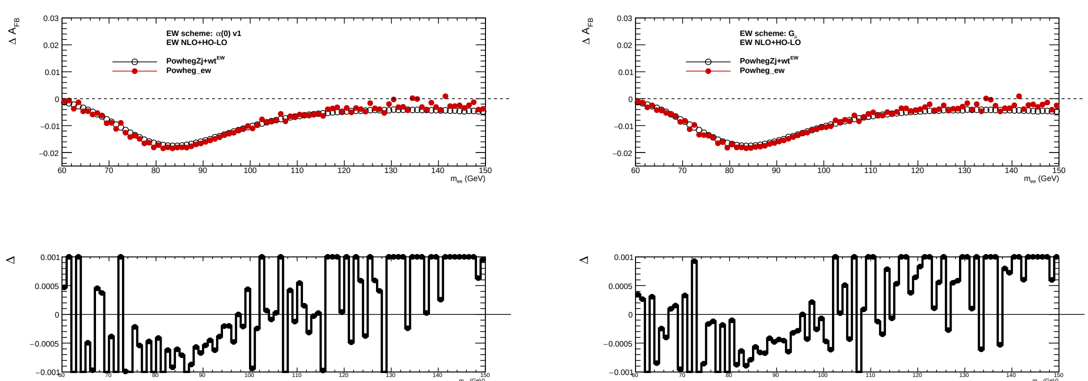

Figure 8: The ΔA_{FB} predictions with `Powheg_ew` and `PowhegZj`+wt^{EW}. Comparisons of the EW NLO+HO-LO difference for $\alpha(0)$ v1 and G_μ schemes. For `PowhegZj`+wt^{EW} EW NLO+HO predictions are calculated with $\alpha(0)$ v0 scheme.
Results with `PowhegZj`+wt^{EW} *updated with* `Dizet 6.45` *and running width.*

3.5 Theoretical uncertainties and conclusions

4 QED emissions

Authors: Alessandro (`HORACE`), Fulvio (`Powheg_ew`), Serge/Lida (`MCSANC`), Scott (`KKMC-hh`), Doreen?(`ZGRAD2`)

Content:

- *Separation of contributions from ISR and IFI.*
- *Photon-induced processes and use of LUXQED PDFs*
- *Short description of calculations and tools used and of their configuration*
- *Numerical results and comparisons*
- *Theoretical uncertainties and conclusions*

4.1 Introduction

4.2 Overview of calculations and tools

4.3 Numerical results for QED ISR and IFI

4.4 Photon-induced processes

4.5 Theoretical uncertainties and conclusions

5 A possible strategy for run-2 measurements and combinations at the LHC

Authors: ATLAS/CMS/LHCb/theorists

Content:

- *Differential observables and expected measurement uncertainties*
- *Intepretation tools*
- *Combination tools*
- *Expected uncertainties and conclusions*

5.1 Introduction

5.2 Observables used for comparisons of expectations between experiments : A_4 and A_{FB}

5.2.1 Pseudo-data representing full run-2 dataset for ATLAS, CMS and LHCb

5.2.2 Compatibility tests between experimental pseudo-data

5.2.3 Combination of experimental pseudo-data

5.3 Interpretation tools

5.3.1 QCD tools: `DYTurbo, NNLOJET`

5.3.2 QED/EW tools: `Dizet, Powheg EW, MC-SANC, ZGRAD2`

5.4 Combined interpretation of experimental measurements

5.4.1 Profile likelihood fit to combination of experimental pseudo-data

5.4.2 Direct extraction of weak mixing angle based on fit of all experimental measurements

5.5 Expected breakdown of uncertainties and conclusions

5.5.1 Measurement uncertainties

5.5.2 PDF uncertainties

5.5.3 QED/EW uncertainties

5.5.4 QCD uncertainties

5.5.5 Parametric uncertainties

5.6 Impact on electroweak fit

5.7 Conclusions

Acknowledgments

References

[1] SLD Electroweak Group, DELPHI, ALEPH, SLD, SLD Heavy Flavour Group, OPAL, LEP Electroweak Working Group, L3 Collaboration, S. Schael *et al.*, *Phys. Rept.* **427** (2006) 257–454, hep-ex/0509008.

[2] D. Yu. Bardin, P. Christova, M. Jack, L. Kalinovskaya, A. Olchevski, S. Riemann, and T. Riemann, *Comput. Phys. Commun.* **133** (2001) 229–395, hep-ph/9908433.

[3] A. B. Arbuzov, M. Awramik, M. Czakon, A. Freitas, M. W. Grunewald, K. Monig, S. Riemann, and T. Riemann, *Comput. Phys. Commun.* **174** (2006) 728–758, hep-ph/0507146.

[4] S. Jadach, B. F. L. Ward, and Z. Was, *Phys. Rev.* **D88** (2013), no. 11 114022, 1307.4037.

[5] G. Altarelli, R. Kleiss, and C. Verzegnassi, eds., *Z physics at LEP-1. Proceedings, Workshop, Geneva, Switzerland, September 4-5, 1989. vol. 1: Standard Physics*, 1989.

[6] F. A. Berends, R. Kleiss, and S. Jadach, *Comput. Phys. Commun.* **29** (1983) 185–200.

[7] E. Richter-Was and Z. Was, *Eur. Phys. J.* **C76** (2016), no. 8 473, 1605.05450.

[8] E. Richter-Was and Z. Was, 1609.02536.

[9] J. H. Kuhn, A. Kulesza, S. Pozzorini, and M. Schulze, *Nucl. Phys.* **B727** (2005) 368–394, hep-ph/0507178.

[10] S. Jadach, B. Ward, and Z. Was, *Comput.Phys.Commun.* **130** (2000) 260–325, hep-ph/9912214.

[11] Z. Czyczula, T. Przedzinski, and Z. Was, *Eur.Phys.J.* **C72** (2012) 1988, 1201.0117.

[12] D. Yu. Bardin, M. S. Bilenky, T. Riemann, M. Sachwitz, and H. Vogt, *Comput. Phys. Commun.* **59** (1990) 303–312.

[13] A. Andonov, A. Arbuzov, D. Bardin, S. Bondarenko, P. Christova, L. Kalinovskaya, V. Kolesnikov, and R. Sadykov, *Comput. Phys. Commun.* **181** (2010) 305–312, 0812.4207.

[14] A. Akhundov, A. Arbuzov, S. Riemann, and T. Riemann, *Phys. Part. Nucl.* **45** (2014), no. 3 529–549, 1302.1395.

[15] Dizet and new version.

[16] Particle Data Group Collaboration, M. Tanabashi *et al.*, *Phys. Rev.* **D98** (2018), no. 3 030001.

[17] A. Freitas *et al.*, 1906.05379.

[18] S. G. Bondarenko and A. A. Sapronov, *Comput. Phys. Commun.* **184** (2013) 2343–2350, 1301.3687.

[19] A. Arbuzov, D. Bardin, S. Bondarenko, P. Christova, L. Kalinovskaya, U. Klein, V. Kolesnikov, L. Rumyantsev, R. Sadykov, and A. Sapronov, *JETP Lett.* **103** (2016), no. 2 131–136, 1509.03052.

[20] H. Burkhardt and B. Pietrzyk, *Phys. Lett.* **B513** (2001) 46–52.

[21] E. Richter-Was and Z. Was, *Eur. Phys. J.* **C79** (2019), no. 6 480, 1808.08616.

[22] S. Alioli *et al.*, *Eur. Phys. J.* **C77** (2017), no. 5 280, 1606.02330.

[23] W. J. Marciano and A. Sirlin, *Phys. Rev.* **D22** (1980) 2695, [Erratum: Phys. Rev.D31,213(1985)].

[24] D. R. Yennie, S. C. Frautschi, and H. Suura, *Annals Phys.* **13** (1961) 379–452.

[25] M. Chiesa, F. Piccinini, and A. Vicini, 1906.11569.

[26] D. Yu. Bardin, P. K. Khristova, and O. M. Fedorenko, *Nucl. Phys.* **B175** (1980) 435–461.

[27] D. Yu. Bardin, P. K. Khristova, and O. M. Fedorenko, *Nucl. Phys.* **B197** (1982) 1–44.

[28] A. Sirlin, *Phys. Rev.* **D22** (1980) 971–981.

[29] F. Jegerlehner, `1711.06089`.

[30] A. Blondel, J. Gluza, S. Jadach, P. Janot, and T. Riemann, eds., *Theory report on the 11th FCC-ee workshop*, 2019.

[31] T. Przedzinski, E. Richter-Was, and Z. Was, *Eur. Phys. J.* **C79** (2019), no. 2 91, `1802.05459`.

[32] T. Przedzinski, E. Richter-Was, and Z. Was, *Eur. Phys. J.* **C74** (2014), no. 11 3177, `1406.1647`.

[33] N. Davidson, G. Nanava, T. Przedzinski, E. Richter-Was, and Z. Was, *Comput.Phys.Commun.* **183** (2012) 821–843, `1002.0543`.

[34] Z. Was and S. Jadach, *Phys. Rev.* **D41** (1990) 1425.

[35] J. C. Collins and D. E. Soper, *Phys. Rev.* **D16** (1977) 2219.

[36] Particle Data Group Collaboration, C. Patrignani *et al.*, *Chin. Phys.* **C40** (2016), no. 10 100001.

[37] L. Barze, G. Montagna, P. Nason, O. Nicrosini, F. Piccinini, and A. Vicini, *Eur. Phys. J.* **C73** (2013), no. 6 2474, `1302.4606`.

[38] S. Jadach, B. F. L. Ward, Z. A. Was, and S. A. Yost, *Phys. Rev.* **D94** (2016), no. 7 074006, `1608.01260`.

[39] S. Jadach, B. F. L. Ward, and Z. Was, *Phys. Rev.* **D63** (2001) 113009, `hep-ph/0006359`.

[40] S. Jadach and S. Yost, *Phys. Rev.* **D100** (2019), no. 1 013002, `1801.08611`.

[41] E. Boos *et al.*, "Generic User Process Interface for Event Generators", in *Physics at TeV colliders. Proceedings, Euro Summer School, Les Houches, France, May 21-June 1, 2001*, 2001, `hep-ph/0109068`.

[42] G. Corcella, I. G. Knowles, G. Marchesini, S. Moretti, K. Odagiri, P. Richardson, M. H. Seymour, and B. R. Webber, *JHEP* **01** (2001) 010, `hep-ph/0011363`.

[43] A. Denner, S. Dittmaier, T. Kasprzik, and A. MÃ$\frac{1}{4}$ck, *Eur. Phys. J.* **C73** (2013), no. 2 2297, `1211.5078`.

[44] S. Dittmaier, A. Huss, and C. Schwinn, *Nucl. Phys.* **B904** (2016) 216–252, `1511.08016`.

[45] S. Dittmaier, A. Huss, and C. Schwinn, *Nucl. Phys.* **B885** (2014) 318–372, `1403.3216`.

[46] C. M. Carloni Calame, G. Montagna, O. Nicrosini, and M. Treccani, *Phys. Rev.* **D69** (2004) 037301, `hep-ph/0303102`.

[47] C. M. Carloni Calame, G. Montagna, O. Nicrosini, and A. Vicini, *JHEP* **12** (2006) 016, `hep-ph/0609170`.

[48] U. Baur, O. Brein, W. Hollik, C. Schappacher, and D. Wackeroth, *Phys. Rev.* **D65** (2002) 033007, `hep-ph/0108274`.

[49] A. D. Martin, W. J. Stirling, R. S. Thorne, and G. Watt, *Eur. Phys. J.* **C63** (2009) 189–285, `0901.0002`.

[50] S. Jadach, B. F. L. Ward, Z. A. Was, and S. A. Yost, *Phys. Rev.* **D99** (2019), no. 7 076016, `1707.06502`.

[51] NNPDF Collaboration, R. D. Ball *et al.*, *Eur. Phys. J.* **C77** (2017), no. 10 663, `1706.00428`.

[52] NNPDF Collaboration, V. Bertone, S. Carrazza, N. P. Hartland, and J. Rojo, *SciPost Phys.* **5** (2018), no. 1 008, `1712.07053`.

[53] A. Manohar, P. Nason, G. P. Salam, and G. Zanderighi, *Phys. Rev. Lett.* **117** (2016), no. 24 242002, `1607.04266`.

[54] S. Jadach, Z. Wąs, R. Decker, and J. H. Kü, *Comput. Phys. Commun.* **76** (1993) 361.

[55] Belle-II Collaboration, T. Abe *et al.*, `1011.0352`.

[56] S. Jadach, W. Placzek, S. Sapeta, A. Siodmok, and M. Skrzypek, *JHEP* **10** (2015) 052, `1503.06849`.

[57] S. Jadach, A. Kusina, W. Placzek, M. Skrzypek, and M. Slawinska, *Phys. Rev.* **D87** (2013), no. 3 034029, `1103.5015`.

A EW schemes

There are several ingredients that goes into definition of *EW schemes*

- Choice of the input parameters
- Renormalisation scheme
- Treatment of other corrections: treatment of self-energy corrections in the propagator (running or fixed width), *on-mass-shell* or *pole* mass in the propagator.
- Something more?

Formally, at the lowest EW order, only three parameters can be set, others are calculated using Standard Model constraints, following structure of $SU(2) \times U(1)$ group. One of such constraint is given in formula (38). The most common choices at hadron colliders, following report [22], are G_μ *scheme* (G_μ, M_Z, M_W) and $\alpha(0)$ *scheme* $(\alpha(0), M_Z, M_W)$. There exists by now family of different modifications of G_μ *scheme*, see discussion in [22], and they are considered as preferred schemes for hadron collider physics.

The Monte Carlo generators usually allow user to define set of input parameters (α, M_Z, M_W), (α, M_Z, G_μ) or (α, M_Z, s_W^2). However within this flexibility, formally multiplicative factor in the Z-boson propagator $\chi_Z(s)$, see formula (20), is always kept to be equal to 1. The

$$\frac{G_\mu \cdot M_z^2 \cdot 16 \cdot c_W^2 \cdot s_W^2}{\sqrt{2} \cdot 8\pi \cdot \alpha} = 1; \tag{8}$$

where $s_W^2 = 1 - m_W^2/m_Z^2$ and $c_W^2 = 1 - s_W^2$. This term is quite often absent in the programs code. Whichever the choice of parameters set is used as primary ones, the others are adjusted to match the constraint (8), regardless if they fall outside their measurement uncertainties or not.

Let us recall, that the calculations of EW corrections available in `Dizet` library work with somewhat different convention of the $\alpha(0)$ *scheme*, defined by the set of input parameters $(\alpha(0), G_\mu, M_Z)$, then M_W is calculated iterating formula (35), which formally brings it beyond EW LO scheme. The value of s_W^2 is calculated from (39) and the EW LO relation (38) does not hold anymore.

For the comparisons performed here we consider following schemes:

A.1 EW scheme: $\alpha(0), G_\mu, M_Z$

This choice will be denoted as $\alpha(0)$ v0 scheme.

Here are formulas to recalculate remaining EW parameters:

$$\begin{aligned} d2 &= \frac{\sqrt{2} \cdot 8\pi \cdot \alpha}{G_\mu \cdot M_z^2} && (9) \\ s_W^2 &= (-1 + \sqrt{1 - d2/4})/2 && (10) \\ m_W^2 &= (1 - s_W^2) \cdot M_Z^2 && (11) \end{aligned}$$

A.2 EW scheme: $\alpha(0), M_W, M_Z$

This choice will be denoted as $\alpha(0)$ v1 scheme.

Here are formulas to recalculate remaining EW parameters:

$$\begin{aligned} s_W^2 &= 1 - M_W^2/M_Z^2 \\ g2 &= 4 \cdot \pi \cdot \alpha / s_W^2 \\ G_\mu &= \sqrt{2} \cdot g2/8/M_W^2 \end{aligned} \tag{12}$$

A.3 EW scheme: G_μ, M_Z, M_W

This choice will be denoted as G_μ scheme.

A convenient set of parameters that describes EW processes at hadron colliders is (G_μ, M_W, M_Z), the so called G_μ scheme. The Fermi constant G_μ measured in muon decay naturally parametrize the CC interaction, while the W and Z masses fix the scale of EW phenomena and the mixing with hyper-charge field. A drawback of this choice is the fact that the coupling of real photons to charge particles is computed from the inputs and in lowest order is equal to

$$\alpha = G_\mu \sqrt{2} M_W^2 (1 - M_W^2/M_Z^2)/\pi \sim 1/132 \tag{13}$$

much larger that the fine structure constant $\alpha(0) = 1/137$, which is a natural value for an on-shell photons.

This drawback can be circumvented by a use of modified G_μ scheme when only LO couplings are re-expressed in terms of α

$$\alpha_{QED} = \alpha(0) \to \alpha(1 - \Delta r) \tag{14}$$

and the Sirlin's parameter Δr [23], representing the complete NLO EW radiative corrections of $O(\alpha)$ to the muon decay amplitude. Both real and virtual relative corrections are calculated at the scale $O(\alpha)$, therefore such an approach may be referred as NLO at $O(\alpha G_\mu^2)$. In this scheme leading universal corrections due to the running of α and connected to the ρ parameter are absorbed in the LO couplings.

Further modifications maybe considered. For the NC DY the gauge invariant separation of complete EW radiative corrections into pure weak and QED corrections (involving virtual and real photons) is possible. Therefore, these two contributions may be considered at different scales, pure weak at $O(G_\mu^3)$, and QED still at $O(\alpha G_\mu^2)$. More refined modifications may be considered, for instance based on defining gauge invariant subsets by using the Yennie-Frautschi-Suura approach [24].

Here are formulas to calculate remaining EW parameters:

$$\begin{aligned} s_W^2 &= 1 - M_W^2/M_Z^2 \\ g2 &= 8 \cdot G_\mu \cdot M_W^2/\sqrt{2} \\ \alpha &= g2 \cdot s_W^2/4/\pi \end{aligned} \tag{15}$$

A.4 EW scheme: $\alpha(0), s_W^2, M_Z$

This choice will be denoted as sin^2_{eff} v1 scheme.

Text to be written, based on recent publication [25]

A.5 EW scheme: G_μ, s_W^2, M_Z

This choice will be denoted as sin^2_{eff} v2 scheme.

Text to be written, based on recent publication [25]

A.6 Benchmark initialisation

Benchmark initialisation of the different EW schemes are chosen such that they share value of one or more input parameters which facilitate comparison of the cross-sections or asymmetries at the EW LO. The $\alpha(0)$ v0 and v1 share same value of α, the $\alpha(0)$ v1 and G_μ schemes same value of M_W (and therefore s_W^2). In all three cases the M_Z and Γ_Z are the same. Common is also choice for the fermion masses, quarks and leptons and for the Higgs boson mass, as shown in Table 12.

Table 12: Values of fermions and Higgs boson massed used for calculating EW corrections.

Parameter	Mass (GeV)	Description
m_e	5.1099907e-4	mass of electron
m_μ	0.1056583	mass of muon
m_τ	1.7770500	mass of tau
m_u	0.0698400	mass of up-quark
m_d	0.0698400	mass of down-quark
m_c	1.5000000	mass of charm-quark
m_s	0.1500000	mass of strange-quark
m_b	4.7000000	mass of bottom-quark
m_t	173.0	mass of top quark
m_H	125.0	mass of Higgs boson

Table 13: The EW parameters used at tree-level EW, with on-mass-shell definition (LEP convention).

Parameter	$(\alpha(0), G_\mu, M_Z)$ $\alpha(0)$ v0	$(\alpha(0), M_W, M_Z)$ $\alpha(0)$ v1	(G_μ, M_Z, M_W) G_μ	$(\alpha(0), s_W^2, M_Z)$ $\sin^2_{eff}$ v1	(G_μ, s_W^2, M_Z) sin^2_{eff} v2
M_Z (GeV)	91.1876	91.1876	91.1876	91.1876	91.1876
Γ_Z (GeV)	2.4952	2.4952	2.4952	2.4952	2.4952
Γ_W (GeV)	2.085	2.085	2.085	2.085	2.085
$1/\alpha$	137.035999139	137.035999139	132.23323	137.035999139	128.744939484
α	0.007297353	0.007297353	0.007562396	0.007297353	0.007767296
G_μ (GeV^{-2})	$1.1663787 \cdot 10^{-5}$	$1.1254734 \cdot 10^{-5}$	$1.1663787 \cdot 10^{-5}$	$1.09580954 \cdot 10^{-5}$	$1.1663787 \cdot 10^{-5}$
M_W (GeV)	80.93886	80.385	80.385	79.93886984	79.93886984
s_W^2	0.2121517	0.2228972	0.2228972	0.231499	0.231499
$\frac{G_\mu \cdot M_z^2 \cdot 16 c_W^2 s_W^2}{\sqrt{2} \cdot 8\pi \cdot \alpha} = 1.0$ $s_W^2 = 1 - m_W^2/m_Z^2$	$\to s_W^2, M_W$	$\to G_\mu, s_W^2$	$\to \alpha, s_W^2$	$\to G_\mu, m_W$	$\to \alpha, m_W$
$\alpha_s(M_Z)$	0.120178900000	0.120178900000	0.120178900000	0.120178900000	0.120178900000

Table 14: The EW parameters used at tree-level EW, with pole definition of the Z, W masses.

Parameter	$(\alpha(0), G_\mu, M_Z)$ $\alpha(0)$ v0	$(\alpha(0), M_W, M_Z)$ $\alpha(0)$ v1	(G_μ, M_Z, M_W) G_μ	$(\alpha(0), s_W^2, M_Z)$ $\sin^2_{eff}$ v1	(G_μ, s_W^2, M_Z) sin^2_{eff} v2
M_Z (GeV)	91.15348	91.15348	91.15348	91.15348	91.15348
Γ_Z (GeV)	2.494266	2.494266	2.494266	2.494266	2.494266
Γ_W (GeV)	2.085	2.085	2.085	2.085	2.085
$1/\alpha$	137.035999139	137.035999139	132.3572336357709	137.035999139	128.84133952
α	0.007297353	0.007297353	0.007555311	0.007297353	0.007761484
G_μ (GeV^{-2})	$1.1663787 \cdot 10^{-5}$	$1.126555497 \cdot 10^{-5}$	$1.1663787 \cdot 10^{-5}$	$1.09663005 \cdot 10^{-5}$	$1.1663787 \cdot 10^{-5}$
M_W (GeV)	80.91191	80.35797	80.35797	79.90895881	79.90895881
s_W^2	0.21208680	0.22283820939	0.22283820939	0.231499	0.231499
$\frac{G_\mu \cdot M_z^2 \cdot 16 c_W^2 s_W^2}{\sqrt{2} \cdot 8\pi \cdot \alpha} = 1.0$ $s_W^2 = 1 - m_W^2/m_Z^2$	$\to s_W^2, M_W$	$\to G_\mu, s_W^2$	$\to \alpha, s_W^2$	$\to G_\mu, m_W$	$\to \alpha, m_W$
$\alpha_s(M_Z)$	0.120178900000	0.120178900000	0.120178900000	0.120178900000	0.120178900000

B Improved Born Approximation

Comment: Content of this section is taken from [21].

At LEP times, to match higher order QED effects with the loop corrections of electroweak sector, concept of electroweak form factors was introduced [5]. This arrangement was very beneficial and enabled common treatment of one loop electroweak effects with not only higher order QED corrections including bremsstrahlung, but also to incorporate higher order loops into Z and photon propagators, see eg. documentation of `KKMC` Monte Carlo [4] or `Dizet` [2]. Such description has its limitations for the LHC applications, but for the processes of the Drell-Yan type with a moderate virtuality of produced lepton pairs is expected to be useful, even in case when high p_T jets are present. For the LEP applications [1], the EW form factors were used together with multiphoton bremsstrahlung amplitudes. For the purpose of this Section we discuss use for parton level Born processes only, no QED ISR/FSR.

The approximation which is discussed here is called *Improved Born Approximation* (IBA) [2]. It absorbs some or all of higher order EW corrections by redefinition of couplings and propagators in the Born spin amplitude, and allows to calculate doubly deconvoluted observables, like various cross-sections and asymmetries.

The initial/final QCD and QED corrections, form separately gauge invariant subsets of diagrams [2]. The QED subset consists of QED-vertices, $\gamma\gamma$ and γZ boxes, bremsstrahlung diagrams. Fermionic self-energies have to be also taken into account. Corresponding subset can be constructed also for the initial/final QCD corrections. All the remaining corrections contribute to the IBA: purely EW loop and boxes and *internal* QCD corrections (lineshape corrections). They can be split into two more gauge-invariant subsets, giving rise to two *improved (or dressed)* amplitudes: (i) improved γ exchange amplitude with running QED coupling where only fermion loops contribute and (ii) improved Z-boson exchange amplitude with four, in general complex, *EW form factors*: $\rho_{\ell f}$, $\mathscr{K}_\ell$, $\mathscr{K}_f$, $\mathscr{K}_{\ell f}$. Components of those corrections are as following:

- Corrections to photon propagator, where only fermion loops contribute, so called vacuum-polarisation corrections.
- Corrections to Z-boson propagator and couplings, called EW form-factors.
- Contribution from the purely weak boxes, the WW and ZZ diagrams. They are negligible at the Z-peak (suppressed by the factor $(s-M_Z^2)/s$), but very important at higher energies. They enter as corrections to form-factors and introduce dependence on $\cos\theta$ of scattering angle.
- Mixed $O(\alpha\alpha_s)$ corrections which originate from gluon insertions to the fermionic components of bosonic self-energies. They also enter as corrections to all form-factors.

Below, to define notation we present formula of the Born spin amplitude $\mathscr{A}^{Born}$. We recall here conventions from [2]. Let us start with defining the lowest order coupling constants (without EW corrections) of the Z boson to fermions: $s_W^2 = 1 - m_W^2/m_Z^2$ defines weak angle $\sin\theta_W^2$ in the on-shell scheme and $T_3^{\ell,f}$ third component of the isospin. The vector v_ℓ, v_f and axial a_ℓ, a_f couplings for leptons and quarks are defined with the formulae below[3]

$$\begin{aligned} v_\ell &= (2\cdot T_3^\ell - 4\cdot q_\ell \cdot s_W^2)/\Delta, \\ v_f &= (2\cdot T_3^f - 4\cdot q_f \cdot s_W^2)/\Delta, \\ a_\ell &= (2\cdot T_3^\ell)/\Delta, \\ a_f &= (2\cdot T_3^f)/\Delta. \end{aligned} \tag{16}$$

where

$$\Delta = \sqrt{16\cdot s_W^2 \cdot (1-s_W^2)}. \tag{17}$$

With this notation, spin amplitude for the $q\bar{q} \to Z/\gamma^* \to \ell^+\ell^-$, denoted as $\mathscr{A}^{Born}$, can be written as:

$$\begin{aligned} \mathscr{A}^{Born} = \frac{\alpha}{s}\{ \quad & [\bar{u}\gamma^\mu v g_{\mu\nu} \bar{v}\gamma^\nu u]\cdot(q_\ell\cdot q_f)\cdot\chi_\gamma(s) + [\bar{u}\gamma^\mu v g_{\mu\nu}\bar{v}\gamma^\nu u\cdot(v_\ell\cdot v_f) \\ & +\bar{u}\gamma^\mu v g_{\mu\nu}\bar{v}\gamma^\nu\gamma^5 u\cdot(v_\ell\cdot a_f) + \bar{u}\gamma^\mu\gamma^5 v g_{\mu\nu}\bar{v}\gamma^\nu u\cdot(a_\ell\cdot v_f) + \bar{u}\gamma^\mu\gamma^5 v g_{\mu\nu}\bar{v}\gamma^\nu\gamma^5 u\cdot(a_\ell\cdot a_f)]\cdot\chi_Z(s) \quad \}, \end{aligned} \tag{18}$$

[3] We will use "ℓ" for lepton, and "f" for quarks.

where u,v denote fermion spinors, Z-boson and photon propagators are defined respectively as:

$$\chi_\gamma(s) = 1, \tag{19}$$

$$\chi_Z(s) = \frac{G_\mu \cdot M_z^2 \cdot \Delta^2}{\sqrt{2}\cdot 8\pi \cdot \alpha} \cdot \frac{s}{s - M_Z^2 + i \cdot \Gamma_Z \cdot s/M_Z}. \tag{20}$$

Then, we redefine vector and axial couplings introducing EW form-factor corrections $\rho_{\ell f}, \mathscr{K}_\ell(s,t), \mathscr{K}_f(s,t), \mathscr{K}_{\ell f}$ as the following:

$$\begin{aligned} v_\ell &= (2 \cdot T_3^\ell - 4 \cdot q_\ell \cdot s_W^2 \cdot \mathscr{K}_\ell(s,t))/\Delta, \\ v_f &= (2 \cdot T_3^f - 4 \cdot q_f \cdot s_W^2 \cdot \mathscr{K}_f(s,t))/\Delta, \\ a_\ell &= (2 \cdot T_3^\ell)/\Delta, \\ a_f &= (2 \cdot T_3^f)/\Delta. \end{aligned} \tag{21}$$

Normalisation correction Z_{V_Π} to Z-boson propagator is defined as

$$Z_{V_\Pi} = \rho_{\ell f}(s,t)\ . \tag{22}$$

Vacuum polarisation corrections Γ_{V_Π} to γ propagator are expressed as

$$\Gamma_{V_\Pi} = \frac{1}{2 - (1 + \Pi_{\gamma\gamma}(s))}, \tag{23}$$

where $\Pi_{\gamma\gamma}(s)$ denotes vacuum polarisation corrections to photon propagator. Both Γ_{V_Π} and Z_{V_Π} are multiplicative correction factors. The $\rho_{\ell f}(s,t)$ can be also absorbed as multiplicative factor into definition of vector and axial couplings.

The EW form-factors $\rho_{\ell f}, \mathscr{K}_\ell(s,t), \mathscr{K}_f(s,t), \mathscr{K}_{\ell f}$ are functions of two Mandelstam invariants (s,t) due to the WW and ZZ box contributions. The Mandelstam variables are defined such that they satisfy the identity

$$s + t + u = 0 \quad where \quad t = -\frac{s}{2}(1 - \cos\theta) \tag{24}$$

and $\cos\theta$ is the cosinus of the scattering angle, i.e. angle between incoming and outgoing fermion directions.

Note, that in this approach the mixed EW and QCD loop corrections, originating from gluon insertions to fermionic components of bosonic self-energies, are included in $\Gamma_{V_\Pi}, Z_{V_\Pi}$ factors.

One has to take also into account the angle dependent double-vector coupling corrections which break factorisation of the couplings shown in (18), into ones associated with either Z boson production or decay. This requires introducing mixed term:

$$\begin{aligned} vv_{\ell f} = \quad & \frac{1}{v_\ell \cdot v_f}[(2 \cdot T_3^\ell)(2 \cdot T_3^f) - 4 \cdot q_\ell \cdot s_W^2 \cdot \mathscr{K}_f(s,t)(2 \cdot T_3^\ell) - 4 \cdot q_f \cdot s_W^2 \cdot \mathscr{K}_\ell(s,t)(2 \cdot T_3^f) \\ & + (4 \cdot q_\ell \cdot s_W^2)(4 \cdot q_f \cdot s_W^2)\mathscr{K}_{\ell f}(s,t)]\frac{1}{\Delta^2}. \end{aligned} \tag{25}$$

Finally, we can write the spin amplitude for Born with EW corrections, $\mathscr{A}^{Born+EW}$, as:

$$\begin{aligned} \mathscr{A}^{Born+EW} = \; & \frac{\alpha}{s}\{[\bar{u}\gamma^\mu v g_{\mu\nu} \bar{v}\gamma^\nu u] \cdot (q_\ell \cdot q_f)] \cdot \Gamma_{V_\Pi} \cdot \chi_\gamma(s) + [\bar{u}\gamma^\mu v g_{\mu\nu} \bar{v}\gamma^\nu u \cdot (v_\ell \cdot v_f \cdot vv_{\ell f}) \\ & + \bar{u}\gamma^\mu v g_{\mu\nu} \bar{v}\gamma^\nu\gamma^5 u \cdot (v_\ell \cdot a_f) + \bar{u}\gamma^\mu\gamma^5 v g_{\mu\nu} \bar{v}\gamma^\nu u \cdot (a_\ell \cdot v_f) + \bar{u}\gamma^\mu\gamma^5 v g_{\mu\nu} \bar{v}\gamma^\nu\gamma^5 u \cdot (a_\ell \cdot a_f)] \cdot Z_{V_\Pi} \cdot \chi_Z(s)\}. \end{aligned} \tag{26}$$

The EW form factor corrections: $\rho_{\ell f}, \mathscr{K}_\ell, \mathscr{K}_f, \mathscr{K}_{\ell f}$ can be calculated using `Dizet` library. This library is also used to calculate vacuum polarisation corrections to photon propagator $\Pi_{\gamma\gamma}$. For the case of pp collisions we do not introduce QCD corrections to vector and axial coupling in initial fermion vertex, as they will be included later as a part of the QCD NLO calculations of the initial state convolution with proton structure functions.

The *Improved Born Approximation* uses spin amplitude $\mathscr{A}^{Born+EW}$ of Eq. (26) and $2 \to 2$ body kinematics to define differential cross-section with EW corrections for $q\bar{q} \to Z/\gamma^* \to ll$ process. Presented above formulae very closely follow the approach taken for implementation[4] of EW corrections to `KKMC` Monte Carlo [4].

[4]Compatibility with this program is also part of the motivation, why we leave updates for the `Dizet` library to the forthcoming work. `Dizet 6.21` is also well documented.

For completeness let us note that above discussion was presented for scattering process, however one may be interested in the decay process only. For this, *effective couplings* of Z-decay are often introduced; there are complex-valued constants as well.

The ratio of effective vector and axial couplings defines g_Z^f (here we use "f" for quark or lepton)

$$g_Z^f = \frac{v_Z^f}{a_Z^f} = 1 - 4|q_f|(K_Z^f s_W^2 + I_f^2) \tag{27}$$

with

$$I_f^2 = \alpha^2(s)\frac{35}{18}[1 - \frac{8}{3}Re(K_Z^f)s_W^2]. \tag{28}$$

and the flavour dependent *effective weak mixing angles* as

$$\sin^2\theta_{eff}^f = Re(\mathscr{K}_Z^f)s_W^2 + I_f^2 \tag{29}$$

C The s dependent Z-boson width

Updated since v03

In formula (20) for the definition of Z propagator running width is used:

$$\chi_Z(s) = \frac{1}{s - M_Z^2 + i \cdot \Gamma_Z \cdot s/M_Z} \tag{30}$$

is often in use.

The form-factors are calculated for the nominal value of M_Z. The so-called s-dependent width is equivalent to further (still partial) resummation of loop corrections, the boson self-energy which is s dependent. This formula was used in many analyses of LEP era.

In many Monte Carlos of LHC era, the definition of Z propagator constant width is used:

$$\chi_Z^{'}(s) = \frac{1}{s - M_Z^2 + i \cdot \Gamma_Z \cdot M_Z}. \tag{31}$$

One can ask the simple question, how analytic forms of (30) and (31) translate to each other. Let us start from (30)

$$\begin{aligned}
\chi_Z(s) &= \frac{1}{s(1 + i \cdot \Gamma_Z/M_Z) - M_Z^2} \\
&= \frac{(1 - i \cdot \Gamma_Z/M_Z)}{s(1 + \Gamma_Z^2/M_Z^2) - M_Z^2(1 - i \cdot \Gamma_Z/M_Z)} \\
&= \frac{(1 - i \cdot \Gamma_Z/M_Z)}{(1 + \Gamma_Z^2/M_Z^2)} \frac{1}{s - \frac{M_Z^2}{1+\Gamma_Z^2/M_Z^2} + i \cdot \frac{\Gamma_Z M_Z}{1+\Gamma_Z^2/M_Z^2}} \\
&= N_Z^{'} \frac{1}{s - {M_Z^{'}}^2 + i\Gamma_Z^{'} M_Z^{'}} \\
M_Z^{'} &= \frac{M_Z}{\sqrt{1 + \Gamma_Z^2/M_Z^2}} \\
\Gamma_Z^{'} &= \frac{\Gamma_Z}{\sqrt{1 + \Gamma_Z^2/M_Z^2}} \\
N_Z^{'} &= \frac{(1 - i \cdot \Gamma_Z/M_Z)}{(1 + \Gamma_Z^2/M_Z^2)} = \frac{(1 - i \cdot \Gamma_Z^{'}/M_Z^{'})}{(1 + {\Gamma_Z^{'}}^2/{M_Z^{'}}^2)}
\end{aligned} \tag{32}$$

The s-dependent width in Z propagator translates into shift in Z propagator mass and width and introduction of the overall complex factor with respect to constant width definition. This last point is possibly least trivial as it effectively mean redefinition of Z coupling. That is why it can not be understood as parameter re-scaling. It points to present in higher order relations between vacuum polarization and vertex. Most of the changes are due to the term Γ_Z^2/M_Z^2 except of the overall phase which result from $1 - i \cdot \Gamma_Z/M_Z$ factor and which change the γZ interference. The shift in M_Z is by about 34 MeV downwards, and the shift in Γ_Z by 1 MeV, due the reparametrisation of the Z-boson propagator.

In Figure 9 shown is comparison of the cross-sections and A_{fb}, between different implementations of $\chi_Z(s)$. Dashed line of reference corresponds to using formula (30). Green line using complete formula (32). Red line corresponds to formula (32) but without $N_Z^{'}$ scaling and blue line to formula (31), with nominal M_Z and Γ_Z.

Table 15: Ratio of the cross-section σ alculated with different form Z-boson propagator, integrated over specified mass windows. Shown in case of EW LO and EW NLO+HO predictions with $O(\alpha(0)$ v0 EW scheme.

σ (Fixed/Running)	$90.5 < m_{ee} < 91.5$ GeV	$89 < m_{ee} < 93$ GeV	$60 < m_{ee} < 81$ GeV	$81 < m_{ee} < 101$ GeV	$101 < m_{ee} < 150$ GeV
EW LO					
with M_Z, Γ_Z shift, no scaling	1.00087	1.00087	1.00062	1.00086	1.00071
no M_Z, Γ_Z shift, no scaling	0.99620	1.00074	0.99716	0.99977	1.00392
EW NLO+HO					
with M_Z, Γ_Z shift, no scaling	1.00113	1.00085	1.00043	1.00083	1.00075
no M_Z, Γ_Z shift, no scaling	0.99746	1.00122	0.99719	1.00013	1.00392

Table 16: Difference in A_{fb} calculated wiht different form of Z-boson propagator, integrated over specified mass windows. Shown in case of EW LO and EW NLO+HO predictions with $O(\alpha(0)$ v0 EW scheme.

ΔA_{fb} (Running - Fixed)	$90.5 < m_{ee} < 91.5$ GeV	$89 < m_{ee} < 93$ GeV	$60 < m_{ee} < 81$ GeV	$81 < m_{ee} < 101$ GeV	$101 < m_{ee} < 150$ GeV
EW LO					
with M_Z, Γ_Z shift, no scaling	-0.00048	-0.00047	-0.00047	-0.00047	-0.00030
no M_Z, Γ_Z shift, no scaling	-0.00006	-0.00026	-0.00012	-0.00040	-0.00005
EW NLO+HO					
with M_Z, Γ_Z shift, no scaling	-0.00053	-0.00053	-0.00052	-0.00053	-0.00024
no M_Z, Γ_Z shift, no scaling	-0.00007	-0.00030	-0.00026	-0.00048	-0.00004

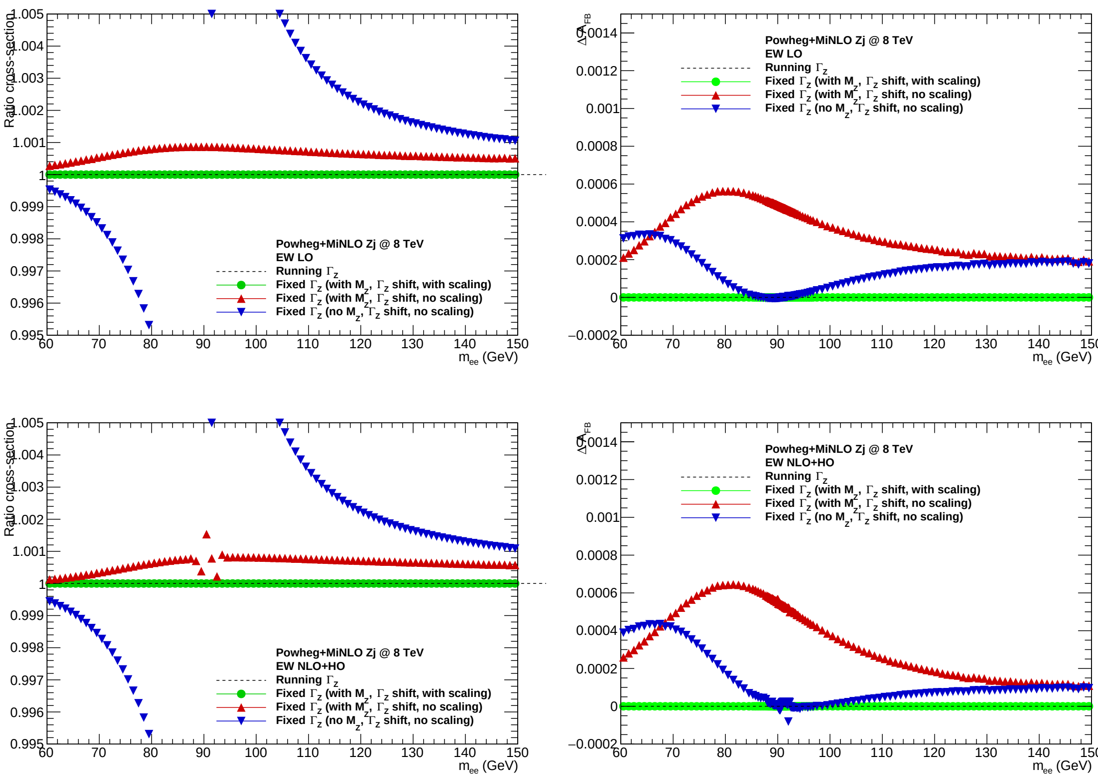

Figure 9: Ratio of the cross-sections (left) and ΔA_{fb} (right) for different form of Z-boson propagator, see text. Top line is for EW LO, bottom line with EW corrections included in the *Improved Born Approximation*.

D Genuine weak and line-shape corrections from `Dizet 6.XX` library

Proposed content:

- *Short introduction to* `Dizet` *package. Description of Improved Born Approximation and introduction of form-factors here if not done in main Sections.*
- *Evolution since version* `6.21`.
- *Theoretical predictions with emphasize on latest updates. Detailed tables + illustrative plots of form-factors.*
- *Theoretical and parametric uncertainties.*

D.1 Input parameters and initialisation flags

The `Dizet` package relies on the so called *on-mass-shell* (OMS) normalisation scheme [26, 27] but modifications are present. The OMS uses the masses of all fundamental particles, both fermions and bosons, electromagnetic coupling constant $\alpha(0)$ and strong coupling $\alpha_s(M_Z)$. The dependence on the ill-defined masses of the light quarks *u, d,c, s* and *b* is solved by dispersion relation, for details see [2]. Another exception is W-boson mass M_W, which still can be predicted with better theoretical error than experimentally measured values, exploiting the very precise knowledge of the Fermi constant in μ-decay G_μ. For this reasons, M_W is usually replaced by G_μ.

The knowledge about the hadronic vacuum polarisation is contained in the quantity denoted as $\Delta\alpha_h^{(5)}(M_Z)$, which is treated as one of the input parameters. It can be either computed from quark masses or, preferably, fitted to experimental low energy $e^+e^- \to hadrons$ data.

The two important constants used are therefore: $\alpha(0)$ - electromagnetic coupling α in Thomson limit and G_μ- Fermi constant in μ-decay. The following parameters are also passed to main `Dizet` subroutine:

$$M_W,\ M_Z,\ m_t,\ \Delta\alpha_h^{(5)}(M_Z),\ \alpha_s(M_Z). \tag{33}$$

Note that the above list is over-complete, only two out of three parameters

$$G_\mu,\ M_W,\ M_Z \tag{34}$$

are independent. They can be selected with appropriate flags setting. The only meaningful choice implemented in `Dizet` library, for calculating EW corrections at the Z-resonance, is to use G_μ and M_Z as input parameters, then calculate M_W.

The M_W is calculated iteratively from the following equation

$$M_W = \frac{M_Z}{\sqrt{2}}\sqrt{1+\sqrt{1-\frac{4A_0^2}{M_Z^2(1-\Delta r)}}}, \tag{35}$$

where

$$A_0 = \sqrt{\frac{\pi\alpha(0)}{\sqrt{2}G_\mu}}. \tag{36}$$

The Sirlin's parameter Δr [28]

$$\Delta r = \Delta\alpha(M_Z) + \Delta r_{EW} \tag{37}$$

is also calculated iteratively, and the definition of Δr_{EW} involves re-summation and higher order corrections. Since this term implicitly depends on M_W and M_Z iterative procedure is needed. The resummation term in formula (37) is not formally justified by renormalisation group arguments, correct generalization is to compute higher order corrections, see more discussion in [2].

Note that once the M_W is recalculated with formula (35), the Standard Model relationship between the weak and electromagnetic couplings

$$G_\mu = \frac{\pi\alpha}{\sqrt{2}M_W^2\sin^2\theta_W} \tag{38}$$

Table 17: The `Dizet` initialisation flags: defaults in different versions.

Input NPAR()	Internal flag	Dizet 6.21 Defaults in [12]	Dizet v6.42 Defaults in [3]	Dizet v6.45	Comments
NPAR(1)	IHVP	1	1	5	$\Delta\alpha^{(5)}_{had}$ param. from [29] in v6.45
NPAR(2)	IAMT4	4	4	8	New devellopment in v6.45
NPAR(3)	IQCD	3	3	3	
NPAR(4)	IMOMS	1	1	1	
NPAR(5)	IMASS	0	0	0	
NPAR(6)	ISCRE	0	0	0	
NPAR(7)	IALEM	3	3	3	
NPAR(8)	IMASK	0	0	0	Not used since v6.21
NPAR(9)	ISCAL	0	0	0	
NPAR(10)	IBARB	2	2	2	
NPAR(11)	IFTJR	1	1	1	
NPAR(12)	IFACR	0	0	0	
NPAR(13)	IFACT	0	0	0	
NPAR(14)	IHIGS	0	0	0	
NPAR(15)	IAMFT	1	3	3	
NPAR(16)	IEWLC	1	1	1	
NPAR(17)	ICZAK	1	1	1	
NPAR(18)	IHIG2	1	1	1	
NPAR(19)	IALE2	3	3	3	
NPAR(20)	IGREF	2	2	2	
NPAR(21)	IDDZZ	1	1	1	
NPAR(22)	IAMW2	0	0	0	
NPAR(23)	ISFSR	1	1	1	
NPAR(24)	IDMWW	0	0	0	
NPAR(25)	IDSWW	0	0	0	

is not fulfilled anymore, unless the G_μ is redefined and not taken at the measured value. This is an approach of some EW LO schemes, but not the one used by `Dizet` and it requires keeping complete expression for $\chi_Z(s)$ propagator in formula for spin amplitude (26), as defined by formula (20).

In the OMS renormalisation scheme the weak mixing angle is defined uniquely through the gauge-boson masses:

$$\sin^2\theta_W = s_W^2 = 1 - \frac{M_W^2}{M_Z^2}. \tag{39}$$

With this scheme, measuring $\sin^2\theta_W$ will be equivalent to indirect measurement of M_W^2 through the relation (39).

Let us return to `Dizet` scheme. After M_W is computed, the list of input parameters of main subroutine is fully specified.

In Table 12 and 13 collected are numerical values for all parameters used in the number presented below (folow collumn with EW scheme $\alpha(0)$ v0 in Table 13).

Default configurations of the initialisation flags, corresponding to each major version of `Dizet` library, are collected in Table 17. Evolution of flags `IAMT4` and `IAMFT` corresponds to improved calculations for fermionic loop corections became gradually available. Evolution of `IHVP` corresponds to including much improved parametrisation of the $\Delta\alpha^{(5)}_{had}$ corrections.

Table 18: The `Dizet` v6.45 recalculated parameters: masses, couplings, etc.., with initialisation as in Tables 17, 12 and 13.

Parameter	Value	Description
$\alpha_{QED}(M_Z^2)$	0.0077549256	calculated using $\Delta\alpha_h^{(5)}(m_Z^2)$ from [29]
$1/\alpha_{QED}(M_Z^2)$	128.950302056	
M_W (GeV)	80.3589356	W mass
$ZPAR(1) = \delta r$	0.03640338	the loop corrections to G_μ
$ZPAR(2) = \delta r_{rem}$	0.01167960	the remainder contribution $O(\alpha)$
$ZPAR(3) = s_W^2$	0.22340108	weak mixing angle defined by weak masses
$ZPAR(4) = G_\mu$ (GeV^{-2})	$1.16614173 \cdot 10^{-5}$	G_μ with loop correct.
$ZPAR(6) = \sin^2\theta^{\ell}_{eff}(M_Z^2)$	0.231499	effective weak mixing angle
$ZPAR(9) = \sin^2\theta^{up}_{eff}(M_Z^2)$	0.231392	effective weak mixing angle
$ZPAR(10) = \sin^2\theta^{down}_{eff}(M_Z^2)$	0.231265	effective weak mixing angle
$ZPAR(14) = \sin^2\theta^{bottom}_{eff}(M_Z^2)$	0.232733	effective weak mixing angle

D.2 Predictions: masses, couplings, EW form-factors

Table 18 collects few benchmark numbers for masses and couplings as calculated by `Dizet 6.45`, with initialisation as in Tables 17, 12 and 13.

Figure 10 shows real parts of the EW form-factors: $\rho_{\ell f}(s,t)$, $\mathscr{K}_f(s,t)$, $\mathscr{K}_\ell(s,t)$, $\mathscr{K}_{\ell f}(s,t)$, for a few values of $\cos\theta$, representing scattering angle between incoming quark and outgoing lepton directions in the centre-of-mass frame of outgoing lepton pairs. The Mandelstam variables (s,t) relate to invariant mass and scattering angle of outgoing leptons as defined in Eq. (24). The $\cos\theta$ dependence of the form-factors is due to box corrections and is more sizeable for the up-quarks.

Note, that at the peak of Z-boson, Born like couplings are not sizeably modified, form-factors are close to 1 and no numerically significant angular dependence is visible. At lower virtualities corrections seem to be larger because Z-boson contributions is non resonant and virtual corrections are by comparison larger. In this region of the phase-space Z-boson is anyway dominated by the contribution from virtual photon. Above the peak, contribution of WW boxes and later also ZZ boxes become gradually sizable and the dependence on $\cos\theta$ angle also appears. Those contributions become double resonant.

D.3 Theoretical and parametric uncertainties

D.3.1 Running $\alpha(s)$

Fermionic loop insertion to the photon propagator, i.e. vacuum polarisation corrections, are summed together as multiplicative factor of formula (23) to the photonic Born term in formula (26). It can be also interpreted as *running QED coupling* $\alpha(s)$ and expressed as

$$\alpha(s) = \frac{\alpha(0)}{1 - \Delta\alpha_h^{(5)}(s) - \Delta\alpha_\ell(s) - \Delta\alpha_t(s) - \Delta\alpha^{\alpha\alpha_s}(s)}. \tag{40}$$

Following [12], the hadronic contribution at M_Z is a significant correction: $\Delta\alpha_h^{(5)}(M_Z^2)$ = 0.0280398 and is calculated in 5-th flavour scheme making use of dispersion relation and experimental input from low energy experiments. This value has been significantly changed over years with new low-energy experiments. Recent estimates [29], which comes also with parametrised formula in very large range of s gives $\Delta\alpha_h^{(5)}(M_Z^2)$ = 0.0275762. The leptonic loop contribution $\Delta\alpha_\ell(s)$ is calculated analytically with up to the 3-loops, and is a comparably significant correction, $\Delta\alpha_\ell(M_Z)$ = 0.0314976. The other contributions are very small. The top contribution depends on the mass of the top quark, and for m_t = 173.8 GeV is $\Delta\alpha_t(s) = -0.585844 \cdot 10^{-4}$. The mixed two-loop $O(\alpha\alpha_s)$ corrections arising from $t\bar{t}$ loops with gluon, for the same top-quark mass and $\alpha_s = 0.119$ is $\Delta\alpha^{\alpha\alpha_s}(M_Z) = -0.103962 \cdot 10^{-4}$.

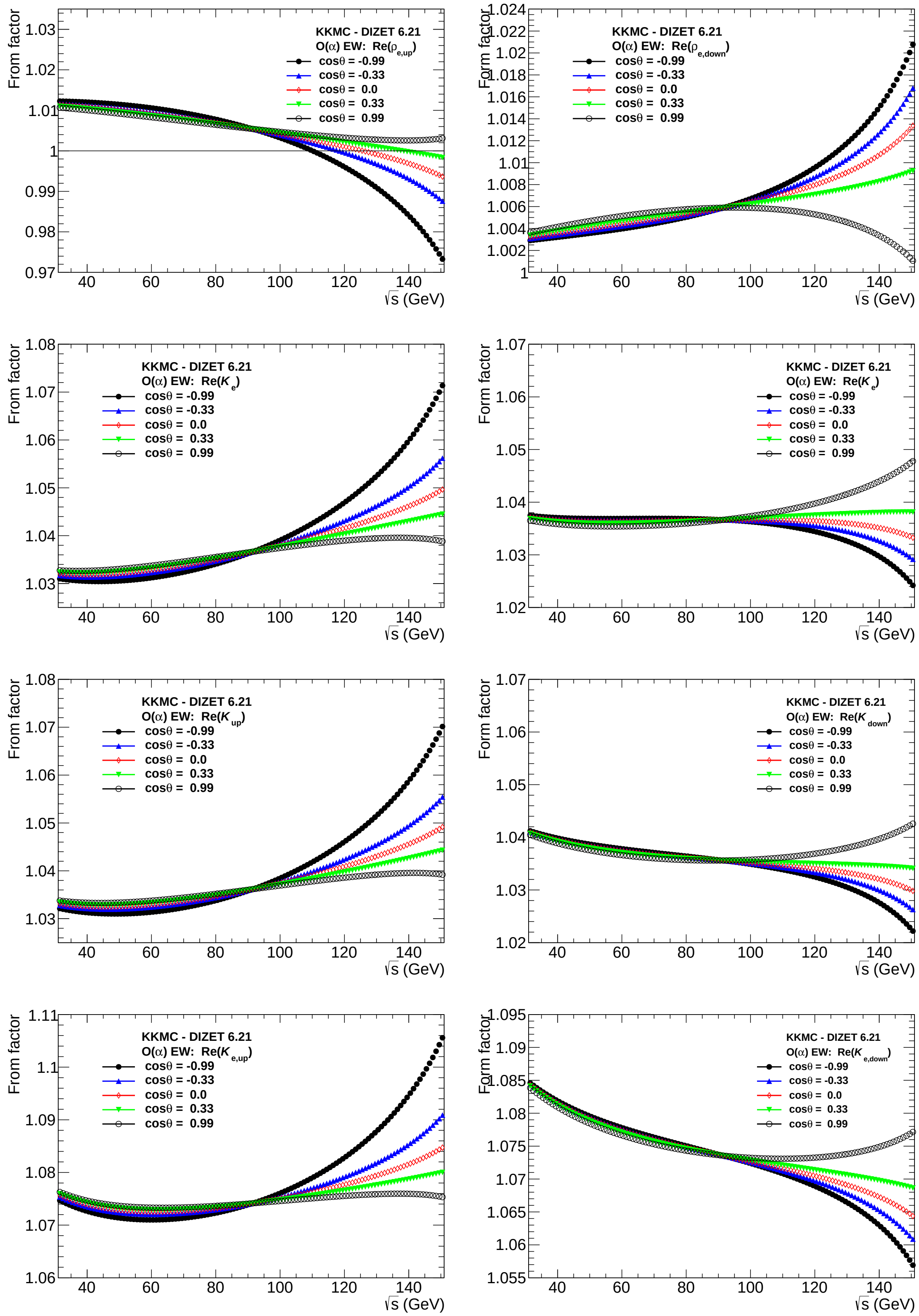

Figure 10: Real part of EW form factors for $q\bar{q} \to Z \to ee$ process: $\rho_{e,up}$, $\mathscr{K}_e$, $\mathscr{K}_{up}$ and $\mathscr{K}_{e,up}$ as a function of $\sqrt{s}$ for few values of $\cos\theta$. For u-type quark flavour left side plots are prepared and for the down-type right side plots. Note that $\mathscr{K}_e$ depend on the flavour of incoming quarks.

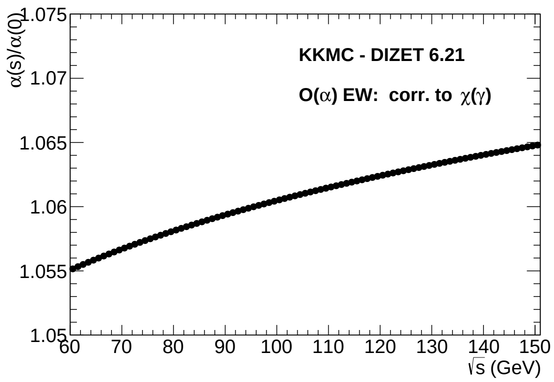

Figure 11: The vacuum polarisation correction to γ propagator, $\alpha(s)/\alpha(0)$ of formula (40), as a function of $\sqrt{s}$. *Plot should be updated with Jegerlehner 2017 parametrisation [29].*

Table 19 summarizes impact from changing predictions on the central value of $\Delta\alpha_h^{(5)}(M_Z^2)$, on the EW corrections to different quantities calculated with $\widehat{\mathrm{D}}$izet library. Figure 11 shows $\alpha(s)/\alpha(0)$ as a function of $\sqrt{s}$.

Uncertainties on the hadronic contributions to the effective fine structure constant $\alpha(s)$ are a problem for electroweak precision physics. Because of the large 6% relative corrections between $\alpha(0)$ and $\alpha(M_Z)$, where 50% of the shift is due to non-perturbative hadronic effects, one is loosing about a factor of five orders of magnitude in precision. Present estimates of the uncertainties of SM input parameters are (from F. Jegerlehner contribution in [30]):

$$\begin{aligned}
\frac{\delta\alpha(0)}{\alpha(0)} &\sim 3.6\cdot 10^{-9}; \frac{\delta G_\mu}{G_\mu} \sim 8.6\cdot 10^{-6}; \frac{\delta M_Z}{M_Z} \sim 2.4\cdot 10^{-5}; \\
\frac{\delta\alpha(0)}{\alpha(0)} &\sim 0.9 - 1.6\cdot 10^{-4} (lost \;\; 10^5 \;\; in \;\; precision); \qquad (41)\\
\frac{\delta M_W}{M_W} &\sim 1.5\cdot 10^{-4}; \frac{\delta m_t}{m_t} \sim 2.3\cdot 10^{-3}; \frac{\delta M_H}{M_H} \sim 1.3\cdot 10^{-3};
\end{aligned}$$

(42)

The $\alpha(M_Z)$ is the least precise among the basic input parameters: $\alpha(M_Z)$, G_μ, M_Z. The present uncertainties on hadronic corrections $\delta\alpha(M_Z)$ = 0.00020 results in the error on predictions $\delta\sin^2\theta_{eff} = 0.00007$ and $\delta M_W/M_W \sim 4.3\cdot 10^{-5}$. For comparison, the uncertainties on m_t contributes $\delta\sin^2\theta_{eff}/ = 0.000002$ and $\delta M_W/M_W \sim 3.0\cdot 10^{-5}$.

The effect of uncertainties on $\Delta\alpha_h^{(5)}(M_Z^2)$, taken as ± 0.0001 on the corrections and quantities calculated by `Dizet` are summarized in Table 20.

D.3.2 Fermionic two-loop corrections

D.3.3 Top quark mass

Table 19: The `Dizet v6.45` predictions for two different parametrisations of $\Delta\alpha_h^{(5)}(M_Z^2)$. Other flags as in Tables 17.

Parameter	$\Delta\alpha_h^{(5)}(M_Z^2)$ = 0.0280398 (param. Jegerlehner 1995)	$\Delta\alpha_h^{(5)}(M_Z^2)$ = 0.0275762 (param. Jegerlehner 2017)	Δ
$\alpha(M_Z^2)$	0.0077587482	0.0077549256	
$1/\alpha(M_Z^2)$	128.8867699646	128.95030224	
s_W^2	0.22356339	0.22340108	- 0.00016
$sin^2\theta_{eff}(M_Z^2)$ (lepton)	0.23166087	0.23149900	- 0.00023
$sin^2\theta_{eff}(M_Z^2)$ (up-quark)	0.23155425	0.23139248	- 0.00016
$sin^2\theta_{eff}(M_Z^2)$ (down-quark)	0.23142705	0.23126543	- 0.00016
M_W (GeV)	80.3505378	80.358936	+8.4 MeV
Δr	0.03690873	0.03640338	
Δr_{rem}	0.01168001	0.01167960	

Table 20: The `Dizet v6.45` predictions: uncertainty from $\Delta\alpha_h^{(5)}(M_Z^2 = 0.0275762)$ (param. Jegerlehner 2017)[29], varied by $\pm$ 0.0001.

Parameter	$\Delta\alpha_h^{(5)}(M_Z^2)$ - 0.0001	$\Delta\alpha_h^{(5)}(M_Z^2)$ = 0.0275762	$\Delta\alpha_h^{(5)}(M_Z^2)$ + 0.0001	$\Delta/2$
$\alpha(M_Z^2)$	0.0077541016	0.0077549256	0.0077557498	
$1/\alpha(M_Z^2)$	128.9640056546	128.95030224	128.9365984574	
s_W^2	0.22336607	0.22340108	0.22343610	0.000035
$sin^2\theta_{eff}(M_Z^2)$ (lepton)	0.23146409	0.23149900	0.23153392	0.000035
$sin^2\theta_{eff}(M_Z^2)$ (up-quark)	0.23135758	0.23139248	0.23142737	0.000035
$sin^2\theta_{eff}(M_Z^2)$ (down-quark)	0.23123057	0.23126543	0.23130029	0.000035
M_W (GeV)	80.3607471	80.358936	80.357124	1.8 MeV
Δr	0.03629414	0.03640338	0.03651261	
Δr_{rem}	0.01167983	0.01167960	0.01167938	

Table 21: The `Dizet v6.45` predictions with improved treatment of two-loop corrections. Other flags as in Tables 17.

Parameter	AMT4= 4	AMT4 = 8	Δ
$\alpha(M_Z^2)$	0.0077549256	0.0077549256	
$1/\alpha(M_Z^2)$	128.9503020560	128.95030224	
s_W^2	0.22333971	0.22340108	+ 0.00006
$sin^2\theta_{eff}(M_Z^2)$ (lepton)	0.23157938	0.23149900	-0.00008
$sin^2\theta_{eff}(M_Z^2)$ (up-quark)	0.23147290	0.23139248	-0.00008
$sin^2\theta_{eff}(M_Z^2)$ (down-quark)	0.23134590	0.23126543	-0.00008
M_W (GeV)	80.361846	80.358936	- 2.9 MeV
Δr	0.03640338	0.03640338	
Δr_{rem}	0.01167960	0.01167960	

Table 22: The `Dizet v6.45` predictions: uncertainty from changing top-quark mass by ±0.5 GeV. Other flags as in Tables 17.

Parameter	m_t - 0.5 GeV	m_t = 173.0 GeV	m_t + 0.5 GeV	$\Delta/2$
$\alpha(M_Z^2)$	0.0077549221	0.0077549256	0.0077549291	
$1/\alpha(M_Z^2)$	128.9503600286	128.95030224	128.9502446106	
s_W^2	0.22345908	0.22340108	0.22334300	0.000058
$sin^2\theta_{eff}(M_Z^2)$ (lepton)	0.23151389	0.23149900	0.23148410	0.000016
$sin^2\theta_{eff}(M_Z^2)$ (up-quark)	0.23140736	0.23139248	0.23137758	0.000016
$sin^2\theta_{eff}(M_Z^2)$ (down-quark)	0.23128031	0.23126543	0.23125053	0.000016
M_W (GeV)	80.355935	80.358936	80.361941	3 MeV
Δr	0.03658500	0.03640338	0.03622132	
Δr_{rem}	0.01167011	0.01167960	0.01168907	

E TauSpinner with EW weights

Comment: Content of this Section was published in [21], now updated with `Dizet 6.45` *form-factors.*

The `TauSpinner` package was initially created as a tool to correct with per-event weight longitudinal spin effects in the generated event samples including τ decays. Implemented there algorithms turned out to be of more general usage. They provide effective approach using reweighting technique to modify matrix elements of the hard processes used in Monte Carlo programs for event production and decay. The most recent summary on its algorithms and their applications is given in [31]. The possibility to introduce one-loop electroweak corrections from `SANC` library [13] in case of Drell-Yan production of the Z-boson became available in `TauSpinner` since [32]. This implementation allowed to introduce per-event weight calculated using pre-tabulated EW corrections for each individual spin configurations of outgoing leptons.

The implementation of EW corrections which is discussed in [21] and summarised here is enhanced. The `TauSpinner` package and algorithms are adapted to allow EW corrections from `Dizet` library directly into spin amplitudes and weight calculations for the Drell-Yan Z-boson production process. In [7, 8] we have shown that separating EW and QCD higher order corrections is possible and the Born-level spin amplitudes, if calculated in the adapted `Mustraal` frame [6], provide very good approximation of the EW LO sector even in case of NLO QCD description of the Drell-Yan processes. The EW corrections are introduced as form-factor corrections to Standard Model couplings and propagators entering Born-level spin amplitudes. This approach was very successful in analyses of LEP precision physics and we use the same strategy for the LHC precision physics around the Z-boson pole.

E.1 Born kinematic approximation and pp scattering

The solution for how to define Born-like kinematics in case of pp scattering is available in the algorithms of `TauSpinner` package [31]. The strategy assumes that hard-process history generated event is not known, in particular flavour and kinematics of incoming partons is therefore reconstructed, entirely from the kinematics of outgoing final states, reaction center of mass energy and with probabilities obtained from parton level cross-sections and PDFs. We briefly recall principles here and explain further optimisations.

E.2 Average over incoming partons flavour

Parton level Born cross-section $\sigma^{q\bar{q}}_{Born}(\hat{s},\cos\theta)$ is convoluted with the structure functions, and averaged over all possible flavours of incoming partons and all possible helicity states of outgoing leptons. The lowest order formula is given below

$$\begin{aligned} d\sigma_{Born}(x_1,x_2,\hat{s},\cos\theta) = \quad & \sum_{q_f,\bar{q}_f} [f^{q_f}(x_1,...)f^{\bar{q}_f}(x_2,...)d\sigma^{q_f\bar{q}_f}_{Born}(\hat{s},\cos\theta) \\ & + f^{q_f}(x_2,...)f^{\bar{q}_f}(x_1,...)d\sigma^{\bar{q}_f q_f}_{Born}(\hat{s},-\cos\theta)], \end{aligned} \tag{43}$$

where x_1, x_2 denote fractions of incoming parton momenta calculated from kinematics of outgoing leptons, $\hat{s} = x_1\ x_2\ s$ and f denotes parton density functions. We assume that kinematics is reconstructed from four-momenta of the outgoing leptons. The sign in front of $\cos\theta$, the cosine of the scattering angle, follows choice of the z-axis orientation being the one of the parton carrying x_1. The two possibilities are taken into account by the two terms of (43). The formula is used for calculating differential cross-section $d\sigma_{Born}(x_1,x_2,\hat{s},\cos\theta)$ of each analysed event, regardless its initial state kinematics and flavours of incoming partons which may be available in the event history entries. The formula can be used to a good approximation in case of NLO QCD spin amplitudes. The kinematics of outgoing leptons is used to construct *effective* kinematics of the Drell-Yan production process and decay, without need for information on the history of the hard-process itself. It can be constructed for events where initial state of Feynman diagrams were quark-gluon or gluon-gluon partons (as stored in the history event entries).

E.3 Effective beams kinematics

The x_1, x_2 are calculated from kinematics of outgoing leptons, following formulae of [33]

$$x_{1,2} = \frac{1}{2} \Big(\pm \frac{p_z^{ll}}{4E} + \sqrt{(\frac{p_z^{ll}}{4E})^2 + 4\,(\frac{m_{ll}^2}{4E^2})^2} \,\Big), \tag{44}$$

where E denotes energy of the proton beam and $p_z^{\ell\ell}$ denotes z-axis momenta of outgoing lepton pairs in the laboratory frame.

E.4 Definition of the polar angle

The $\cos\theta$, in case of $q\bar{q} \to Z \to \ell\ell$ process, can be defined as a weighted average of the angles of the outgoing leptons with respect to the beams directions [34]. It will be denoted as $\cos\theta^*$. Extending this definition to pp collisions, requires choice which direction along z-axis is of the quark and of the anti-quark, and then boosting their four-momenta into rest frame of the lepton pair system. The $\cos\theta^*$ distribution is calculated as follows:

$$\cos\theta_1 = \frac{\tau_x^{(1)} b_x^{(1)} + \tau_y^{(1)} b_y^{(1)} + \tau_z^{(1)} b_z^{(1)}}{|\vec{\tau}^{(1)}||\vec{b}^{(1)}|}, \quad \cos\theta_2 = \frac{\tau_x^{(2)} b_x^{(2)} + \tau_y^{(2)} b_y^{(2)} + \tau_z^{(2)} b_z^{(2)}}{|\vec{\tau}^{(2)}||\vec{b}^{(2)}|}, \tag{45}$$

finally

$$\cos\theta^* = \frac{\cos\theta_1 \sin\theta_2 + \cos\theta_2 \sin\theta_1}{\sin\theta_1 + \sin\theta_2} \tag{46}$$

where $\vec{\tau}^{(1)}, \vec{\tau}^{(2)}$ denote 3-vectors of outgoing leptons and $\vec{b}^{(1)}, \vec{b}^{(2)}$ denote 3-vectors of incoming beams with sign of the z-axis accordingly which term of (43) is considered. All 3-vectors are of lepton pair centre-of-mass system.

The definition of cosine polar angle (46) is a default of `TauSpinner` algorithms. Alternatively, one can use also polar angle from `Mustraal` [6] or `Collins-Soper` [35] frames. We will come later to the choice with the discussion on the preferred frame used in case of NLO QCD corrections included in the production process of generated events.

E.5 Concept of the EW weight

The EW corrections enter expression for the $\sigma_{Born}(\hat{s}, \cos\theta)$ through the definition of the vector and axial couplings and propagators of photon and Z-boson. They modify normalisation of the cross-sections, the line-shape of the Z-boson, polarisation of the outgoing leptons and asymmetries.

Given that to a good approximation we were able to factorise QCD and EW components of the cross-section we can now define per-event weight which specifically corrects for EW effects. Applying such weight allows to modify events generated with EW LO to the one including the EW corrections. This is very much the same idea as already implemented in `TauSpinner` for introducing corrections for different effects: spin correlations, production process, etc.

The per-event weight wt^{EW} is defined as ratio of the Born-level cross-sections with and without EW corrections

$$wt^{EW} = \frac{d\sigma_{Born+EW}(s, \cos\theta)}{d\sigma_{Born}(s, \cos\theta)}, \tag{47}$$

where $\cos\theta$ can be taken according to $\cos\theta^*$, $\cos\theta^{Mustraal}$ or $\cos\theta^{CS}$ definition. Introducing weight wt^{EW} allows for flexible and straightforward implementation of the higher order EW corrections using `TauSpinner` framework and form-factors calculated eg. with `Dizet` library.

The formula for wt^{EW} can be used to reweight from one to another EW LO scheme. In that case both the numerator and denominator of Eq. (47) will use lowest order $d\sigma_{Born}$, but calculated in different EW schemes.

E.6 EW corrections to doubly-deconvoluted observables

Having defined all components needed for calculating wt^{EW}, we will show now selected examples of numerical results for doubly-deconvoluted observables around the Z-pole.

The `Powheg+MiNLO` Monte Carlo, with NLO QCD and LO EW matrix elements, was used to generate $Z+j$ events with $Z \to e^+e^-$ decays in pp collisions at 8 TeV. No selection is applied to generated events, except requiring invariant mass of outgoing electrons in the range $70 < m_{ee} < 150$ GeV. For events generation, the EW parameters as shown in left-most column of Table 4, were used. The values for α and s_W^2 are close to the ones of MSbar discussed in [36]. Note that they are not at the values of precise measurements by LEP experiments at the Z-pole [1]. The initialisation with G_μ *scheme* of Table 4 is often used as a default for phenomenological studies at LHC and we will show later the estimated size of EW corrections for this setup.

To quantify the effect of the EW corrections, we reweight generated MC events to EW LO in the scheme used by the `Dizet` library and then introduce gradually EW corrections and form-factors calculated with that library. For each step appropriate numerator of the wt^{EW} is calculated, while for the denominator the EW LO $\mathscr{A}^{Born}$ matrix element is used, parameterised as in the left-most column of Table 4. The sequential steps, in which we illustrate effects of EW corrections are given below:

1. Reweight with wt^{EW}, from EW LO scheme with s_W^2= 0.23113 to EW LO scheme with s_W^2= 0.21215, see Table 4. The $\mathscr{A}^{Born}$ matrix element, Eq. (18), is used for calculating numerator of wt^{EW}.

2. As in step (1), but include EW corrections to m_W, effectively changing value of s_W^2 to s_W^2= 0.223401084 in calculation of wt^{EW}. Relation of formula (38) is not obeyed anymore.

3. As in step (2), but include EW loop corrections to the normalisation of Z-boson and γ propagators, i.e. QCD/EW corrections to $\alpha(0)$ and $\rho_{\ell f}(s)$ form-factor calculated without box corrections. The $\mathscr{A}^{Born+EW}$ is used for calculating numerator of wt^{EW}.

4. As in step (3), but include EW corrections to Z-boson vector couplings: $\mathscr{K}_f, \mathscr{K}_e, \mathscr{K}_{\ell f}$, calculated without box corrections. The $\mathscr{A}^{Born+EW}$ is used for calculating numerator of wt^{EW}.

5. Replace $\rho_{\ell f}, \mathscr{K}_f, \mathscr{K}_e, \mathscr{K}_{\ell f}$ form-factors by the ones including box corrections. The $\mathscr{A}^{Born+EW}$ is used for calculating numerator of wt^{EW}.

After step (1) the predictions are according to EW LO and QCD NLO, but with different EW scheme than used originally for events generation. Then steps (2)-(5) introduce EW corrections. Step (3) effectively changes back α to be close to initial $\alpha(M_Z)$, while steps (4)-(5) effectively shift back value of s_W^2 to be close to the one used for events generation. Given the fact that EW LO scheme used for generating events has parameters already close to measured at the Z-pole, we expect the total EW corrections to the generated sample to be roughly at percent level.

In the following, we will also estimate how precise it would be to use effective Born approximation with *v0*, *v1* or *v2* parametrisations instead of complete EW corrections. To obtain those predictions similar to step (1) listed above reweight is needed, but in the numerator of wt^{EW} the $\mathscr{A}^{Born}$ parametrisations as specified in the right two columns of Table 4 are used. For *v1* the $\rho_{\ell,f} = 1.005$ is included, while for *v2* both s_W^2 and ρ included are flavour dependent.

The important flexibility of proposed approach is that wt^{EW} can be calculated using $d\sigma_{Born}$ in different frames: $\cos\theta^*$, `Mustraal` or `Collins-Soper`. For some observables, frame choice used for wt^{EW} calculation is not relevant at all and the simplest $\cos\theta^*$ frame can be used. We show later an example, where only using `Mustraal` frame for the wt^{EW} calculation leads to correct results of the reweighting procedure.

Table 6 details numerical values for EW corrections, integrated in the range $80 < m_{ee} < 100$ GeV and $89 < m_{ee} < 93$ GeV. Numbers for calculating EW weight using $\cos\theta^*$ definition of the scattering angle are shown. In Table 24 results obtained with wt^{EW} calculated in different frames are compared. When using *Mustraal* frame or *Collins-Soper* frame instead of $\cos\theta^*$ one, the differences are at most at the 5-th digit.

In Table 28 compared are results with wt^{EW} calculated in different frames. When using *Mustraal* frame or *Collins-Soper* frame instead of $\cos\theta^*$, the differences are at most at the 5-th digit.

Table 23: EW corrections to cross-sections around Z-pole, $89 < m_{ee} < 93$ GeV. The EW weight is calculated with $\cos\theta^*$, $\cos\theta^{Mustraal}$ or $\cos\theta^{CS}$ definitions for scattering angle.
Updated with `Dizet 6.45` *form-factors.*

Corrections to cross-section ($89 < m_{ee} < 93$ GeV)	$wt^{EW}(\cos\theta^*)$	$wt^{EW}(\cos\theta^{Mustraal})$	$wt^{EW}(\cos\theta^{CS})$
σ(EW corr. to m_W)/σ(EW LO $\alpha(0)$)	0.97145	0.97144	0.97145
σ(EW corr. to $\chi(Z),\chi(\gamma)$)/σ(EW LO $\alpha(0)$)	0.98274	0.98247	0.98271
σ(EW/QCD FF no boxes)/σ(EW LO $\alpha(0)$)	0.96505	0.96523	0.96506
σ(EW/QCD FF with boxes)/σ(EW LO $\alpha(0)$)	0.96510	0.96527	0.96510
σ(Eff. v0)/σ(EW/QCD FF with boxes)	1.01142	1.01152	1.01142
σ(Eff. v1)/σ(EW/QCD FF with boxes)	1.00130	1.00149	1.00130
σ(Eff. v2)/σ(EW/QCD FF with boxes)	0.99989	0.99992	0.99989

Table 24: The difference in forward-backward asymmetry, ΔA_{FB} around Z-pole, m_{ee} = 89 - 93 GeV. The difference is calculated using $\cos\theta^{CS}$ to define forward and backward hemisphere. The EW weight is calculated with $\cos\theta^*$, $\cos\theta^{Mustraal}$ or $\cos^{CS}$.
Updated with `Dizet 6.45` *form factors.*

Corrections to A_{FB} ($89 < m_{ee} < 93$ GeV)	$wt^{EW}(\cos\theta^*)$	$wt^{EW}(\cos\theta^{ML})$	$wt^{EW}(\cos\theta^{CS})$
A_{FB}(EW/QCD corr. to m_W) - A_{FB}(EW LO $\alpha(0)$)	-0.02076	-0.02091	-0.02080
A_{FB}(EW/QCD corr. to $\chi(Z),\chi(\gamma)$) - A_{FB}(EW LO $\alpha(0)$)	-0.02047	-0.02062	-0.02051
A_{FB}(EW/QCD FF no boxes) - A_{FB}(EW LO $\alpha(0)$)	-0.03491	-0.03517	-0.03497
A_{FB}(EW/QCD FF with boxes) - A_{FB}(EW LO $\alpha(0)$)	-0.03489	-0.03516	-0.03496
A_{FB}(Eff. v0) - A_{FB}(EW/QCD FF with boxes)	0.00039	0.00037	0.00039
A_{FB}(Eff. v1) - A_{FB}(EW/QCD FF with boxes)	0.00042	0.00038	0.00042
A_{FB}(Eff. v2) - A_{FB}(EW/QCD FF with boxes)	0.00022	0.00024	0.00022

E.7 Comparisons of σ and A_{fb} in different EW schemes

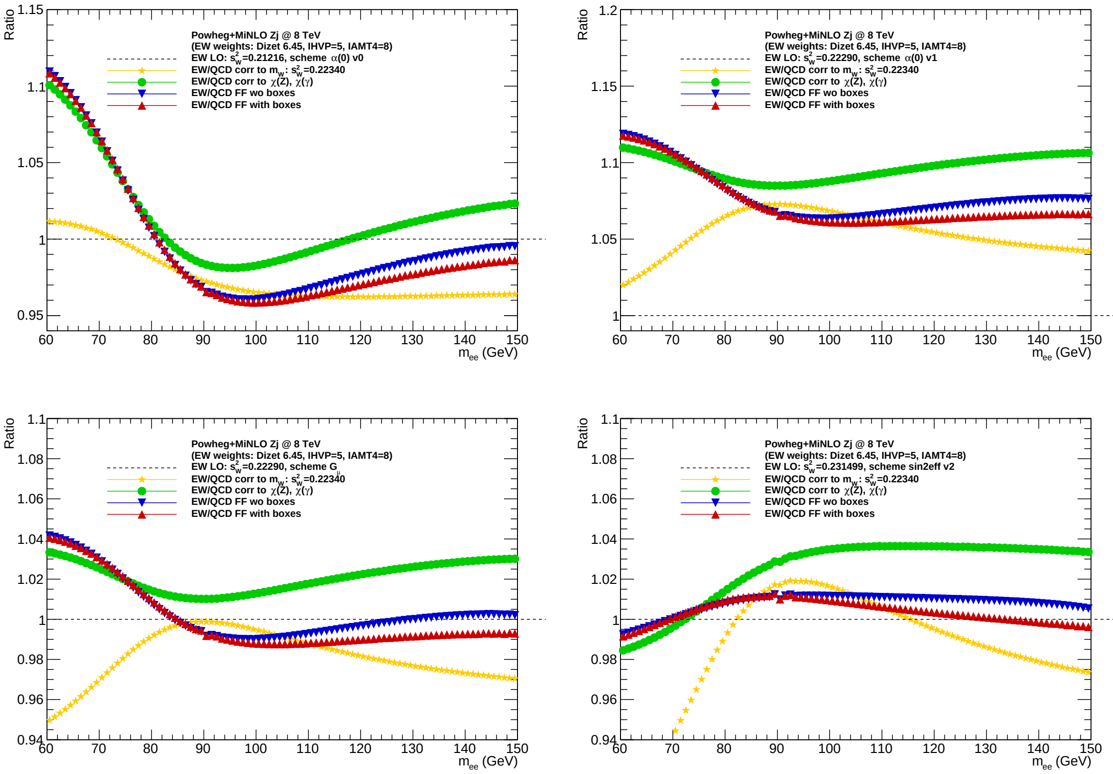

Figure 12: Ratio of the cross-sections, shown predictions from Improved Born Approximation with EW NLO+HO form-factors calculated in EW α_0 v0 scheme, reference is Born at EW LO in different EW schemes specified in Table 13. With color lines shown is effect of increamental inclusions of different groups of EW corrections. EW form factors calculated with `Dizet 6.45` library.

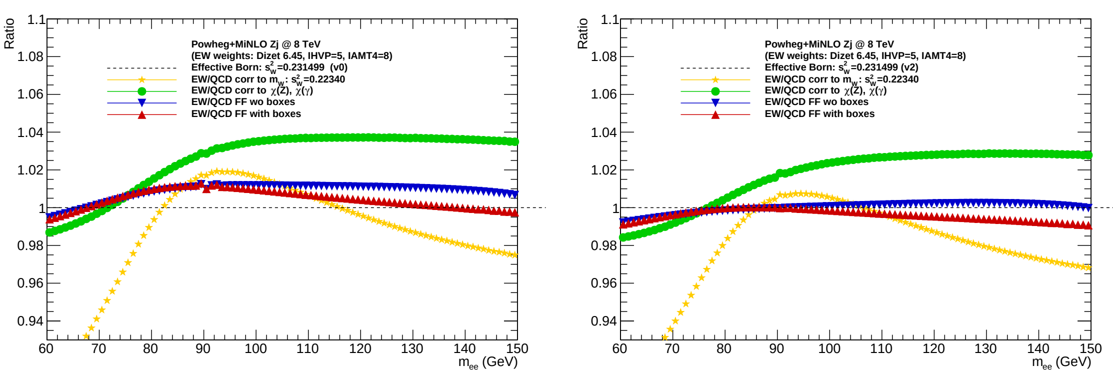

Figure 13: Ratio of the cross-sections, shown predictions from Improved Born Approximation with EW NLO+HO form-factors calculated in EW α_0 v0 scheme, reference is Effective Born parametrised as specified in Table 4. With color lines shown is effect of increamental inclusions of different groups of EW corrections. EW form factors calculated with `Dizet 6.45` library.

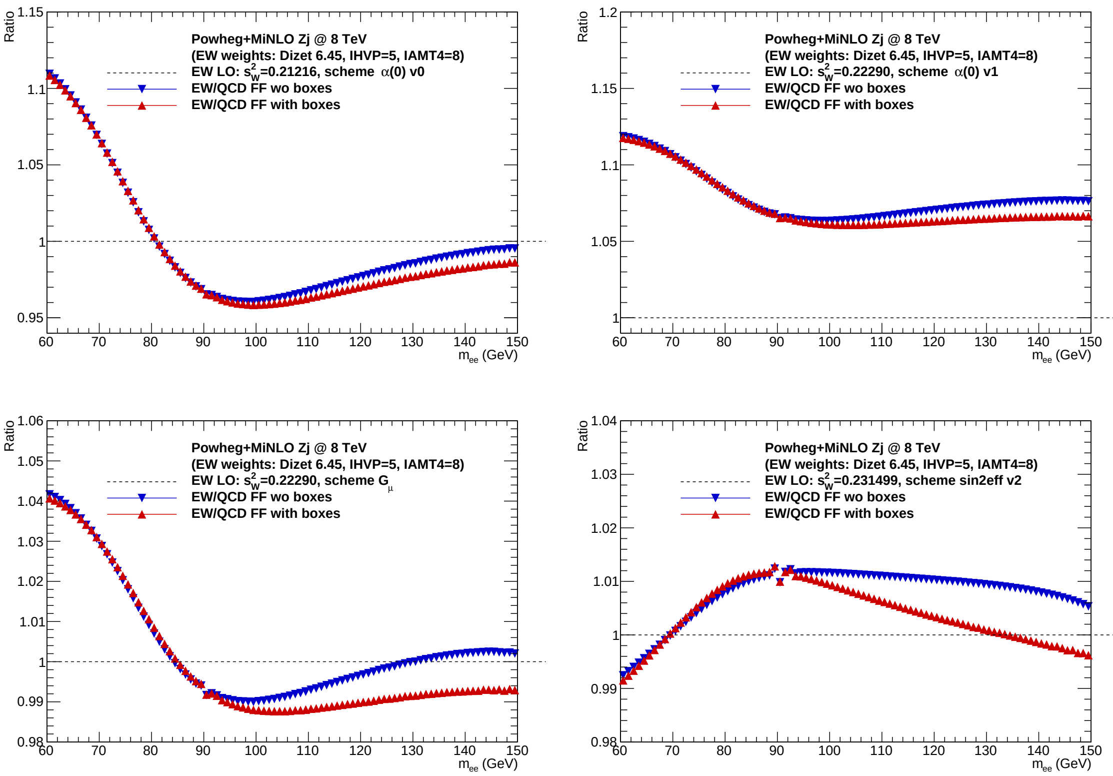

Figure 14: Same as Figure 12 but without shown effects of group of corrections, yellow and green lines removed, vertical scales zoomed.

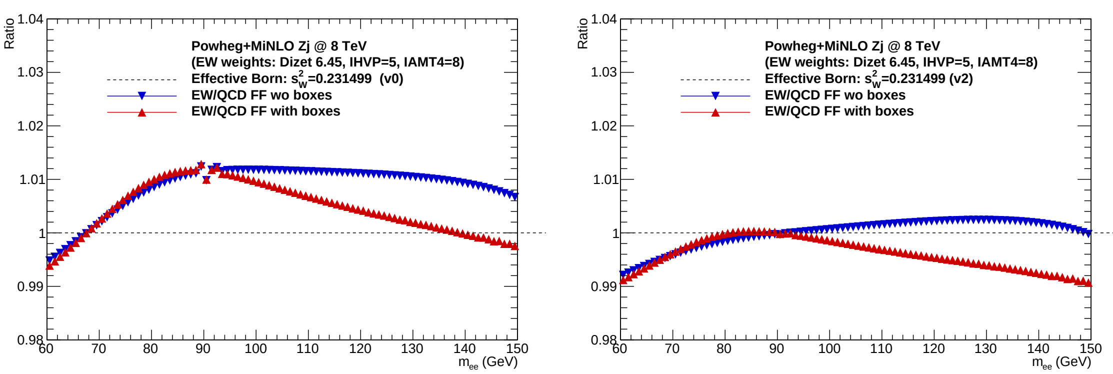

Figure 15: Same as Figure 13 but without shown effects of group of corrections, yellow and green lines removed, vertical scales zoomed.

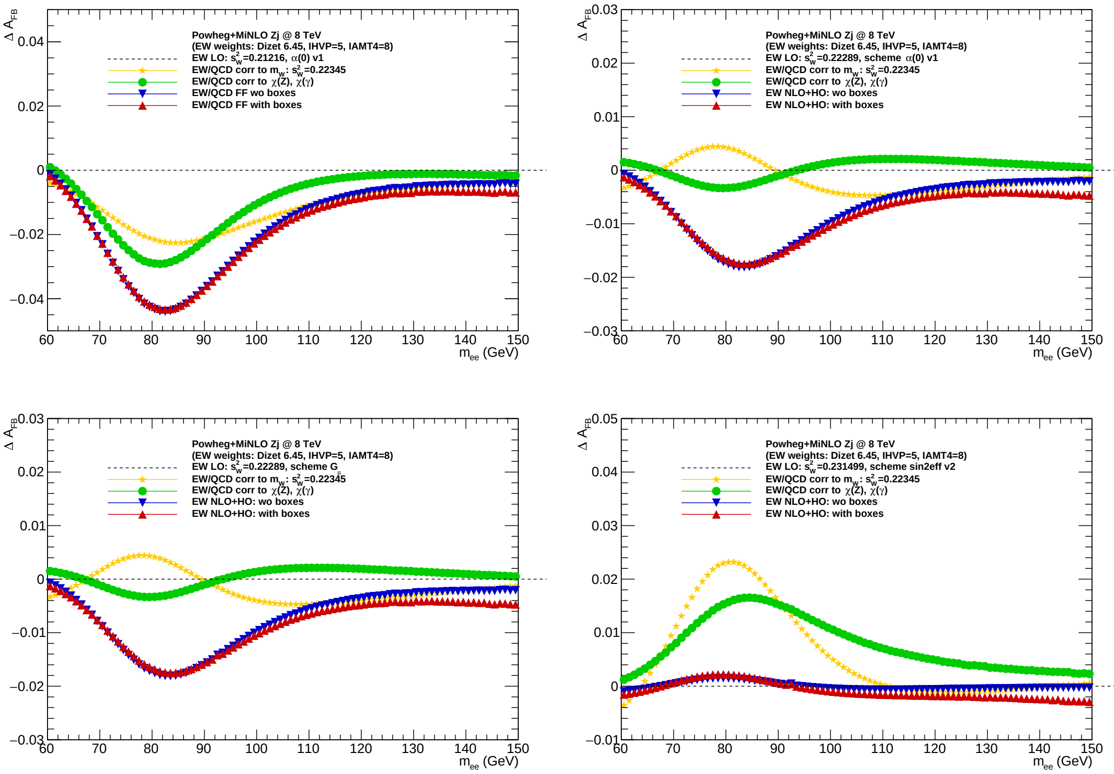

Figure 16: Ratio of the cross-sections, shown predictions from Improved Born Approximation with EW NLO+HO form-factors calculated in EW α_0 v0 scheme, reference is Born at EW LO in different EW schemes specified in Table 13. With color lines shown is effect of increamental inclusions of different groups of EW corrections. EW form factors calculated with `Dizet 6.45` library.

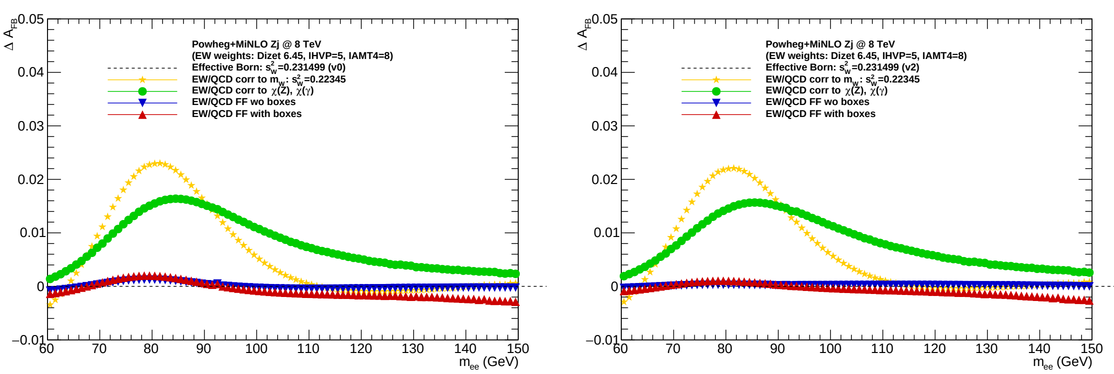

Figure 17: Ratio of the cross-sections, shown predictions from Improved Born Approximation with EW NLO+HO form-factors calculated in EW α_0 v0 scheme, reference is Effective Born parametrised as specified in Table 4. With color lines shown is effect of increamental inclusions of different groups of EW corrections. EW form factors calculated with `Dizet 6.45` library.

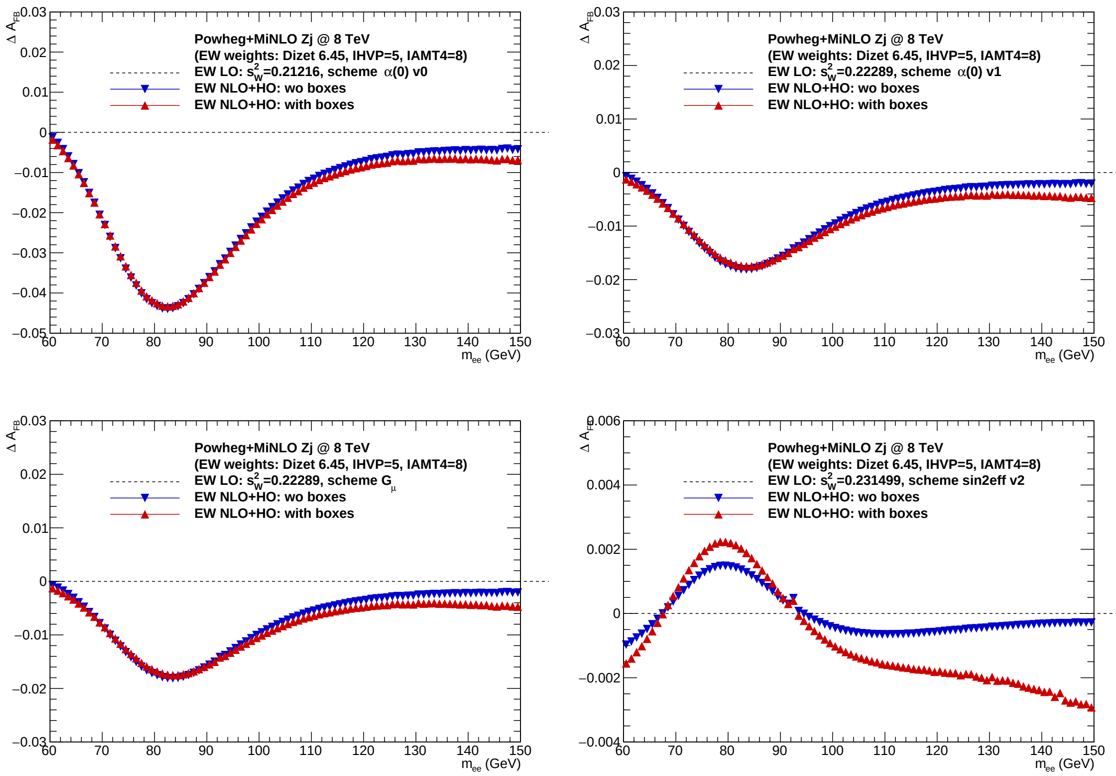

Figure 18: Same as Figure 16 but without shown effects of group of corrections, yellow and green lines removed, vertical scales zoomed.

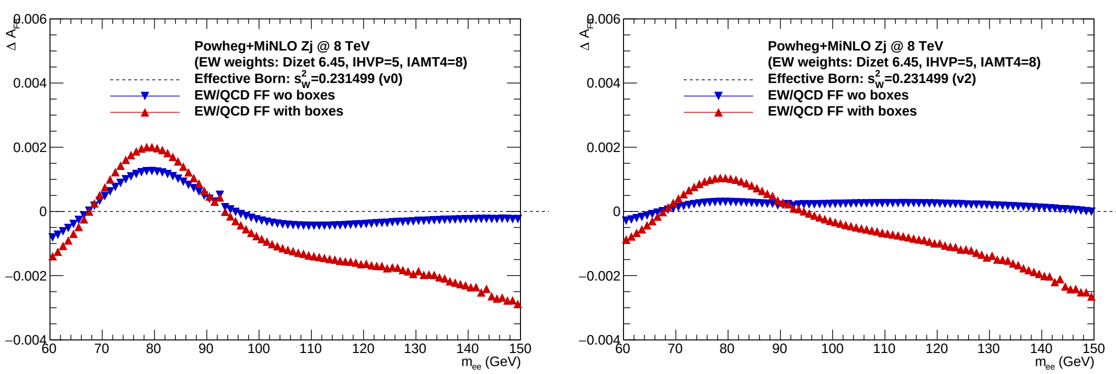

Figure 19: Same as Figure 17 but without shown effects of group of corrections, yellow and green lines removed, vertical scales zoomed.

Table 25: Ratio of the reference $\sigma^{ref}(NLO+HO)$ cross-section calculated with Improved Born Approximation and `Dizet 6.45` form-factors and the $\sigma(LO)$, calculated with EW LO Born and different EW schemes, as in Table 13. Ratio of cross-sections integrated in different mass windows.
Updated with `Dizet 6.45` *form-factors.*

$\sigma^{ref}(NLO+HO)/\sigma(LO)$	$89 < m_{ee} < 93$ GeV	$60 < m_{ee} < 81$ GeV	$81 < m_{ee} < 101$ GeV	$101 < m_{ee} < 150$ GeV
EW scheme $\alpha(0)$) v0	0.96510	1.04695	0.96632	0.96508
EW scheme $\alpha(0)$) v1	1.06558	1.09892	1.06613	1.06202
EW scheme G_μ	0.99211	1.02321	0.99264	0.98884
EW scheme $\sin^2\theta_{eff}$ v2	1.01141	1.00293	1.01132	1.00572

Table 26: Ratio of reference $\sigma^{ref}(NLO+HO)$ cros-section calculated with Improved Born Approximation and `Dizet 6.45` form-factors and the $\sigma(effect.)$, calculated with Effective Born parametrised as in Table 4. Ratios of cross-sections integrated in different mass windows.
Updated with `Dizet 6.45` *form-factors.*

$\sigma^{ref}(NLO+HO)/\sigma(effect.)$	$89 < m_{ee} < 93$ GeV	$60 < m_{ee} < 81$ GeV	$81 < m_{ee} < 101$ GeV	$101 < m_{ee} < 150$ GeV
Effective v0	1.01142	1.00411	1.01135	1.00627
Effective v1	1.00130	0.99780	1.00132	0.99800
Effective v2	0.99989	0.99701	0.99987	0.99654

Table 27: Difference between reference $A_{fb}^{ref}(NLO+HO)$ asymmetry calculated with Improved Born Approximation and `Dizet 6.45` form-factors and the $A_{fb}(LO)$, calculated with EW LO Born and different EW schemes, as in Table 13. Difference of asymmetries integrated in different mass windows.
Updated with `Dizet 6.45` *form-factors.*

$A_{fb}^{ref}(NLO+HO)-A_{fb}(LO)$	$89 < m_{ee} < 93$ GeV	$60 < m_{ee} < 81$ GeV	$81 < m_{ee} < 101$ GeV	$101 < m_{ee} < 150$ GeV
EW scheme $\alpha(0)$) v0	-0.03489	-002880	-0.03514	-0.01334
EW scheme $\alpha(0)$) v1	-0.01508	-0.01104	-0.01515	-0.00684
EW scheme G_μ	-0.01507	-0.01104	-0.01514	0.00684
EW scheme $\sin^2\theta_{eff}$ v2	-0.00039	0.00115	-0.00046	-0.00171

Table 28: Difference between reference $A_{fb}^{ref}(NLO+HO)$ asymmetry calculated with Improved Born Approximation and `Dizet 6.45` form-factors and the $A_{fb}(effect.)$, calculated with Effective Born parametrised as in Table 4. Difference is asymmetries integrated in different mass windows.
Updated with `Dizet 6.45` *form-factors.*

$A_{fb}^{ref}(NLO+HO)-A_{fb}(effect.)$	$89 < m_{ee} < 93$ GeV	$60 < m_{ee} < 81$ GeV	$81 < m_{ee} < 101$ GeV	$101 < m_{ee} < 150$ GeV
Effective v0	0.00039	0.00104	0.00042	-0.00153
Effective v1	0.00042	0.00068	0.00042	-0.00094
Effective v2	0.00022	0.00052	0.00024	-0.00087

E.8 How to vary $sin^2\theta_W^{eff}$ beyond the EW LO schemes.

In the EW scheme discussed so far, the s_W^2 is not an input. It is calculated from SM, relation (8). One possibility to vary this parameter is to stay within Standard Model framework and vary some other physical constants which impact the s_W^2 values. Candidates for such constants within Standard Model, which are also inputs to the `Dizet` library, are G_μ or m_t. From the simple estimates, those parameter will have to be varied far beyond their presently best measured values, to allow for the variation of s_W^2 parameter by $\pm 100 \cdot 10^{-5}$.

Alternative is to extend formulae for $\mathscr{A}^{Born+EW}$ (26) beyond the Standard Model, by introducing additional v-like coupling to Z-boson. This can be introduced as the shift δ_{S2W} or shift δ_V in the v_ℓ, v_f couplings. Below we give few more details how this was implemented into $\mathscr{A}^{Born+EW}$ calculations:

- `optME = 1`: introducing unknown heavy particle coupling to the Z-boson, redefines vector couplings to fermions as

$$\begin{aligned}
v_\ell = & \quad (2 \cdot T_3^\ell - 4 \cdot q_\ell \cdot (s_W^2 + \delta_{S2W}) \cdot \mathscr{K}_\ell(s,t))/\Delta, \\
v_f = & \quad (2 \cdot T_3^f - 4 \cdot q_f \cdot (s_W^2 + \delta_{S2W}) \cdot \mathscr{K}_f(s,t))/\Delta, \\
vv_{\ell f} = & \quad \frac{1}{v_\ell \cdot v_f}[(2 \cdot T_3^\ell)(2 \cdot T_3^f) \\
& -4 \cdot q_\ell \cdot (s_W^2 + \delta_{S2W}) \cdot \mathscr{K}_f(s,t)(2 \cdot T_3^\ell) \\
& -4 \cdot q_f \cdot (s_W^2 + \delta_{S2W}) \cdot \mathscr{K}_\ell(s,t)(2 \cdot T_3^f) \\
& +(4 \cdot q_\ell \cdot s_W^2)(4 \cdot q_f \cdot s_W^2)\mathscr{K}_{\ell f}(s,t) \\
& +2 \cdot (4 \cdot q_\ell))(4 \cdot q_f \cdot) \cdot s_W^2 \cdot \delta_{S2W})\mathscr{K}_{\ell f}(s,t)] \ \frac{1}{\Delta^2}
\end{aligned} \tag{48}$$

  without altering definition of

$$\Delta = \sqrt{16 \cdot s_W^2 \cdot (1 - s_W^2)} \tag{49}$$

  or any other couplings in the $\mathscr{A}^{Born+EW}$ (26) or in calculations of the EW form-factors.

- `optME = 2`: breaking the relation of the Standard Model $s_W^2 = 1 - M_W^2/M_Z^2$ and changing $s_W^2 \to s_W^2 + \delta_{S2W}$ everywhere in the formulae of $\mathscr{A}^{Born+EW}$.

- `optME = 3`: similar as `optME = 1` but now redefining vector couplings to fermions with δ_V instead of δ_{S2W}. We keep relative normalisation (charge structure) of δ_V similar to δ_{S2W}, to facilitate comparisons.

$$\begin{aligned}
v_\ell = & \quad (2 \cdot T_3^\ell - 4 \cdot q_\ell \cdot (s_W^2 \cdot \mathscr{K}_\ell(s,t) + \delta_V))/\Delta, \\
v_f = & \quad (2 \cdot T_3^f - 4 \cdot q_f \cdot (s_W^2 \cdot \mathscr{K}_f(s,t) + \delta_V))/\Delta, \\
vv_{\ell f} = & \quad \frac{1}{v_\ell \cdot v_f}[(2 \cdot T_3^\ell)(2 \cdot T_3^f) \\
& -4 \cdot q_\ell \cdot (s_W^2 + \cdot \mathscr{K}_f(s,t) + \delta_V)(2 \cdot T_3^\ell) \\
& -4 \cdot q_f \cdot (s_W^2 \cdot \mathscr{K}_\ell(s,t) + \delta_V)(2 \cdot T_3^f) \\
& +(4 \cdot q_\ell \cdot s_W^2)(4 \cdot q_f \cdot s_W^2)\mathscr{K}_{\ell f}(s,t) \\
& +2 \cdot (4 \cdot q_\ell))(4 \cdot q_f \cdot) \cdot s_W^2 \cdot \mathscr{K}_{\ell f}(s,t) \cdot \delta_V] \ \frac{1}{\Delta^2}.
\end{aligned} \tag{50}$$

  The δ_V shift is almost equivalent to shift in $\sin^2\theta^f_{eff}$, but it is (s,t) independent.

The `optME = 1, 2`, in case of form-factors not being recalculated, formally differ by the term proportional to δ_{S2W}^2 in the expression of $vv_{\ell f}$. Changing input parameters G_μ or m_t as a source of s_W^2 variations corresponds to `optME = 2` with additional changes of the couplings in ME and recalculating form-factors. All discussed options can be realised using implementation of `Tauola/TauSpinner` package and were invstigated in [21], showing very consistent slop of the predictions from Improved Born Approximations as function of $\sin^2\theta_W^{eff}$, for all options specified above.

In Figure 20 we show updated results from option `optME = 3` and EW corrections calculated with `Dizet 6.45` library, applied to Effective Born and to Improved Born. The changes in A_{fb} are shown as a function of $\sin^2\theta_W^{eff}$. Note that the slope is slightly changing depending if one or the other aproximation is used. Also at the nominal value of $\sin^2\theta_W^{eff}$ = 0.231499 between Improved Born and Effective Born predictions are $\Delta A_{fb}(EW)$ = 0.0004, similar for mass ranges $m_{ll} = 89 - 93$ GeV and $m_{ll} = 80 - 100$ GeV.

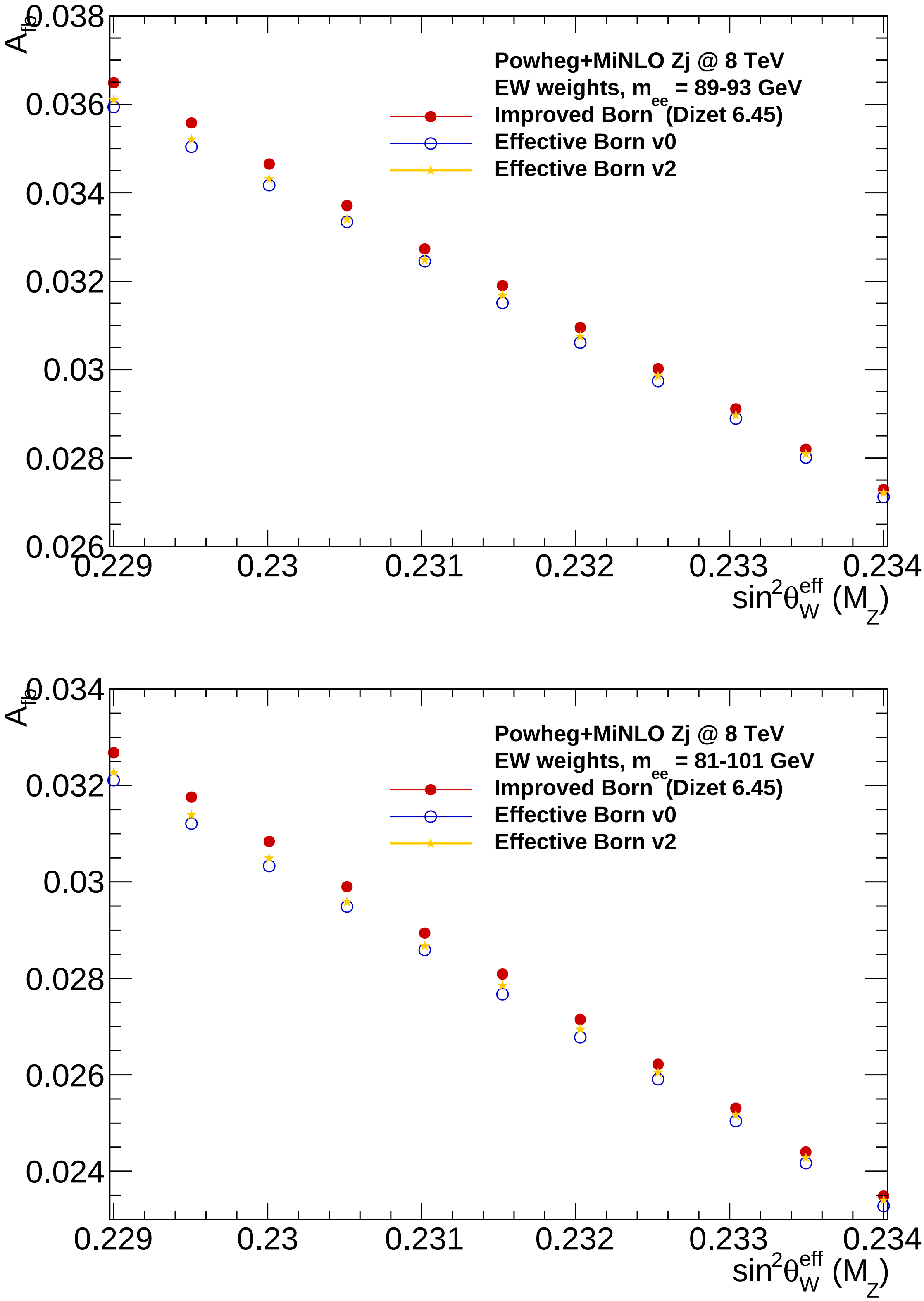

Figure 20: Scan of A_{fb} vs $\sin^2\theta_W^{eff}(M_Z)$ for Improved and Effective Born implementation of wt^{EW} weight. EW forma factors calculated with `Dizet 6.45` library.

Table 29: The binning in M_{bin}, Y_{bin} for tabulating A_4 sensitivity to $\sin^2\theta_W^{eff}$.

Observable	Bin thresholds
M_{bin}	[60, 66, 76, 86, 96, 106, 116, 150] GeV
Y_{bin}	[0.0, 0.4, 0.8, 1.2, 1.6, 2.0, 2.4, 2.8, 3.2, 3.6]

E.9 The A_4 in the full phase-space and with experimental bining.

The `Powheg+MiNLO` Zj sample have been used to calculate predicted A_4 in the full phase space, in the experimental bins of lepton pair M_{bin}, Y_{bin}. Binning used is specified in Table 29:

In Tables 30 and 31 shown are predictions for A_4 with full EW corrections applied using `TauSpinner` weight wt^{EW}. In Tables 32 and 33 shown are predictions using Effective Born v0. In Tables 34 and 35 shown are just ΔA_4 for $\Delta\sin^2\theta_W = +0.00050$, estimated with Full EW corrections and Effective Born v0.

Figure 21 show respectively A_4 (top plot), the ΔA_4 between full EW corrections and Effective Born v0 (middle plot) and ΔA_4 for $\Delta\sin^2\theta_W = \pm 0.00050$ vs nominal value art Z-pole. Shown on 1D histograms with horisontal axis representing bins in (M, Y) as specifie in Table 29.

Table 30: The A_4 caculated including full EW corrections, in experimental bins M_{bin}, Y_{bin}. *Updated with* `Dizet 6.45` *form factors.*

M_{bin}, Y_{bin}	$\sin^2\theta_W^{eff} = 0.23100$	$\sin^2\theta_W^{eff} = 0.23150$	$\sin^2\theta_W^{eff} = 0.23200$	Δ_P	Δ_M
1 , 1	-0.04712	-0.04716	-0.04720	0.00004	-0.00004
1 , 2	-0.13503	-0.13515	-0.13528	0.00012	-0.00012
1 , 3	-0.24463	-0.24485	-0.24506	0.00021	-0.00021
1 , 4	-0.37830	-0.37862	-0.37893	0.00032	-0.00032
1 , 5	-0.52417	-0.52461	-0.52505	0.00044	-0.00045
1 , 6	-0.69617	-0.69676	-0.69735	0.00059	-0.00059
1 , 7	-0.87865	-0.87940	-0.88013	0.00074	-0.00075
1 , 8	-1.04540	-1.04630	-1.04719	0.00089	-0.00090
1 , 9	-1.22346	-1.22447	-1.22548	0.00100	-0.00101
2 , 1	-0.04599	-0.04610	-0.04621	0.00011	-0.00011
2 , 2	-0.15099	-0.15133	-0.15168	0.00035	-0.00035
2 , 3	-0.25526	-0.25587	-0.25648	0.00061	-0.00061
2 , 4	-0.41167	-0.41258	-0.41349	0.00091	-0.00091
2 , 5	-0.56949	-0.57077	-0.57204	0.00127	-0.00128
2 , 6	-0.76368	-0.76537	-0.76705	0.00168	-0.00169
2 , 7	-0.97291	-0.97501	-0.97710	0.00209	-0.00210
2 , 8	-1.17256	-1.17506	-1.17755	0.00249	-0.00250
2 , 9	-1.35532	-1.35813	-1.36092	0.00279	-0.00281
3 , 1	-0.02223	-0.02245	-0.02267	0.00022	-0.00022
3 , 2	-0.07747	-0.07815	-0.07884	0.00068	-0.00068
3 , 3	-0.13806	-0.13926	-0.14046	0.00120	-0.00120
3 , 4	-0.20723	-0.20904	-0.21085	0.00181	-0.00181
3 , 5	-0.28220	-0.28473	-0.28726	0.00253	-0.00253
3 , 6	-0.38354	-0.38690	-0.39024	0.00335	-0.00335
3 , 7	-0.49968	-0.50390	-0.50810	0.00421	-0.00421
3 , 8	-0.61852	-0.62357	-0.62861	0.00504	-0.00505
3 , 9	-0.72616	-0.73188	-0.73758	0.00571	-0.00572
4 , 1	0.00742	0.00721	0.00691	0.00030	-0.00021
4 , 2	0.02350	0.02285	0.02204	0.00081	-0.00065
4 , 3	0.04065	0.03950	0.03811	0.00139	-0.00114
4 , 4	0.06283	0.06111	0.05904	0.00207	-0.00172
4 , 5	0.08847	0.08604	0.08324	0.00280	-0.00243
4 , 6	0.11597	0.11267	0.10908	0.00359	-0.00330
4 , 7	0.14134	0.13709	0.13271	0.00438	-0.00424
4 , 8	0.16457	0.15941	0.15424	0.00517	-0.00516
4 , 9	0.18159	0.17575	0.16990	0.00585	-0.00584
5 , 1	0.03252	0.03232	0.03213	0.00020	-0.00020
5 , 2	0.11502	0.11441	0.11380	0.00061	-0.00061
5 , 3	0.19154	0.19047	0.18940	0.00107	-0.00107
5 , 4	0.28932	0.28773	0.28612	0.00160	-0.00160
5 , 5	0.39524	0.39303	0.39083	0.00220	-0.00220
5 , 6	0.52786	0.52499	0.52213	0.00287	-0.00286
5 , 7	0.66747	0.66395	0.66042	0.00353	-0.00352
5 , 8	0.77857	0.77447	0.77035	0.00411	-0.00411
5 , 9	0.86671	0.86218	0.85764	0.00454	-0.00453

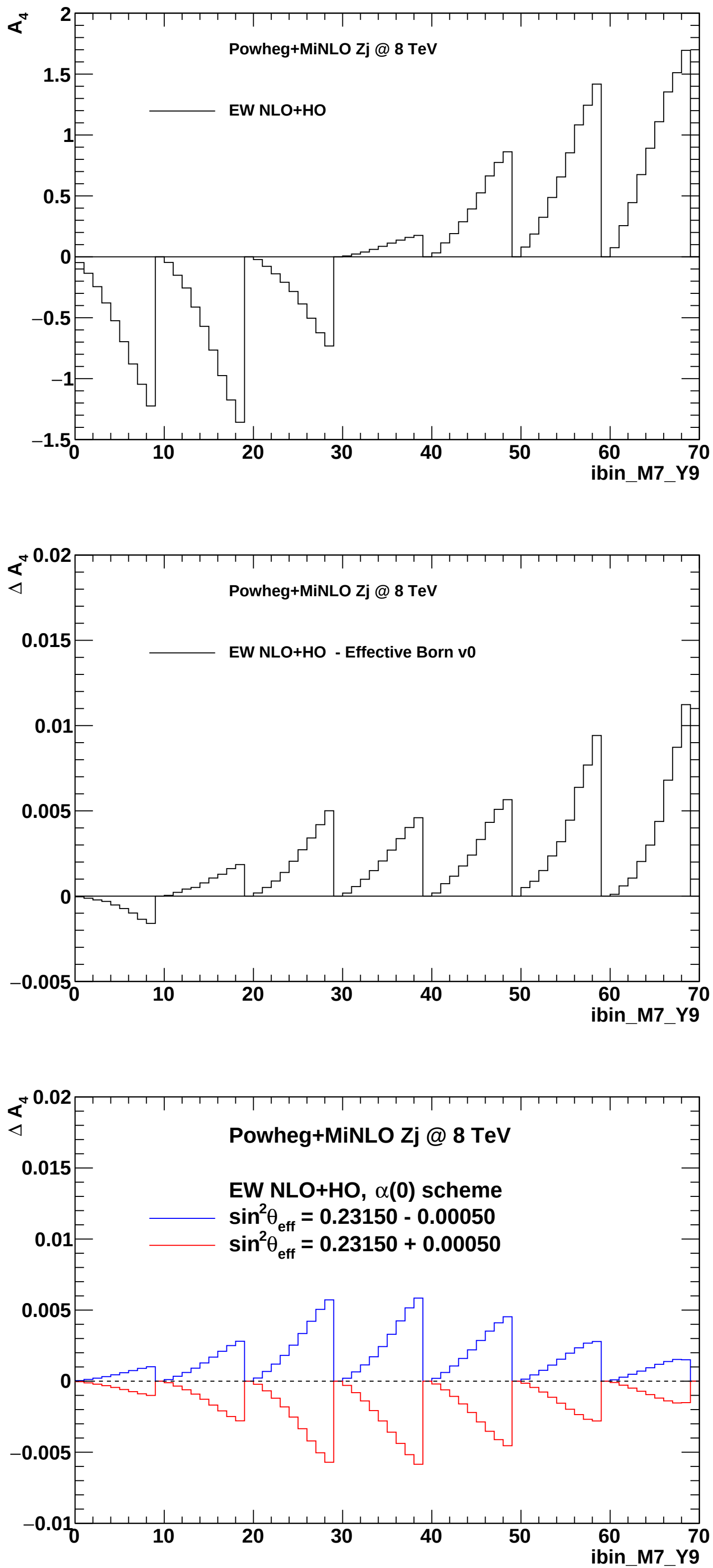

Figure 21: Predictions for A_4 (top), ΔA_4 between full EW corrections and Effective Born v0 (middle), and ΔA_4 for $\Delta \sin^2\theta_W = \pm 0.00050$ vs nominal value at Z-pole. Shown on 1D histograms with horisontal axis representing bins in (M,Y) as specifie in Table 29.

Table 31: The A_4 caculated including full EW corrections, in experimental bins M_{bin},Y_{bin}. Continuation of Table 30. *Updated with* `Dizet 6.45` *form factors.*

M_{bin},Y_{bin}	$\sin^2\theta_W^{eff} = 0.23100$	$\sin^2\theta_W^{eff} = 0.23150$	$\sin^2\theta_W^{eff} = 0.23200$	Δ_P	Δ_M
6 , 1	0.08041	0.08027	0.08013	0.00014	-0.00014
6 , 2	0.18749	0.18705	0.18660	0.00044	-0.00044
6 , 3	0.32530	0.32454	0.32378	0.00076	-0.00076
6 , 4	0.48828	0.48715	0.48602	0.00113	-0.00113
6 , 5	0.65712	0.65557	0.65402	0.00155	-0.00155
6 , 6	0.85586	0.85389	0.85191	0.00198	-0.00197
6 , 7	1.08547	1.08313	1.08078	0.00235	-0.00234
6 , 8	1.24701	1.24433	1.24165	0.00268	-0.00267
6 , 9	1.42075	1.41796	1.41516	0.00280	-0.00279
7 , 1	0.07507	0.07498	0.07489	0.00009	-0.00009
7 , 2	0.25610	0.25582	0.25553	0.00028	-0.00028
7 , 3	0.44532	0.44484	0.44435	0.00049	-0.00049
7 , 4	0.67565	0.67494	0.67423	0.00071	-0.00071
7 , 5	0.89229	0.89135	0.89041	0.00095	-0.00094
7 , 6	1.11025	1.10907	1.10788	0.00119	-0.00119
7 , 7	1.35502	1.35364	1.35226	0.00139	-0.00138
7 , 8	1.51281	1.51129	1.50975	0.00153	-0.00153
7 , 9	1.69631	1.69481	1.69330	0.00151	-0.00150

Table 32: The A_4 caculated with Effective Born v0, in experimental bins M_{bin}, Y_{bin}.

M_{bin}, Y_{bin}	$\sin^2\theta_W^{eff} = 0.23100$	$\sin^2\theta_W^{eff} = 0.23150$	$\sin^2\theta_W^{eff} = 0.23200$	Δ_P	Δ_M
1 , 1	-0.04709	-0.04713	-0.04716	0.00004	-0.00004
1 , 2	-0.13492	-0.13503	-0.13514	0.00011	-0.00011
1 , 3	-0.24443	-0.24462	-0.24482	0.00019	-0.00020
1 , 4	-0.37801	-0.37831	-0.37860	0.00029	-0.00029
1 , 5	-0.52369	-0.52409	-0.52450	0.00040	-0.00041
1 , 6	-0.69549	-0.69604	-0.69657	0.00054	-0.00054
1 , 7	-0.87772	-0.87840	-0.87908	0.00068	-0.00068
1 , 8	-1.04412	-1.04494	-1.04576	0.00082	-0.00082
1 , 9	-1.22195	-1.22288	-1.22379	0.00091	-0.00093
2 , 1	-0.04604	-0.04615	-0.04625	0.00010	-0.00010
2 , 2	-0.15122	-0.15155	-0.15188	0.00033	-0.00033
2 , 3	-0.25571	-0.25629	-0.25686	0.00057	-0.00058
2 , 4	-0.41223	-0.41309	-0.41395	0.00086	-0.00086
2 , 5	-0.57033	-0.57154	-0.57274	0.00120	-0.00121
2 , 6	-0.76484	-0.76644	-0.76802	0.00158	-0.00160
2 , 7	-0.97431	-0.97630	-0.97826	0.00197	-0.00198
2 , 8	-1.17431	-1.17667	-1.17901	0.00234	-0.00236
2 , 9	-1.35734	-1.35998	-1.36260	0.00262	-0.00264
3 , 1	-0.02243	-0.02264	-0.02285	0.00021	-0.00021
3 , 2	-0.07801	-0.07866	-0.07932	0.00065	-0.00065
3 , 3	-0.13899	-0.14015	-0.14129	0.00115	-0.00115
3 , 4	-0.20869	-0.21043	-0.21216	0.00173	-0.00174
3 , 5	-0.28436	-0.28678	-0.28920	0.00242	-0.00242
3 , 6	-0.38640	-0.38961	-0.39281	0.00320	-0.00321
3 , 7	-0.50327	-0.50731	-0.51133	0.00402	-0.00404
3 , 8	-0.62293	-0.62776	-0.63257	0.00481	-0.00483
3 , 9	-0.73141	-0.73688	-0.74233	0.00545	-0.00547
4 , 1	0.00725	0.00703	0.00681	0.00022	-0.00022
4 , 2	0.02298	0.02229	0.02155	0.00074	-0.00069
4 , 3	0.03972	0.03851	0.03721	0.00130	-0.00121
4 , 4	0.06141	0.05962	0.05769	0.00193	-0.00179
4 , 5	0.08642	0.08398	0.08135	0.00263	-0.00245
4 , 6	0.11317	0.10997	0.10656	0.00341	-0.00320
4 , 7	0.13780	0.13372	0.12951	0.00422	-0.00407
4 , 8	0.16030	0.15539	0.15042	0.00497	-0.00492
4 , 9	0.17675	0.17115	0.16560	0.00555	-0.00559
5 , 1	0.03233	0.03214	0.03195	0.00019	-0.00019
5 , 2	0.11426	0.11368	0.11310	0.00058	-0.00058
5 , 3	0.19031	0.18930	0.18829	0.00101	-0.00101
5 , 4	0.28747	0.28596	0.28444	0.00151	-0.00151
5 , 5	0.39271	0.39063	0.38854	0.00208	-0.00208
5 , 6	0.52438	0.52167	0.51897	0.00271	-0.00271
5 , 7	0.66295	0.65962	0.65630	0.00332	-0.00333
5 , 8	0.77326	0.76938	0.76551	0.00387	-0.00388
5 , 9	0.86079	0.85652	0.85226	0.00426	-0.00427

Table 33: The A_4 caculated Effective Born v0, in experimental bins M_{bin}, Y_{bin}. Continuation of Table 32.

M_{bin}, Y_{bin}	$\sin^2\theta_W^{eff} = 0.23100$	$\sin^2\theta_W^{eff} = 0.23150$	$\sin^2\theta_W^{eff} = 0.23200$	Δ_P	Δ_M
6 , 1	0.07990	0.07977	0.07963	0.00013	-0.00013
6 , 2	0.18659	0.18618	0.18577	0.00041	-0.00041
6 , 3	0.32375	0.32304	0.32233	0.00071	-0.00071
6 , 4	0.48585	0.48479	0.48374	0.00105	-0.00105
6 , 5	0.65382	0.65238	0.65094	0.00144	-0.00144
6 , 6	0.85126	0.84943	0.84761	0.00183	-0.00183
6 , 7	1.07892	1.07675	1.07458	0.00217	-0.00217
6 , 8	1.23912	1.23665	1.23418	0.00247	-0.00247
6 , 9	1.41110	1.40854	1.40599	0.00256	-0.00256
7 , 1	0.07496	0.07488	0.07479	0.00008	-0.00008
7 , 2	0.25547	0.25521	0.25496	0.00025	-0.00025
7 , 3	0.44422	0.44378	0.44334	0.00044	-0.00044
7 , 4	0.67355	0.67291	0.67228	0.00064	-0.00064
7 , 5	0.88920	0.88836	0.88751	0.00085	-0.00085
7 , 6	1.10575	1.10469	1.10362	0.00106	-0.00106
7 , 7	1.34808	1.34684	1.34561	0.00123	-0.00123
7 , 8	1.50391	1.50256	1.50120	0.00136	-0.00136
7 , 9	1.68489	1.68358	1.68226	0.00131	-0.00132

Table 34: The ΔA_4 for $\Delta \sin^2\theta_W = +0.00050$, estimated with full EW corrections and Effective Born v0, in experimental bins M_{bin}, Y_{bin}. *Updated with* `Dizet 6.45` *form factors.*

M_{bin}, Y_{bin}	ΔA_4 (full EW)	ΔA_4 (Effective v0)
1 , 1	0.00004	0.00004
1 , 2	0.00012	0.00011
1 , 3	0.00021	0.00019
1 , 4	0.00032	0.00029
1 , 5	0.00044	0.00040
1 , 6	0.00059	0.00054
1 , 7	0.00074	0.00068
1 , 8	0.00089	0.00082
1 , 9	0.00100	0.00091
2 , 1	0.00011	0.00010
2 , 2	0.00035	0.00033
2 , 3	0.00061	0.00057
2 , 4	0.00091	0.00086
2 , 5	0.00127	0.00120
2 , 6	0.00168	0.00158
2 , 7	0.00209	0.00197
2 , 8	0.00249	0.00234
2 , 9	0.00279	0.00262
3 , 1	0.00022	0.00021
3 , 2	0.00068	0.00065
3 , 3	0.00120	0.00115
3 , 4	0.00181	0.00173
3 , 5	0.00253	0.00242
3 , 6	0.00335	0.00320
3 , 7	0.00421	0.00402
3 , 8	0.00504	0.00481
3 , 9	0.00571	0.00545
4 , 1	0.00030	0.00022
4 , 2	0.00081	0.00074
4 , 3	0.00139	0.00130
4 , 4	0.00207	0.00193
4 , 5	0.00280	0.00263
4 , 6	0.00359	0.00341
4 , 7	0.00438	0.00422
4 , 8	0.00517	0.00497
4 , 9	0.00585	0.00555
5 , 1	0.00020	0.00019
5 , 2	0.00061	0.00058
5 , 3	0.00107	0.00101
5 , 4	0.00160	0.00151
5 , 5	0.00220	0.00208
5 , 6	0.00287	0.00271
5 , 7	0.00353	0.00332
5 , 8	0.00411	0.00387
5 , 9	0.00454	0.00426

Table 35: The ΔA_4 for for $\Delta \sin^2\theta_W = +0.00050$, estimated with full EW corrections and Effective Born v0, in experimental bins M_{bin}, Y_{bin}. Continuation of Table 34. *Updated with* `Dizet 6.45` *form factors.*

M_{bin}, Y_{bin}	ΔA_4 (full EW)	ΔA_4 (Effective v0)
6 , 1	0.00014	0.00013
6 , 2	0.00044	0.00041
6 , 3	0.00076	0.00071
6 , 4	0.00113	0.00105
6 , 5	0.00155	0.00144
6 , 6	0.00198	0.00183
6 , 7	0.00235	0.00217
6 , 8	0.00268	0.00247
6 , 9	0.00280	0.00256
7 , 1	0.00009	0.00008
7 , 2	0.00028	0.00025
7 , 3	0.00049	0.00044
7 , 4	0.00071	0.00064
7 , 5	0.00095	0.00085
7 , 6	0.00119	0.00106
7 , 7	0.00139	0.00123
7 , 8	0.00153	0.00136
7 , 9	0.00151	0.00131

F Powheg_ew

Comments:
This text should be completed by the authors, for now as placeholders some tables from past meetings.
Recently presented materials:
https://indico.cern.ch/event/829225/contributions/3481094/attachments/1871705/3080271/piccinini.pdf

Details (for benchmarking with other codes in G_μ scheme):

- PDF set: MSTW2008nlo68cl PDF set, member number 0, version 2; LHAPDF ID = 21100
- Fact/ren scales: virtuality of the (born) leptonic pair i.e. when there is QED FSR it is the virtuality of the l lbar gamma system
- Deltar = 2.97632672697318683E-002
- Re(delta alpha(60.000000000000000)) = 5.46493045419893034E-002
  1/alpha(60) = 129.54706939050510 neglecting the imaginary part
- Re(delta alpha (91.153480619182758)) = 5.89760567146062550E-002 1/alpha(MZ) = 128.95414861873800 neglecting the imaginary part

F.1 Benchmark results for different EW schemes

Comments:
Those tables should be completed by the authors, for now as placeholders.
Recently presented materials:
https://indico.cern.ch/event/829225/contributions/3481094/attachments/1871705/3080271/piccinini.pdf

Tables:

- Table 36: Cross-section and cross-section ratios at EW LO, NLO, NLO+HO, different EW schemes, `Powheg_ew` Monte Carlo. *Status of December 2018.*
- Table 37: Cross-sections, cross-sections difference in forward and backward hemispheres and forward-backward asymmetry, `Powheg_ew` Monte Carlo, EW LO, NLO, NLO+HO, different schemes.*Status of December 2018.*
- Table 38: Forward-backward asymmetry differences between different EW schemes, as estimated by `Powheg_ew`, different EW schemes at LO, NLO, NLO+HO.*Status of December 2018.*

Table 36: Cross-sections and cross-sections ratios estimated with `Powheg_ew` for three mass windows. The pole definition is used for input parameters as in Table 14.

	EW order	m_{ee} = 89 - 93 GeV	m_{ee} = 80 - 100 GeV	m_{ee} = 70 - 120 GeV
$\alpha(0)$ v0	LO	630.848722	906.156051	959.658977
$\alpha(0)$ v1	LO	571.411296	821.363274	870.729908
G_μ	LO	612.514433	880.446121	933.363827
$\alpha(0)$ v1	NLO	600.185042	863.142557	915.580114
G_μ	NLO	607.142292	873.173294	926.253246
$\alpha(0)$ v1	NLO+HO	607.551746	873.717147	926.761229
G_μ	NLO+HO	607.515354	873.655348	926.681425
$\alpha(0)$ v1	NLO/LO	1.050350	1.05087	1.05151
G_μ	NLO/LO	0.991230	0.99174	0.99238
$\alpha(0)$ v1	NLO+HO/LO	1.063247	1.063740	1.064349
G_μ	NLO+HO/LO	0.991038	0.992287	0.992840
$\alpha(0)$ v1 / $\alpha(0)$ v0	LO	0.90578	0.906426	0.90733
G_μ / $\alpha(0)$ v1	LO	1.07193	1.07193	1.07193
G_μ / $\alpha(0)$ v1	NLO	1.01159	1.01162	1.01166
G_μ / $\alpha(0)$ v1	NLO+HO	0.99994	0.99993	0.99991
G_μ / $\alpha(0)$ v0	LO	0.97094	0.97163	0.97260

Table 37: Cross-sections, cross-sections difference in forward and backward hemispheres and forward-backward asymmetry as estimated by `Powheg_ew`, for three mass windows. The pole definition is used for input parameters as in Table 14.

	EW order	m_{ee} = 89 - 93 GeV	m_{ee} = 80 - 100 GeV	m_{ee} = 70 - 120 GeV
σ $\alpha(0)$ v0	LO	630.848722	906.156051	959.658977
σ $\alpha(0)$ v1	LO	571.411296	821.363274	870.729908
σ G_μ	LO	612.514433	880.446121	933.363827
Δ_{FB} σ $\alpha(0)$ v0	LO	42.2123628	57.9248406	60.0147094
Δ_{FB} σ $\alpha(0)$ v1	LO	26.5928310	35.6782853	36.6828324
Δ_{FB} σ G_μ	LO	42.2123628	57.9248406	60.0147094
A_{FB} $\alpha(0)$ v0	LO	0.06691361	0.06392369	0.06253754
A_{FB} $\alpha(0)$ v1	LO	0.04653886	0.04343789	0.04212883
A_{FB} G_μ	LO	0.04653886	0.04343789	0.04212883
σ $\alpha(0)$ v1	NLO	600.185042	863.142557	915.580114
σ G_μ	NLO	607.142292	873.173294	926.253246
Δ_{FB} σ $\alpha(0)$ v1	NLO	18.0312902	23.2253069	23.5291169
Δ_{FB} σ G_μ	NLO	17.6425904	22.6341188	22.8962216
A_{FB} $\alpha(0)$ v1	NLO	0.03004289	0.02690785	0.02569858
A_{FB} G_μ	NLO	0.02905841	0.02592168	0.02471918
ΔA_{FB} $\alpha(0)$ v1	NLO-LO	-0.0164959	-0.0165300	-0.0164302
ΔA_{FB} G_μ	NLO-LO	-0.0174805	-0.0175162	-0.0174096
σ $\alpha(0)$ v1	NLO+HO	607.551746	873.717147	926.761229
σ G_μ	NLO+HO	607.515356	873.655348	926.681425
Δ_{FB} σ $\alpha(0)$ v1	NLO+HO	18.7322427	24.2066243	24.5563891
Δ_{FB} σ G_μ	NLO+HO	18.7739638	24.2682506	24.6205407
A_{FB} $\alpha(0)$ v1	NLO+HO	0.03083234	0.02770533	0.02649700
A_{FB} G_μ	NLO+HO	0.03090286	0.02777783	0.02656851
ΔA_{FB} $\alpha(0)$ v1	NLO+HO-LO	-0.0157065	-0.0157326	-0.0156318
ΔA_{FB} G_μ	NLO+HO-LO	-0.0156360	-0.0156596	-0.0155603

Table 38: Forward-backward asymmetry differences between different EW schemes, as estimated by `Powheg_ew`, for three mass windows. The pole definition is used for input parameters as in Table 14.

ΔA_{FB}	EW order	m_{ee} = 89 - 93 GeV	m_{ee} = 80 - 100 GeV	m_{ee} = 70 - 120 GeV
$\alpha(0)$ v1 - $\alpha(0)$ v0	LO	-0.020375	-0.020486	-0.020487
G_μ - $\alpha(0)$ v0	LO	-0.020375	-0.020486	-0.0204871
G_μ - $\alpha(0)$ v1	LO	0.0	0.0	0.0
G_μ - $\alpha(0)$ v1	NLO	-0.00098	-0.00098	-0.00098
G_μ - $\alpha(0)$ v1	NLO + HO	-0.00007	-0.00007	-0.00007

G MCSANC

Comments:
This text should be completed by the authors, for now as placeholders some tables from past meetings.
Recently presented materials:

G.1 Benchmark results for different EW schemes

Table 39: Cross-sections and cross-sections ratios estimated with `MCSANC` for three mass windows. The pole mass definition is used for input parameters as in Table 14.
Numbers updated on 16.10.2019 to configuration of that Table.

σ [pb]	EW order	m_{ee} = 89 - 93 GeV	m_{ee} = 80 - 100 GeV	m_{ee} = 70 - 120 GeV
$\alpha(0)$ v1	LO	571.41(1)	821.36(1)	870.72(1)
G_μ	LO	612.53(1)	880.47(1)	933.39(1)
$\alpha(0)$ v1	NLO	600.08(1)	863.00(1)	915.42(1)
G_μ	NLO	607.41(1)	873.57(1)	926.66(1)
$\alpha(0)$ v1	NLO+HO			
G_μ	NLO+HO			
$\alpha(0)$ v1	NLO/LO	1.05017	1.05070	1.05134
G_μ	NLO/LO	0.991641	0.992163	0.992790
$\alpha(0)$ v1	NLO+HO/LO			
G_μ	NLO+HO/LO			
G_μ / $\alpha(0)$ v1	LO	1.071962	1.071966	1.071975
G_μ / $\alpha(0)$ v1	NLO	1.012215	1.012245	1.012278
G_μ / $\alpha(0)$ v1	NLO+HO			

Table 40: Forward-backward asymmetry and differences estimated with `MCSANC` for three mass windows. The pole mass definition is used for input parameters as in Table 14.
Numbers updated on 16.10.2019 to configuration of that Table.

A_{FB}	EW order	m_{ee} = 89 - 93 GeV	m_{ee} = 80 - 100 GeV	m_{ee} = 70 - 120 GeV
$\alpha(0)$ v1	LO	0.004655(1)	0.004347(1)	0.004215(1)
G_μ	LO	0.004656(1)	0.004347(1)	0.004215(1)
$\alpha(0)$ v1	NLO	0.003058(1)	0.002746(1)	0.002623(1)
G_μ	NLO	0.002964(1)	0.002652(1)	0.002530(1)
$\alpha(0)$ v1	NLO+HO			
G_μ	NLO+HO			
$\alpha(0)$ v1	NLO - LO	-0.001597(1)	-0.001601(1)	-0.001591(1)
G_μ	NLO - LO	-0.001691(1)	-0.001695(1)	-0.001685(1)
$\alpha(0)$ v1	NLO+HO - LO			
G_μ	NLO+HO - LO			
G_μ - $\alpha(0)$ v1	LO	0.0	0.0	0.0
G_μ - $\alpha(0)$ v1	NLO	0.000094	0.000094	0.000093
G_μ - $\alpha(0)$ v1	NLO+HO			

Table 41: The $\sin^2\theta_W^{eff}$ predictions in EW G_μ scheme.

$\sin^2\theta_W^{eff}$	EW LO	EW NLO	EW NLO+HO	Comments
lepton	0.2228972225239183	0.2323557983674498		
neutrino	0.2228972225239183	0.2320009933224815		
up-quark	0.2228972225239183	0.2322559935838819		
down-quark	0.2228972225239183	0.2321377252355592		
bottom-quark	0.2228972225239183	0.2337274233845253		

H Results from analytical programs

These results were prepared by S. Dittmaier, come from private code.

I KKMC_hh

This test is from proceedings contribution at RADCOR 2019 conference S.A/Yost et al. ISR and IFI in Precision AFB Studies with KKMC-hh

$\mathcal{KK}$MC-hh is a hadronic event generator for Z boson production and decays, which includes exponentiated multi-photon radiation and first-order electroweak corrections. We have used $\mathcal{KK}$MC-hh to investigate the role of initial sate radiation (ISR) and initial-final interference (IFI) in precision electroweak analyses at the LHC. We compare the effect of this radiation on angular distributions and forward-backward asymmetry, which are particularly important for the measurement of the weak mixing angle. We discuss the relation of the ISR implementation in $\mathcal{KK}$MC-hh to ISR from parton distribution functions with QED corrections.

I.1 Introduction

Angular distributions for $pp \to Z/\gamma^* \to$ leptons are important for a precision measurement of the weak mixing angle at the LHC. The inputs for calculating the weak mixing angle can come from measurements of the forward-backward asymmetry $A_{\rm FB}$ or the angular coefficient $A_4 = 4\langle\cos\theta\rangle$. In either case, the relevant angle is taken to be the Collins-Soper (CS) angle in the rest frame of the final state lepton pair.[35]

The angular distribution is sensitive to radiative corrections. In the presence of final state radiation (FSR) from the leptons, the photon momenta can be subtracted to find the CM momentum of the Z boson. Initial state radiation (ISR) complicates this because it cannot be unambiguously distinguished from FSR. ISR also interferes with FSR at the quantum level, and this initial-final interference (IFI) creates an ambiguity in the Z boson rest frame that cannot be resolved, even in principle. These radiative effects are presently under investigation using a variety of programs in addition to $\mathcal{KK}$MC-hh, including POWHEG-EW[37] and MC-SANC[18, 19].

We present studies of radiative corrections to angular distributions using $\mathcal{KK}$MC-hh[38], a hadronic event generator based on CEEX[39], an amplitude-level soft photon exponentiation scheme originally developed for electron-positron collisions in the LEP era, which implemented for e^+e^- scattering in the $\mathcal{KK}$MC generator[10] and extended to quark initial states in $\mathcal{KK}$MC 4.22[4]. CEEX is similar to YFS soft photon exponentiation[24], but implemented at the amplitude level rather than the cross section level, which facilitates the exponentiation of interference effects, in particular IFI. An extensive review and explanation of the implementation of IFI in the CEEX framework can be found in Ref. [40].

$\mathcal{KK}$MC-hh events can be exported in an LHE-compatible [41] event record and showered by any external shower generator, or they can be showered by an internal implementation of HERWIG 6.5[42]. This assumes an approximation in which QCD and QED effects factorize, which is true at leading log and should be a good approximation at $O(\alpha_s\alpha)$.[43, 44, 45] Unshowered events will be presented here, since the number of events needed to see the effect of radiative corrections on $A_{\rm FB}$ or A_4 is on the order of 10^9 or more, requiring substantial computer resources, especially in the presence of the shower. A smaller sample of showered events was included in the RADCOR 2019 by S. A. Yost, but was not discussed in detail and is not included here. It is expected that those results will be included in a more detailed analysis to be published soon.

$\mathcal{KK}$MC-hh includes an *ab initio* calculation of QED radiation including quark masses, so that the results are finite in the collinear limit. This differs from other programs capable of addressing ISR effects in hadron scattering, such as POWHEG-EW, MC-SANC, Horace [46, 47], and ZGRAD2 [48], which factorize collinear QED radiation with the assumption that its effect is included in the parton distribution functions (PDFs). Factorizing the collinear QED has the advantage of avoiding the issue of quark masses, but setting a high factorization scale could limit the ability to address non-collinear ISR. Also, such factorization is not readily combined with CEEX soft photon exponentiation in $\mathcal{KK}$MC-hh.

Including quark masses in the calculation raises the question of what value should be assigned to them. The first parton distributions to include QED corrections was the MRST QED PDF set[49], which assumed current quark masses. This is consistent with the expectation that for deep inelastic scattering, the colliding quarks couple perturbatively to the spectator quarks, so that the recoil when a photon is emitted should be governed by the current quark mass, not the constituent mass. However, some controversy remains on this issue, which was addressed in a study[50] applying $\mathcal{KK}$MC-hh to LHC phenomenology relevant to the W mass measurement by varying the quark masses. The mass dependence is logarithmic, so varying the light quark masses by a factor of 10 only changes the ISR contribution by about 10%. Since ISR typically contributes at the order of around 0.1% for most distributions, the mass dependence is usually insignificant.

I.2 The Effect of Initial-State QED Radiation on Angular Distributions

In this section, we focus on CS angle distributions, particularly A_{FB} and A_4, and compare the effect of including QED corrections in the PDFs to the effect of adding ISR via $\mathcal{KK}$MC-hh. All results are from $\mathcal{KK}$MC-hh runs without a QCD shower, producing 5.7×10^9 muon events at 8 TeV. Since $\mathcal{KK}$MC-hh includes collinear ISR, it must be used with pure-QCD parton distributions. These runs use NNPDF3.1[51] ($\alpha_s(M_Z) = 0.21018$). For comparison, we also show results for $\mathcal{KK}$MC-hh with ISR off, but with a NNPDF3.1luxQED[52] parton distribution functions, which include LuxQED photon ISR[53].

NLO electroweak corrections are added using DIZET 6.21[2], which uses an input scheme with parameters G_μ, $\alpha(0)$, and M_Z. The quark masses in DIZET are selected internally based on the vacuum polarization option, for which the default fit is used. Photonic radiative corrections are calculated using $\alpha(0)$ and PDG values[16] for the quark current masses. Otherwise, all parameters are consistent with the LHC electroweak benchmark study, Ref. [22].

All results include dilepton mass cut 60 GeV $< M_{ll} <$ 116 GeV, including those labeled "uncut." The "cut" results include an additional constraint $p_{\text{T}} > 25$ GeV on the transverse momentum of each muon, and $|\eta| < 2.5$ on the pseudorapidity of each muon. The forward-backward asymmetry A_{FB} is calculated from the cut events, while A_4 is calculated using uncut events. Final state radiation is included in all cases. Initial-final interference (IFI) is not included. IFI effects are discussed separately in the next section. In Table 1, the column labeled "No ISR" have ISR turned off in $\mathcal{KK}$MC-hh and use a non-QED NNPDF3.1 set. The LuxQED column has ISR turned off in $\mathcal{KK}$MC-hh and uses the NNPDF3.1luxQED. The "$\mathcal{KK}$MC-hh ISR" column has ISR turned on in $\mathcal{KK}$MC-hh and uses a non-QED NNPDF3.1 set. Differences are shown comparing ISR on and off both ways, using LuxQED or $\mathcal{KK}$MC-hh. In the case of the cross-section, the differences are shown as percentages, while for the asymmetries, the straight differences are shown.

	No ISR	LuxQED ISR	LuxQED−no ISR	$\mathcal{KK}$MC-hh ISR	ISR−no ISR
Uncut σ	939.858(7) pb	944.038(7) pb	0.445(1)%	944.99(2) pb	0.546(2)%
Cut σ	439.103(7) pb	440.926(7) pb	0.415(1)%	442.36(1) pb	0.742(3)%
A_{FB}	0.01125(3)	0.01145(2)	$(1.9 \pm 0.3) \times 10^{-4}$	0.1129(2)	$(3.9 \pm 2.8) \times 10^{-5}$
A_4	0.06102(4)	0.06131(3)	$(2.9 \pm 0.5) \times 10^{-4}$	0.06057(3)	$(-4.4 \pm 0.5) \times 10^{-4}$

Table 1. Effect of ISR added via LuxQED or $\mathcal{KK}$MC-hh

Both LuxQED and $\mathcal{KK}$MC-hh show that ISR shifts the cut and uncut cross-section by about half a percent, with differences on the order of a per-mil. LuxQED also shows a shift in A_{FB} and A_4 on the order of a few per-mil, but the ISR effect in $\mathcal{KK}$MC-hh is much smaller for A_{FB}, and has the opposite sign for A_4.

Figures 1 and 2 compare Collins-Soper angular distributions $\cos(\theta_{\text{CS}})$ in three cases: "FSR only" has no ISR and a non- QED PDF set, "FSR + ISR" includes $\mathcal{KK}$MC-hh ISR with a non-QED PDF set, and "FSR + LuxQED" uses a LuxQED PDF set with no ISR from $\mathcal{KK}$MC-hh. Fig. 1 does not include the additional lepton cuts, and is the distribution relevant to A_4, while Fig. 2 includes the lepton cuts, and is relevant to A_{FB}.

Figures 3 and 4 show the effect of ISR on A_{FB} as a function of the dilepton mass and rapidity, respectively. In Fig. 3, the ISR contribution to A_{FB} is less than 10^{-3} for the entire range of M_{ll}, and in the vicinity of $M_Z \approx 91$ GeV, it is less than 3×10^{-4}, for both LuxQED and $\mathcal{KK}$MC-hh. In Fig. 4, the ISR effect from $\mathcal{KK}$MC-hh is below 10^{-4} in all bins, and consistent with zero in the central bin. However, LuxQED would give a larger ISR contribution for $Y_{ll} < 2$.

Figures 5 and 6 show the effect of ISR on A_4 as a function of the dilepton mass and rapidity. In Fig. 6, the ISR contribution is again typically of order 10^{-3}, and $\mathcal{KK}$MC-hh shows that it is approximately consistent with zero in the vicinity of M_Z. In Fig. 7, the ISR contribution from $\mathcal{KK}$MC-hh increases for large rapidity, but is on the order of 10^{-4} for $Y_{ll} < 2$. The LuxQED prediction is consistently below 5×10^{-4}, but significantly different from $\mathcal{KK}$MC-hh.

I.3 The Effect of Initial-Final Interference on Angular Distributions

In this section, we consider the effect of quantum interference between initial and final state QED radiation (IFI) on the CS angular distributions, forward-backward asymmetry, and A_4. The use of A_{FB} or A_4 in determining the weak mixing angle is complicated by IFI, it a quantum uncertainty in any attempt to back out FSR from the

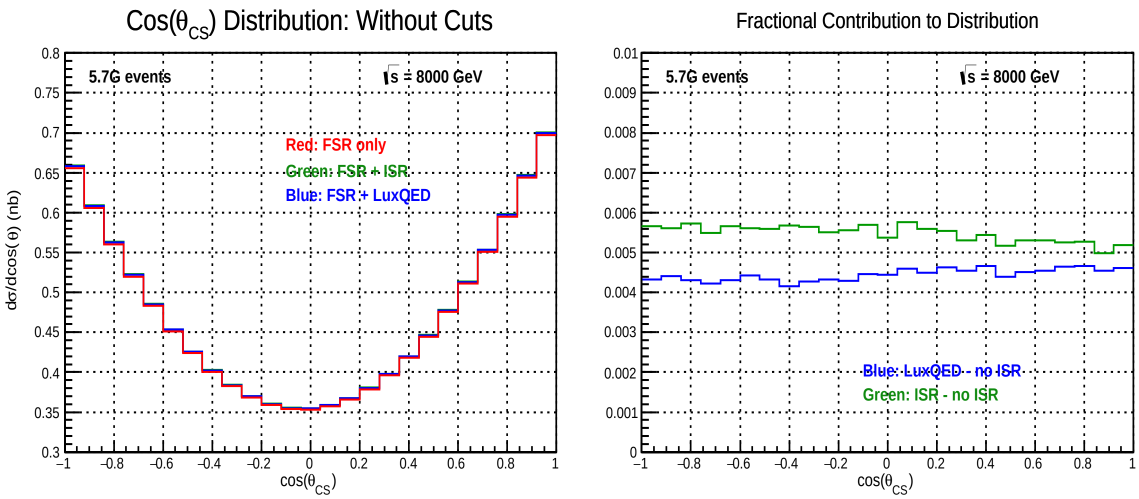

Figure 22: ISR contributions to $\cos(\theta_{\mathrm{CS}})$ distributions, without lepton cuts.

measurement.

All comparisons are without a QCD shower and use NNPDF3.1 parton distributions without QED corrections, since these are included in $\mathcal{KK}$MC-hh. The parameters are the same as in the previous section.

Table 2 shows the effect of ISR on the uncut and cut cross sections as well as on the forward-backward asymmetry A_{FB} and on A_4. The differences are shown relative to $\mathcal{KK}$MC-hh with both ISR and ISR on, but IFI off. For the cross sections, percent differences are shown, while for the asymmetries, the differences are shown directly. The comparisons were calculated within a single run by reweighting, and the errors take into account the weight correlations, which reduce the uncertainty.

	without IFI	with IFI	difference
uncut σ	944.99(2)	944.91(2)	$-0.0089(4)\%$
cut σ	442.36(1)	442.33(1)	$-0.0070(5)\%$
A_{FB}	0.01129(2)	0.01132(2)	$(2.9 \pm 1.1) \times 10^{-5}$
A_4	0.06057(3)	0.061024	$(4.5 \pm 0.3) \times 10^{-4}$

Table 2. Effect of Initial-Final Interference

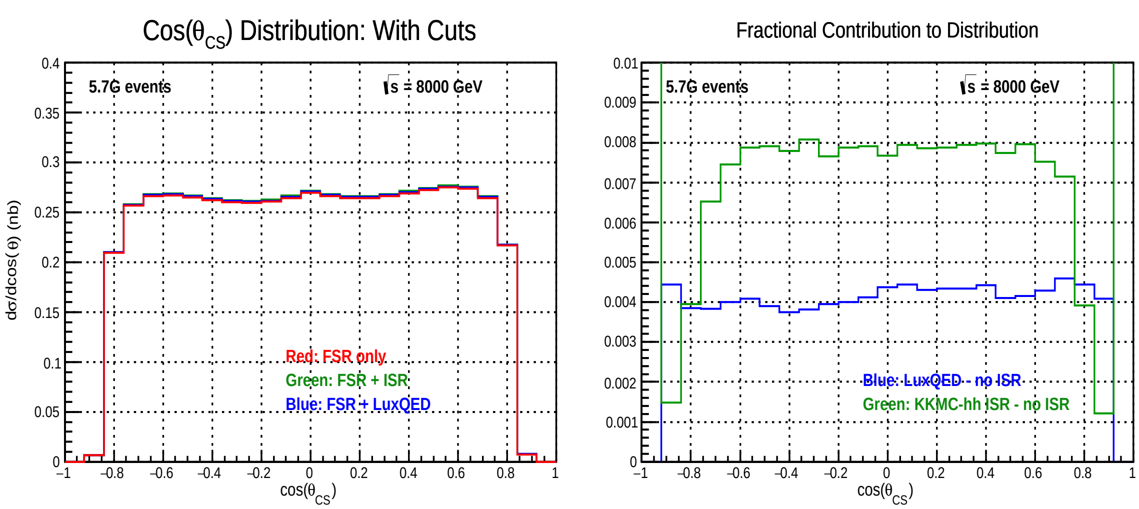

Figure 23: ISR contributions to $\cos(\theta_{\mathrm{CS}})$ distributions, with lepton cuts.

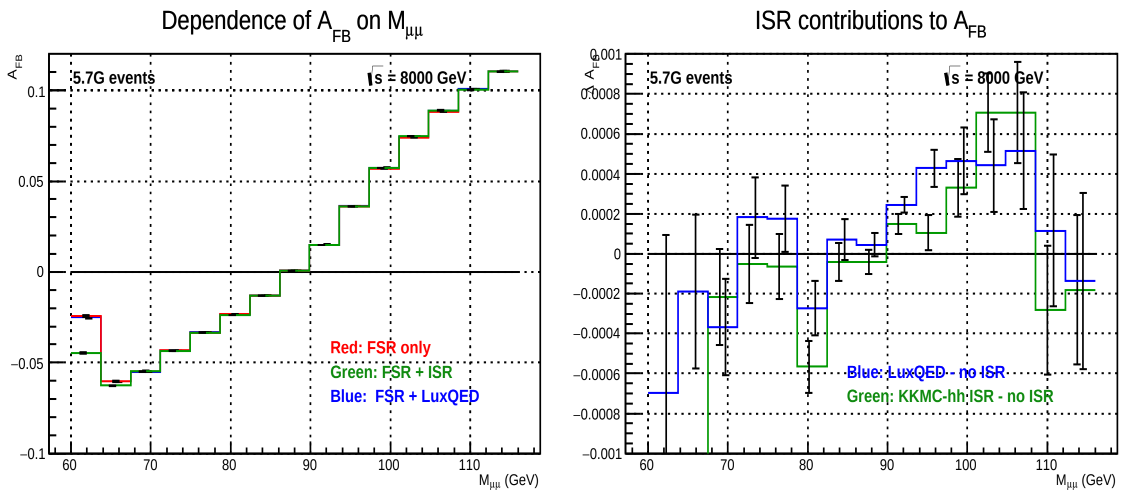

Figure 24: Effect of ISR on $A_{\rm FB}$in terms of dilepton mass.

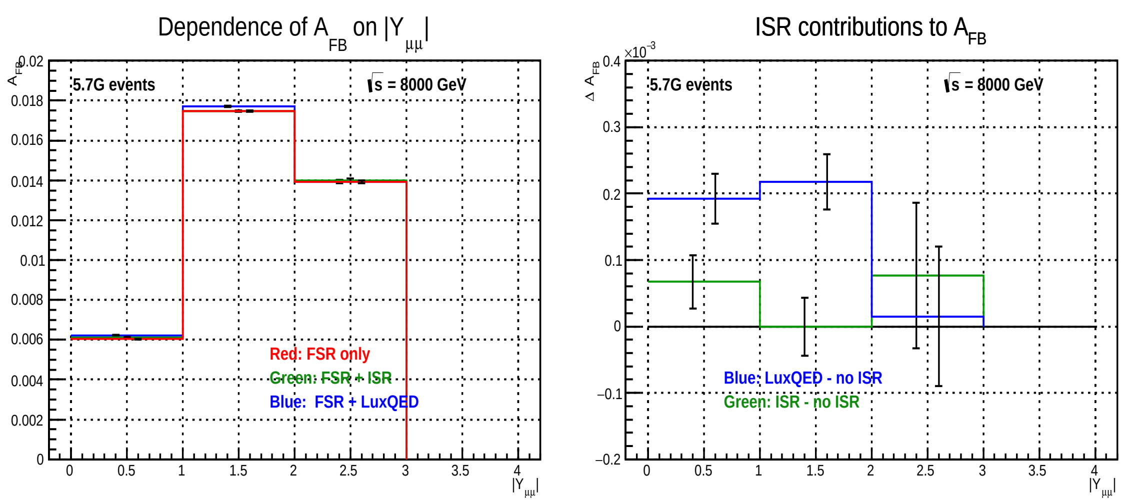

Figure 25: Effect of ISR on $A_{\rm FB}$in terms of dilepton rapidity.

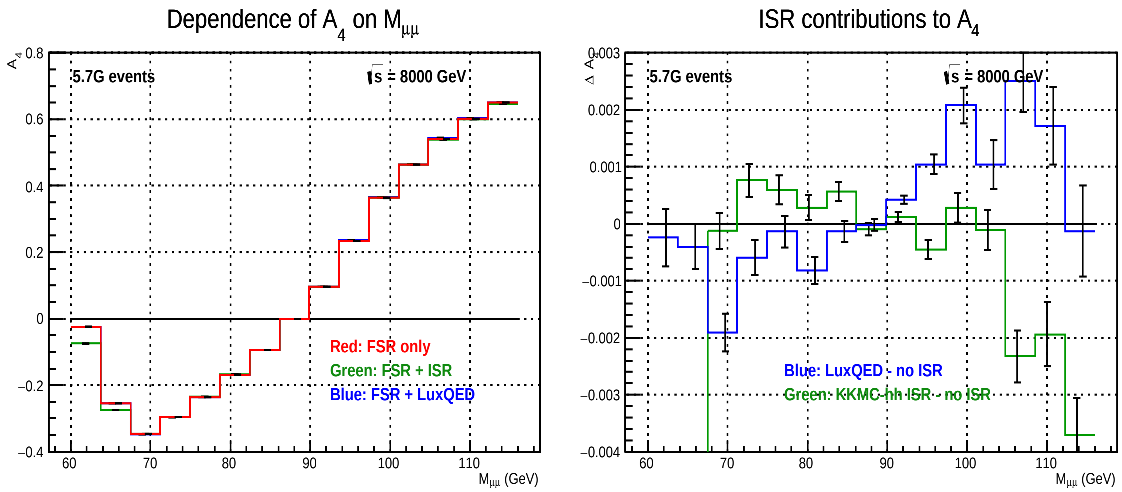

Figure 26: Effect of ISR on A_4 in terms of dilepton mass.

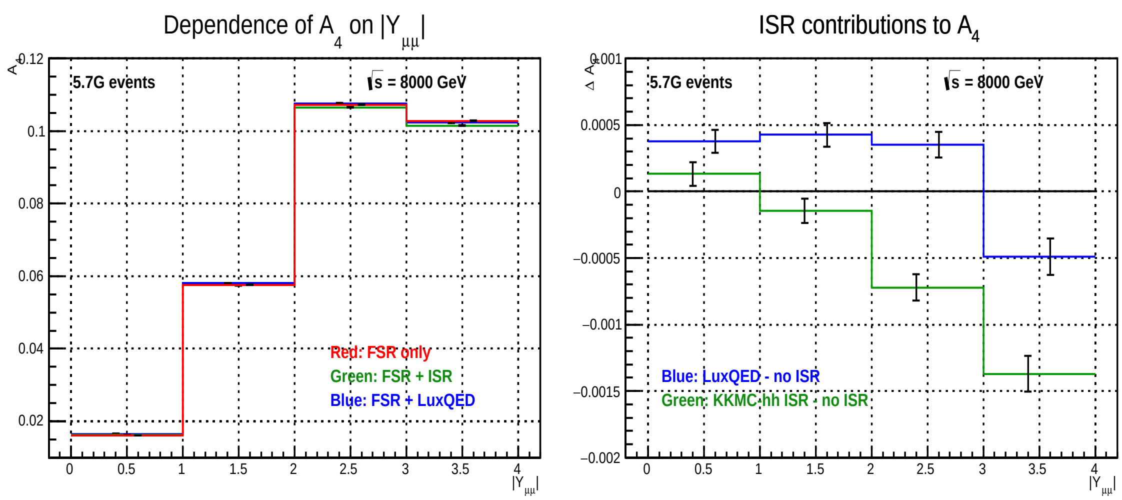

Figure 27: Effect of ISR on A_4 in terms of dilepton rapidity.

The contribution of IFI on cross sections is very small, of the order 0.01%, while the effect of IFI on $A_{\rm FB}$ and A_4 is of order 10^{-5} and 10^{-4}, respectively. The IFI-dependence of the uncut and cut CS angle distributions are shown in Fig. 7. The effect is typically a fraction of a per-mil, and angle-dependent. The uncut distribution (left) is relevant to A_4, and the cut distribution (right) is relevant to $A_{\rm FB}$.

Fig. 8 shows the IFI effect on the forward-backward asymmetry, as a function of the dilepton mass on the left, and the dilepton rapidity on the right. Fig. 9 shows similar comparisons for A_4. The IFI contribution to both $A_{\rm FB}$ and A_4 is consistent with zero near M_Z and at low dilepton rapidity. However, A_4 is more sensitive to IFI than $A_{\rm FB}$ in general.

I.4 Conclusions

$\mathcal{KK}$MC-hh provides a precise tool for calculating exponentiated photonic corrections to hadron scattering. We have presented estimates for the contributions of ISR and IFI to the $A_{\rm FB}$ and A_4 angular distributions which will be useful for determining the weak mixing angle from LHC data. $\mathcal{KK}$MC-hh is particularly well suited to evaluating IFI due to its CEEX exponentiation, which was developed in part to facilitate the calculation of interference effects. The ISR contribution is large enough that it cannot be neglected in precision studies, and needs to be incorporated in some manner, at least by including collinear photon emission in the PDFs, and preferably by including exponentiated photon emission in the generator, as in $\mathcal{KK}$MC-hh.

The *ab initio* calculation of QED emission from the quarks is unique to the approach of $\mathcal{KK}$MC-hh: other generators use calculations matched to a QED-corrected PDF set. Studies comparing these approaches are in progress, and the results will be interesting not just at the computational level, but also conceptually, for better understanding the role of QED emission in hadron scattering.

Finally, we note that $\mathcal{KK}$MC-ee and $\mathcal{KK}$MC-hh are still under development. Thanks to the program's modular design, improvements in the pure electroweak calculation can be readily incorporated in KKMC as they become available. Such an upgrade will be important in $\mathcal{KK}$MC-ee for future e^+e^- colliders[30], and $\mathcal{KK}$MC-hh will benefit at the same time. In particular, an updated parametrization of $\alpha_{\text{QED,eff}}$ [30] is available, as well as updated DIZET libraries 6.42[3] and the recent version 6.45.

Tests of $\mathcal{KK}$MC-hh to date have focused on muon decays. $\mathcal{KK}$MC supports τ lepton decays via TAUOLA[54], which has still needs to be tested in the context of $\mathcal{KK}$MC-hh to insure proper interplay with the shower. In addition, TAUOLA will eventually require an update, at least for future e^+e^- colliders, especially in the context of precision measurements of τ polarization effects.[30] Future results from Belle II [55] are likely to provide valuable input for reaching a higher level of precision in modeling τ decays.

In the near future, we expect to be able to address NLO QCD issues as well, at first by adding a capability to add photonic corrections to events provided by any event generator, rather than running events generated by $\mathcal{KK}$MC-hh afterward. To the extent that QCD and QED radiation factorize, which is true at leading log and probably beyond that to some degree[43, 44, 45], the two orders of showering should give equivalent results, but allowing the QCD shower to run run first increases the program's utility, and also provides a quantitative test of the factorization of QCD and QED radiation in this context. Eventually, we anticipate incorporating NLO QCD internally, perhaps via the KrkNLO scheme.[56, 57]

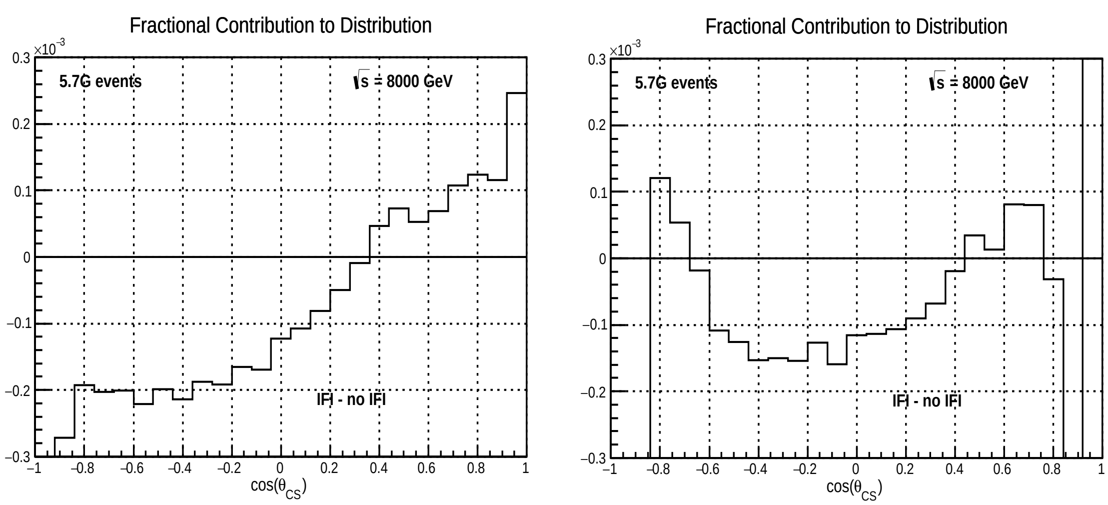

Figure 28: Dependence of the Collins-Soper angular distribution on initial-final interference, without lepton cuts (left) and with them (right).

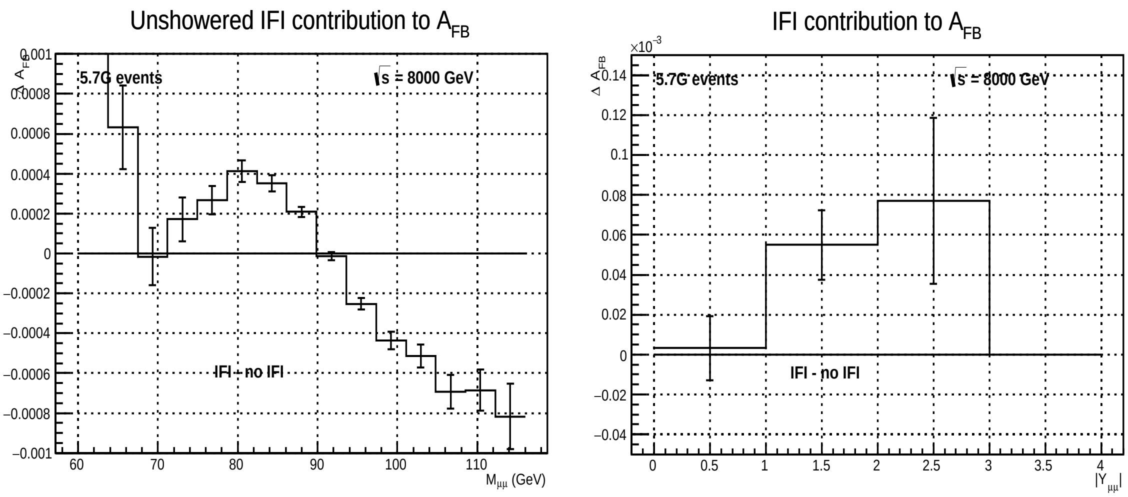

Figure 29: The IFI contribution to A_{FB}as a function of M_{ll} (left) and Y_{ll} (right).

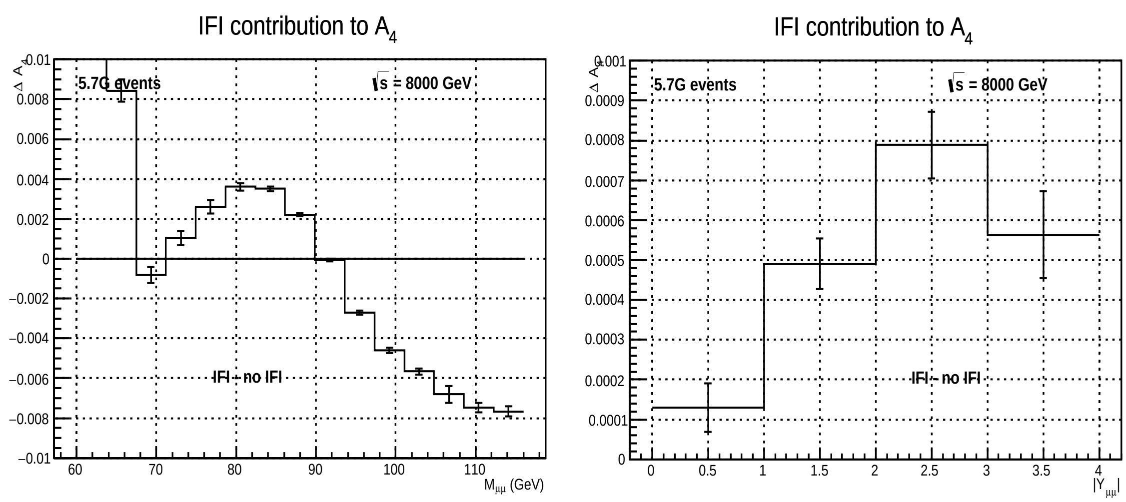

Figure 30: The IFI contribution to A_4 as a function of M_{ll} (left) and Y_{ll} (right).

J HORACE

Comments:
This text should be completed by the authors

K Multi MC comparisons in the G_μ EW scheme

Table 42: Cross-section (pb) in the mass window 60-120 GeV, predictions with different codes.

EW order	Program	G_μ scheme	Comments
LO	MCSANC	951.755(4)	
	POWHEG_ew	951.74(1)	
	ZGRAD2	951.472(8)	
LO+PW	MCSANC	945.813(4)	
	POWHEG_ew	945.69(1)	
	ZGRAD2	945.85(1)	
PW	MCSANC	-5.942(4)	
	POWHEG_ew	-6.05(1)	
	ZGRAD2	-5.625(3)	
LO+PW+HO	MCSANC	946.139(4)	
	POWHEG_ew	946.12(1)	
	ZGRAD2	945.39(1)	
PW+HO	MCSANC	-5.616(5)	
	POWHEG_ew	-5.62(2)	
	ZGRAD2	-6.08(1)	
HO	MCSANC	0.326(4) $O[(\Delta\rho)^2]$	
		-0.43(1) $O[(\Delta\rho)]$	
	POWHEG_ew	0.43(1)	
	ZGRAD2	-0.46(1)	
LO+ISR	MCSANC	955.23(1)	
	POWHEG_ew		
	ZGRAD2	955.12(1)	
ISR	MCSANC	3.53(1)	
	POWHEG_ew		
	ZGRAD2	3.645(4)	
LO+IFI	MCSANC	951.93(1)	
	POWHEG_ew		
	ZGRAD2	951.39(1)	
IFI	MCSANC	0.177(2)	
	POWHEG_ew		
	ZGRAD2	-0.0847(7)	
LO+FSR	MCSANC	935.89(2)	
	POWHEG_ew		
	ZGRAD2	935.70(2)	
FSR	MCSANC	-15.87(2)	
	POWHEG_ew		
	ZGRAD2	-15.77(2)	

Table 43: Forward-backward asymmetry in the mass window 60-120 GeV, predictions with different codes.

EW order	Program	G_μ scheme	Comments
LO	MCSANC	0.03683(1)	
	POWHEG_ew	0.03682(1)	
	ZGRAD2	0.03683(2)	
LO+PW	MCSANC	0.01997(1)	
	POWHEG_ew	0.01949(1)	
	ZGRAD2	0.01973(2)	
[LO+PW]-[LO]	MCSANC	-0.01686(1)	
	POWHEG_ew	-0.01733(1)	
	ZGRAD2	-0.01710(3)	
LO+PW+HO	MCSANC	0.02180(1)	
	POWHEG_ew	0.02085(1)	
	ZGRAD2	0.02156(2)	
[LO+PW+HO]-[LO]	MCSANC	-0.01503(1)	
	POWHEG_ew	-0.01596(1)	
	ZGRAD2	-0.01527(3)	
LO+ISR	MCSANC	0.03678(1)	
	POWHEG_ew		
	ZGRAD2	0.03683(2)	
[LO+ISR] - [LO]	MCSANC	-0.00005(2)	
	POWHEG_ew		
	ZGRAD2	0.00000(3)	
LO+IFI	MCSANC	0.03652(1)	
	POWHEG_ew		
	ZGRAD2	0.03660(2)	
[LO+IFI] - [LO]	MCSANC	-0.00031(2)	
	POWHEG_ew		
	ZGRAD2	-0.00023(3)	
LO+FSR	MCSANC	0.03729(5)	
	POWHEG_ew		
	ZGRAD2	0.03751(4)	
[LO+FSR] - [LO]	MCSANC	0.00055(6)	
	POWHEG_ew		
	ZGRAD2	0.00068(4)	

Table 44: Cross-section (pb) in the mass window 60-120 GeV, predictions with different codes.

EW order	Program	G_μ scheme	Comments
[LO+PW+HO]/[LO]	MCSANC	0.994993(4)	
	POWHEG_ew	0.994950(10)	
	ZGRAD2	0.993607(8)	
	TauSpinner + wtEW	0.99410	

Table 45: Forward-backward asymmetry in the mass window 60-120 GeV, predictions with different codes.

EW order	Program	G_μ scheme	Comments
[LO+PW+HO]-[LO]	MCSANC	-0.01503(1	
	POWHEG_ew	-0.01596(1)	
	ZGRAD2	-0.01527(3)	
	TauSpinner + wtEW	-0.01509	